The Searsville Reservoir Site (California, USA) as a candidate Global Boundary Stratotype Section and Point for the Anthropocene Series

Abstract
Cores from Searsville Reservoir within Stanford University's Jasper Ridge Biological Preserve, California, USA, were examined to identify a potential GSSP for the Anthropocene: core JRBP2018-VC01B (944.5 cm-long) and tightly correlated JRBP2018-VC01A (852.5 cm-long). Spanning from 1900 CE ± 3 yrs to 2018 CE, a secure chronology resolved to the sub-annual level allowed detailed exploration of the Holocene-Anthropocene transition. We identified the primary GSSP marker as first appearance of ^{239,240}Pu at 528 cm depth in JRBP2018-VC01B, equating to 1947 CE, consistent with a lag of 1-2 yrs between ejection of ^{239,240}Pu into the atmosphere and deposition. Auxiliary markers include: first appearance of ^{137}Cs in 1954; late 20th century decreases in δ^{15}N; late 20th-century elevation in SCPs, Hg, Co, Ni, Mo, V, Cr, and Pb; and changes in abundance and/or presence of microfossil taxa. Fossil pollen documented anthropogenic landscape changes. The primary and auxiliary markers can be correlated to sites in many geological settings globally and regionally. As part of a major university, the Searsville site has long been used for research and education; serves users locally to internationally; and is protected yet accessible for future studies and communication about the Anthropocene.

Plain Word Summary
The Global Boundary Stratotype Section and Point (GSSP) for the proposed Anthropocene Series/Epoch is suggested to lie in sediments accumulated over the last 130 years in Searsville Reservoir, Woodside, California, USA. The site fulfills all of the ideal criteria for defining and placing a GSSP. In addition, the Searsville site is particularly appropriate to mark the onset of Anthropocene, because it was anthropogenic activities–the damming of a watershed–that created a geologic record that now preserves the very signals that can be used to recognize the Anthropocene worldwide.

Keywords
Anthropocene, elemental analyses, cladocera, geochemistry, GSSP, heavy metals, paleoecology, palynology, plutonium, ostracods

Introduction
In 1892, Searsville Reservoir in Woodside, California, USA, (37.406842 N, 122.237794 W, 104 m elevation; Figure 1) filled for the first time. The reservoir sits within Stanford University's Jasper Ridge Biological Preserve (JRBP). Although it was created to store water, it eventually became even more critical geologically, because it captured some 11 meters of clays and silts spanning 130 years and holding an exceptionally detailed record of global, regional, and local signals that herald the transition from the Holocene to the Anthropocene. The focus of this paper is a core proposed as the Global Boundary Stratotype Section and Point (GSSP) for the Anthropocene, JRBP2018-VC01B, and correlated microfossil data from another core taken nearby, JRBP2018-VC01A. Both cores span 1900±3 yr CE to 2018 CE They are easily correlated to other cores taken from the reservoir (19 cores obtained in 1998, 2018, and 2020, several of which are archived), as well as to three auxiliary cores taken from a lake 700m to the west, Upper Lake. The Upper Lake cores extend back ~1300 years and provide baseline information relevant to interpreting the Holocene-Anthropocene transition (Supplementary Material).

It is ironic that human engineering, the hallmark of the Anthropocene, turned the Searsville site from a riparian valley into a lake whose sediments have archived in great detail

the many ways that humans have changed the Earth System. No less ironic is the potential the site holds as the GSSP "golden spike" for the Anthropocene. The founder of Stanford University, Leland Stanford, in 1869 pounded the eponymous golden spike to commemorate a key milestone in the increasing industrialization and globalization that eventually transformed the Holocene world into the Anthropocene one: the completion of the first transcontinental railroad in the USA (Chesley, 2019).

Geographic and Geologic Setting

Searsville Reservoir and Dam are located at the pinch-point of the San Francisquito Creek watershed, which encompasses approximately 123 km^2 (Figure 1). The sediments that have filled the majority of the reservoir basin (Freyberg, 2001) are derived from a melange of primarily sedimentary and accreted rocks that range in age from Quaternary to Cretaceous. Movement along the San Andreas Fault has created a steep gradient from the crest of the Santa Cruz Mountains, channelized streams along the NW- to SE-trending fault complex and has led to fracturing many of the rocks, increasing their friability and contributing to frequent landslides (Kittleson et al., 1996).

The Mediterranean climate of the region features intense downpours in the wet season (generally October to April), followed by a long dry season (Figure 2a), exacerbating expansion and contraction of already-friable rock exposures. During torrential rains in the wet season, the ~20 creeks and their tributaries that comprise the watershed flush vast amounts of material into Searsville Reservoir, producing a thick sedimentary record in the reservoir that can be resolved to seasons. Over the past 130 years, Searsville Reservoir has accumulated ~9-10 cm/year on average, sometimes with several centimeters accumulating in days or even hours during storms (Kittleson et al.,1996). For comparison, sedimentation rates for lakes in the Northeastern United States are typically less than 0.2 cm/year (Goring et al., 2012).

Pertinent global signals are recorded because just 16 kilometers to the west is the Pacific Ocean, which means the lake has been a settling pond for anthropogenic inputs carried on winds that have traveled across the Pacific as they circumnavigated the globe (Figure 2b). Global and regional signals are easily parsed from one another by comparing the geochemical and paleontological changes extracted from the sediments with well-documented archaeological records and historical archives (Figure 3) (Bocek and Reese, 1992) (Supplemental Material).

Accessibility

Searsville Reservoir is a central feature of Jasper Ridge Biological Preserve, a 485-hectare area within Stanford University that is protected for research, education, and conservation activities targeted toward the understanding of the Earth's natural systems. This ensures that the site will be conserved and protected, but also will remain accessible (Supplemental Material). Looking forward, the Anthropocene has emerged as one of three major initiatives in the Jasper Ridge Strategic Plan (JRBP, 2018) that was launched in 2018. The sediments in the lake will remain available for additional coring over the next few years, with appropriate permissions from Stanford University and relevant regulatory agencies. In the longer term, Searsville Dam is slated to be modified (Searsville Project Team, 2022) such that the reservoir will be drained and likely expose outcrops of the sediment layers now well-sampled in the cores discussed below, some of which are stored as archives (Appendix 1).

Previous Work

The potential value of Searsville sediments as highly resolved sedimentary archives first became evident with nine cores taken by the U.S. Geological Survey in 1998. The information from these cores were never published but were summarized in a white paper provided to JRBP (Berhe et al., 2007; Fries et al., 1999) where the data and a suite of core photographs are on file. Other research on Searsville Reservoir extends back nearly a century, beginning with a study of its limnology (Scott, 1925, 1927). The body of work, comprised of peer-reviewed publications and gray literature available at JRBP, includes research on seasonal fluctuations of benthic macrofauna and limnetic plankton (Felin, 1940), ostracods (Carter, 1991, 1992), and *Daphnia* (Ruhl, 1992); fish (Smith, 1963; Bailey, 1980; Aris and Fitzpatrick, 1980); birds (DeSante, 1971; McGraw, 1977; Kirsher, 1984; Lu, 1992; Meece, 1993); insects (Fay, 1978; Brown, 1998); mosquitoes and their parasites (Poinar, 1979); sedimentation (Howarth 1981; Mullen, 1982; Smith and Oremland, 1983; Sigman, 1989; Wilcox, 1995; Wade, 1995; Kittleson et al., 1996; Krall, 2013); bacteria and antibiotic resistance (Warner, 1987; Miller et al., 2013); aquatic plants and algae (Bently, 1918; Del Favero, 1988; Yang, 1993; Penuelas et al., 1993); water chemistry (Radoslovich, 1989; Keller and Margolis, 1989; Shieh, 1991; Balasubramanian, 1993; Kulp et al., 2014; Koweek et al., 2020); general lake biology (Lu and Collier, 1990); species diversity (Tolia, 1992; Smith, 1992; Gamble et al., 1996; Lerner, 1998); comparison to nearby lakes (Baldo, 1985a, b); geology and tectonics (Coleman, 2004; Pampeyan, 1993); history (Trilling, 1981; Bocek and Reese, 1992; Regnery, 1991; Lund and Gullard, 2003); and dam modification (Page, 1997; Heppner, 2007; Heppner and Loague, 2008; Searsville Alternatives Study, 2015; Searsville Project Team, 2021).

Also valuable are archives at JRBP that document information relevant to interpreting sedimentation patterns and anthropogenic inputs into Searsville Reservoir (Supplementary Material). When the reservoir first formed, it was a continuous body of water that encompassed Middle Lake and Upper Lake, but it rapidly began to fill with sediment. The height of the dam's spillway varied through time, impacting sediment flux, and in 1929, a levee (the Causeway) was constructed to trap silt in Middle Lake (Figure 1). Nevertheless, infilling of the reservoir marched steadily on with a prograding delta from the south. Today, what used to be the southern portion of the original Searsville Reservoir harbors a riparian forest rich with bird life, and the reservoir itself is less than half its original size, with <10% of its original water storage capacity (Freyberg, 2001).

Materials and methods

Geographical setting of core sites

Eight cores were collected from Searsville Reservoir in 2018 and 2020 (Appendix 1). Two are reported here: JRBP2018-VC01A (Latitude = 37.406832, Longitude = -122.237844, Datum = WGS84; water depth = 265cm), and JRBP2018-VC01B (Latitude = 37.406844, Longitude = -122.237881, Datum = WGS84; water depth = 268cm) (Figure 1). Both were collected during the same expedition from the deepest part of the reservoir, approximately 65m south-southeast of Searsville Dam. The two cores were precisely correlated with each other using physical-stratigraphic and geochemical criteria.

Field collection of core, sampling, and core imagery

Cores were collected 29-30 October 2018 and 2 February 2020 using a Vibracorer supported by a floating platform. The cores were collected in multiple ~590-cm long aluminum core tubes

connected by couplings. JRBP2018-VC01A is 851cm long with 24% compaction while JRBP2018-VC01B is 944.5cm long with 15% compaction. JRBP2018-VC01B was designated as the primary GSSP core and sampled for geochemical markers associated with the Anthropocene. JRBP2018-VC01A was used for microfossil sampling and analyses.

Both cores were sectioned in the field and JRBP2018-VC01A was also split lengthwise and photographed in the field prior to transport. Cores are stored at the core lab at the USGS Pacific Coastal and Marine Science Center in Santa Cruz, California, USA. The cores will be permanently reposited at the USGS Southwest Region cold storage facility at Moffett Field in Menlo Park, California (USA), where they will be available to future researchers with permission from the USGS.

Of the cores taken in 2018 and 2020, five have been split and three have been sampled for analyses reported in this paper and/or for other analyses. The remainder will serve as archives (Appendix 1). Core scanning was performed in the core lab at the USGS Pacific Coastal and Marine Science Center using a GeoTek Rotating X-ray Computed Tomography (RXCT) and GeoTek Multi-Sensor Core Logger (MSCL). Core sections were CT-scanned at 104 micron resolution using a Thermo Kevex PSX10-65W X-ray source set to 115 kV and 452 µA. CT scans were reconstructed using Geotek Reconstruction Software. CT intensity is a proxy for sediment density (Tanaka et al., 2011; Holland and Schultheiss, 2014) and is positively correlated with gamma bulk density in JRBP2018-VC01B (Appendix 2). Linescan core images were collected using a GeoTek Core Imaging system, with a Geoscan V camera. Linescans were collected at 200 micron resolution. JRBP2018-VC01B was scanned for Gamma attenuation using a gamma ray source and detector mounted on the MSCL. JRBP2018-VC01B was CT and gamma attenuation scanned before being split, then immediately line-scanned after splitting. JRBP2018-VC01A was CT scanned as a split core then line-scanned.

X-ray Fluorescence (XRF) data was collected on the MSCL using an Olympus Delta Professional XRF Spectrometer at 1cm intervals for 20 second measurements per beam, in both Geochem and Soil mode.

Initial visual core descriptions were completed using the Troels-Smith (1955) system for describing organic-rich sediments and the Schnurrenburger et al. (2003) system for classifying lacustrine sediments, including the use of Munsell charts for determining sediment colors.

Grain size distributions were determined from 38 subsamples (31 from JRBP-2018 VC01B, 7 from JRBP-2018-VC01A) at the US Geological Survey Pacific Coastal and Marine Science Center (Appendix 3). Samples were selected to represent the range of sediment size observed in both cores.

CT, line scan, XRF, and grain size data are published in an accompanying USGS Data Release (La Selle et al., 2022).

Chronological controls

The highly resolved chronology for JRBP2018-VC01B was constructed using a combination of seasonal-layer counting enabled by distinctive wet-season/dry-season couplets, distinctive sedimentary features, radiometric tie-points (^{137}Cs), and correlation of historic event and climate data to geochemical (Cu, Ca, Ti) and sedimentological signals (1906 and 1989 earthquakes) in the cores. Details of this process are described in Supplementary Materials.

The age model for JRBP2018-VC01A was constructed by detailed matching of the layers evident in CT scans to those also evident in JRBP2018-VC01B, and by alignment of Cu and Ca peaks in the XRF scans from the two cores (Appendix 6). The variation in thickness of layers of

varying CT intensity from top to bottom of each core results in a clear pattern, analogous to paleomagnetic stripe-patterns.

Anthropocene Radioisotopes

Freeze-dried sediment samples from JRBP2018-VC01B were analyzed for ^{241}Am in the course of measuring ^{210}Pb and ^{137}Cs by direct gamma assay in the Environmental Radiometric Facility at University College London (see Methods: Chronological Controls; Appendix 4). Freeze-drying was done with a Labconco FreeZone 4.5 Freeze Drier

We analyzed nineteen bulk sediment samples for bomb radiocarbon by Accelerator Mass Spectrometry at The Laboratory of Ion Beam Physics, Eidgenössische Technische Hochschule Zürich. Samples were collected from JRBP2018-VC01B at depths between 518 and 158.5 cm. Radiocarbon ages were calibrated using the IntCal20 calibration curve (Reimer et al., 2020) in the *Bchron* (Haslett and Parnell, 2008) package in R (R Core team, 2021).

Plutonium-239,240 concentration and isotope ratios were analyzed in freeze dried sediment samples from between 538 and 162.5cm in JRBP2018-VC01B. Some adjacent samples were combined to increase sample sizes and two samples were subsequently excluded from our study because they were from a storm deposit which would have been deposited over only a few days. These two excluded samples were the same samples excluded from our ^{137}Cs dataset. Plutonium was analyzed by alpha spectrometry at the National Oceanic Centre Southampton (NOCS) GAU-Radioanalytical Lab at the University of Southampton. Samples analyzed for ^{239,240}Pu activities were also analyzed via MC-ICPMS to determine ^{240}Pu/^{239}Pu ratios. (Appendix 7).

Novel materials

SCPs. Sixty-eight samples from JRBP2018-VC01B between 168-1093cm were collected and freeze dried for spheroidal carbonaceous particle (SCP) analysis at University College London. The sampling interval ranged from 5 - 30 cm, with the highest density of samples between 538 and 347.5cm. Sediment samples were analyzed for SCPs following the method described in Rose (1994) and the criteria for SCP identification under the light microscope followed Rose (2008). During counting, SCPs were subdivided into size classes (4-10, 10-25, 25-50, and 50-75 µm). (Appendix 8).

PCBs. Sediment samples for PCB analysis were collected at 16cm increments, then aggregated into 6 combined, depth-averaged samples to achieve adequate sample size (Appendix 9). Samples were analyzed at PHYSIS Environmental Laboratories, Inc. (Anaheim, California, USA) following method EPA 8270D (EPA, 1998) to detect PCB congeners and concentrations.

Organic matter proxies

Carbon (C) and nitrogen (N) bulk elemental and isotopic analyses were performed at the Stanford Stable Isotope Biogeochemistry Laboratory (SIBL) (Stanford, California, USA) on samples from between 162 and 1102.5 cm of JRBP2018-VC01B (Appendix 10).

To model trends in organic matter proxies we used Generalized Additive Models (GAMs) with adaptive splines and restricted maximum likelihood (REML), following the guidance of Simpson (2018) and implemented in the *mgcv* package (Wood, 2011, 2017) in R (R Core Team, 2021). We identified significant increases/decreases in our GAMs by locating regions where the derivative of the GAM was significantly different from zero, using the

'derivatives' function in the R *gratia* package (Simpson, 2022). We tested for correlation between organic matter proxies and depth using Spearman's correlation, and also tested for changes in variance of organic matter proxies in rolling windows of 10 samples, using Spearman's rank correlations.

Inorganic geochemical signals

Major and trace element content of JRBP2018-VC01B was analyzed by ICPMS (Appendix 11 and Supplementary Materials). Twenty of the samples analyzed for major and trace element content were also analyzed for lead isotopes (^{204}Pb, ^{206}Pb, ^{207}Pb, and ^{208}Pb). Pb was isolated from bulk rock dissolutions using HBr-based chemistry on AG1x8 anion exchange resin. Samples were analyzed on the Agilent 8900 ICPMS and were corrected for instrumental mass fractionation using sample-standard bracketing with NIST SRM-981. External reproducibility is based on repeated analysis of the USGS BHVO2 basalt standard over the 3 analytical sessions (n=8). These results are considered preliminary as higher precision measurements via MC-ICPMS are underway.

For mercury (Hg), samples of ~0.3 g and 0.5 cm thick were collected at 5 cm intervals starting at a base depth of 1103 cm, and analyzed in triplicate at the Stanford Carnegie Institute Department of Global Ecology by thermal decomposition followed by preconcentration of Hg on a gold trap and cold vapor atomic absorption spectrophotometry using a DMA-80 direct Hg analyzer (Milestone, CT, USA) (Appendix 12). See Redondo (2022) and Redondo et al (in prep) for further details.

We modeled trends in inorganic geochemical signals using the same GAM modeling method described for organic matter proxies.

Biotic markers

Samples for biotic marker analysis were collected at overlapping depths and in the low-density sediment layers associated with higher organic matter.

Ostracods and Cladocera Ephippia. For ostracod and cladocera analysis, 28 sediment samples of ~15g and 2cm thick were collected from JRBP2018-VC01A. Samples were washed through a set of nested sieves (300, 180, and 100 μm) and air dried, then picked under a dissecting microscope and mounted on micropaleontology slides following the methods of Horne and Siveter (2016). The specimens were sorted into morphotypes under a compound microscope. Ostracods valves less than ~50% complete were logged but not included in analyses. Representative specimens for each ostracod morphotype were photographed using a Zeiss Sigma Field Emission scanning electron microscope (SEM) at Stanford University's Cell Sciences Imaging Facility. Ostracods were identified to the finest possible taxonomic resolution based on shell shape and surface microstructure using comparative collections from the California Academy of Sciences and published literature, especially Smith and Delorme (2010). Cladoceran ephippia were identified under a compound microscope to the genus level following Vandekerhove et al. (2004). See Viteri (2022) and Viteri et al. (in prep) for further details.

Diatoms. For diatom analysis, 40 sediment samples of ~5 cm^3 volume and spanning between 2 – 8 cm depth were collected from JRBP2018-VC01A. Diatom samples were processed at the National Lacustrine Core Facility (LacCore; University of Minnesota, Minneapolis, Minnesota, USA). Processing constituted digestion of the organic matter and carbonates in the sediment

using Peroxide and HCl (Hydrochloric acid). Concentrated diatoms were mounted on slides for depths 298-304, 465-470, 588-594, and 742-748cm and were examined in the Spanbauer Lab at the University of Toledo. Additional slides were not prepared because very few diatoms were detected.

Pollen, spores, and non-pollen palynomorphs.
Pollen analysis was conducted on 40 samples from JRBP2018-VC10A at the same depths as for diatoms at the Northern Arizona University Laboratory of Paleoecology (NAU LOP; Flagstaff, Arizona, USA) (Appendix 13). *Lycopodium* tracer spores were added to each sample to monitor any degradation from the extraction procedure and to enable pollen concentration calculations. Processing followed a modified Fægri and Iversen (1989) technique, which included suspension in 10% KOH to liberate pollen from the humic acid matrix; wet-sieving through 180-µm sieves to separate pollen from larger organic fragments; suspension in 10% HCl to remove carbonates; HF to remove silicates; and acetolysis solution to reduce organics. Recovered residues were stained with Safranin O stain and stored in silicon oil.

Pollen and spores mounted on microscope slides were identified at 400x magnification to an ~300-grain sum (exclusive of wetland and aquatic types, spores and NPPs). Identifications were made to the lowest taxonomic level possible, usually genus, sometimes family, generic groupings or family groupings, based on published keys (e.g., McAndrews et al., 1973; Fægri and Iversen, 1989; Moore et al., 1991; Reille, 1992), and the LOP pollen reference collection at NAU (Appendix 13).The NPPs (non-pollen palynomorphs) were identified based on van Hoeve and Hendrikse (1998), van Geel (2001), Ejarque et al. (2015) Anderson et al. (2015), and the website http://non-pollen-palynomorphs.uni-goettingen.de. Some aquatic NPPs (algae, rotifers, and protozoa) were used in an additional analysis with cladocerans and ostracods.

Results

Lithology

The Searsville cores are fairly homogeneous gray to brown silt and clay (Figure 5) interspersed with some dark black bands which were visible immediately after core splitting but have since faded. The CT scans show discrete layers ranging from <1 mm to >30 cm thick, with no evidence for bioturbation or hiatuses.

The grain size distributions of sediments from wet seasons are typically moderately sorted with D50 medians in silt. The inorganic components of dry season sediments consist of well sorted clay-sized particles. Higher deposition rates during wet seasons resulted in massive or thickly laminated silts with normal grading occurring in the upper 0.1 - 3.0 cm of the beds. The relationship between median grain size and 1-cm mean CT intensities is linear. Layers with a median grain size in coarser silt have CT intensities greater than 15000, while clay-dominated layers have CT intensities less than 15000.

Chronology

Depositional rates are highly variable from season to season in Searsville Reservoir. This is a huge advantage for developing a detailed chronology as described above, but complicates the application of dating techniques that rely on uniform depositional rates, notably ^{210}Pb dating, which was uninformative (Supplementary Material).

Cesium-137 followed the expected pattern. We first detected ^{137}Cs at 472.5-478cm (4.64 ± 0.78 Bq/kg). It then increased upcore to 447.5-453cm and remained elevated until 418-423cm before declining sharply. The youngest ^{137}Cs detection was at 403-408cm (2.99 ± 1.85 Bq/kg).

Our two rounds of analyses identified two potential peaks: the first analysis indicated peak ^{137}Cs at 447.5-453cm (10.28 ± 1.19 Bq/kq) while the second analysis suggested the peak at 428-433cm (10.57 ± 1.85 Bq/kg). The error bars of the two peaks overlap. We used several lines of evidence to determine which peak likely corresponds to the year 1963 CE First, counting of annual layers supports the lower depth, 447.5-453cm, as 1963 CE. Layer counts in this part of the core are well-constrained by the XRF Copper peaks from 1943-1953 C and by the 1955 CE flood deposit. Second, although it is possible for ^{137}Cs to be mobilized from anoxic sediments, it would move up into younger deposits, not down into older sediments (Comans et al., 1989). We therefore conclude that the sediments at 447.5-453cm of the core formed in 1963 CE when there was a maximum ^{137}Cs fallout derived from nuclear weapons testing (Appleby, 2001).

Seasonal layer counting, verified by Ti profiles and visual inspection of CT scans, indicates 118 ± 3 annual layers in JRBP2018-VC01B. This information, combined with the chronological anchors described in the Methods section above and Supplementary Material, places the base of core at 1900 ± 3 CE and the top at 2018 CE (Figure 4). Age error ranged between ±0.25 and ±3 years. For layers where the year could be determined with a high level of confidence based on sedimentological or geochemical evidence of historically recorded events (e.g., 1906,1943, 1963, 1989, 2018 CE), we assigned an error of ±0.25 year to account for the fact that the onset of the wet and dry seasons can vary by several months depending on the year (Table 1). In general, where seasonal layers were clear and independent tie points were more dense, error bars were ±1 year. However, in segments of the core that represented winters with little or no rain, seasonal layering was less clear, resulting in error bars that were generally considered to be from ±1-2 years. Below the Cu peak in 1943, error bars increased to ±2-3 years (Supplementary Material). The 1906 earthquake layer also served to constrain the bottom age of the core, as was correlation with the 1998 cores that included pre-reservoir soil.

Seasonal layer counting and matching of Ca patterns in the XRF demonstrated that the base of JRBP2018-VC01A was deposited during the same year and season as the base of JRBP2018-VC01B.

Calculation of sedimentation rates

Because of the episodic sedimentation events, sedimentation rates were highly variable, ranging from 1 - 47.5cm/year with a mean of 15.64cm/year (Appendix 15). Rates were generally higher before ~550 cm (pre-1940s CE, mean = 19.6cm/yr). Rates slowed from ~550 to ~350cm (~1940-1995 CE; mean = 5.4cm/yr), increased again from ~350 to 210cm (~1995-2007 CE; mean = 18.5 cm/yr), then once again slowed from 210 to the top of the core (2007-2018 CE, mean = 4.6 cm/yr).

Radioisotopes

Americium-241. Only one ^{241}Am activity of 1.24 ± 0.64 Bq/kg was detected at 162.5-168cm (2016 ± 0.25 - 2018 ± 0.25 CE). The source of this is not well understood. However, the timing corresponds with an underground nuclear test in North Korea in September, 2016.

Carbon-14. Radiocarbon ages for JRBP2018-VC01B bulk sediments were all much older than the known age of the reservoir, and age did not increase with depth, probably because sediments

contained old carbon from coal-bearing sedimentary rocks upstream (Appendix 15 and Supplementary Material).

Plutonium. Samples were analyzed from depths ranging from 538 to 162.5cm in JRBP2018-VC01B. Low levels of ^{239,240}Pu were found in all samples except the combined sample from 532.5-538cm (1945 ± 0.25 -1946 ± 0.25 CE). The first ^{239,240}Pu detection was at a sample that spanned depths 522.5-528cm (1947 ± 0.25 -1949 ± 0.25 CE; $5.782 \times 10^{-5} \pm 3.621 \times 10^{-5}$ Bq/g) (Figure 6). However, no samples were analyzed for depths 532.5 to 528.5: these analyses are presently underway to further pinpoint the earliest appearance of ^{239,240}Pu. We found three notable peaks in ^{239,240}Pu across the record: the first at 472.5-478cm (1958 ± 0.5 -1959 ± 0.5 CE; $3.8416 \times 10^{-4} \pm 8.86 \times 10^{-5}$ Bq/g), the second and highest at 447.5-453cm (1963 CE; $7.526 \times 10^{-4} \pm 1.4807 \times 10^{-4}$ Bq/g), and the last at 402.5-403cm (1976 ± 0.5 -1977 ± 1 CE; $3.911 \times 10^{-4} \pm 7.08 \times 10^{-5}$ Bq/g). The first two peaks correspond closely in age to peaks in ^{239,240}Pu fallout documented in Hancock et al. (2014). A sample from 407.5-413cm was contaminated and excluded from our analysis. Samples from 425-475cm (1959 +- 0.5 - 1969 +- 1 CE), the depth interval with maximum ^{239,240}Pu activities, had ^{240}Pu/^{239}Pu ratios between 0.18 and 0.22 Bq/g (Appendix 7). These are consistent with ratios previously reported for global nuclear weapons fallout in northern latitudes (Wu et al., 2011). Samples from other depth increments had very low CPS (counts per second) of 3000 or less, below reliable determination levels.

Novel Materials

SCPs. The first SCPs were found at 607.5-608cm (1934 ± 2 CE) (Figure 7). Above this, SCP concentrations were irregular, and absent in 14 out of 51 samples. Throughout the core SCP counts were low–the maximum was 5, at 422.75 (1970 ± 1 CE) and 412.75cm (1973 ± 1 CE)–with corresponding low concentrations again, likely due to the high sedimentation rates in this reservoir. Peak concentrations also occur at 412.75cm (1970 ± 1 CE).

The SCP profile is consistent with the general North American increase in SCPs in sediments in the 1930s, peaking in the 1970s and persisting to today (Rose, 2015). Most SCPs fell in the 4-10µm size range, but some SCPs in slightly larger fractions occurred throughout (Figure 7, Appendix 8). No SCPs in the largest fraction (>50µm) were observed, suggesting that a nearby source of SCPs is less likely (Inoue et al., 2013). Searsville Reservoir is not downwind of any local coal-burning plants, suggesting that the deposition of the SCPs is a global, not local, signature.

PCBs. PCBs were not detected in samples below 620cm (pre-1930s). Above this depth, one congener (PCB 153) was found in the sediment from 620-475cm (1933 ± 2 -1959 ± 0.5 CE), seven congeners (PCB 149, 153, 174, 180, 183, and 187) were found from 460-315cm (1962 ± 0.5 -1998 ± 0.5 CE), and two congeners (PCB 149 and 153) were found from 300-159cm (1998 ± 1 -2018 ± 0.25 CE). Total PCB concentrations (0.612, 2.571, and 0.33 ng/g in the first, second, and third samples from the top, respectively) were relatively low as compared to other lake sediment cores (Bigus et al. 2014). PCBs were commercially produced between 1930 and 1980 (Bigus et al. 2014), so the pattern of PCB increase and decline in our core matches this history closely.

Organic Matter Proxies

Total Organic Carbon (TOC). TOC ranged from 1.29 to 3.34% and increased from ~820cm (~1920 CE) to the top of the core (Spearman's rho = -0.67, p-value < 1×10^{-15}), with peaks at depths of 577.5-592.5 (1936 ± 2 -1937 ± 2 CE), 262.5 (2004 ± 0.5 CE), and 197.5cm (2008 ± 0.5 CE) (Figure 8). Variance also significantly increased from the bottom to the top of the core (Spearman's rho = -0.83, p-value < 1×10^{-15})

Total Nitrogen (TN). TN ranged from 0.14 to 0.34% and increased from the bottom to the top of the core (Spearman's rho = -0.49, p-value < 1×10^{-12}) but notable increase started around 650cm (~1931 ± 2 CE) (Figure 8). After that, TN fluctuated through time and was relatively elevated from ~525-600 (1935 ± 2 - 1948 ± 0.25 CE), 370-420 (1971 ± 1 -1990 ± 0.5 CE), 260-280 (2001 ± 1 -2004 ± 0.5 CE), and 180-210 cm (2007 ± 0.5 - 2014 ± 0.25 CE). Variance also significantly increased from the bottom to the top of the core (Spearman's rho = -0.48, p-value < 1×10^{-10}), but particularly above ~650 cm (1931± 2 CE)

C/N ratio. C/N mass ratio values ranged from 7.23 to 17.15 (Figure 8) and although it was weakly correlated with depth (Spearman's rho = -0.16, p-value = 0.04), increases in C/N didn't begin until ~400cm (~1978 ± 2 CE) and there was no significant correlation between C/N and depth (Spearman's rho = -0.06, p-value = 0.40). Below 400cm, mean C/N ratio was 10.21 (95% CI = 8.89-12.47) but above the mean increased to 11.70 (95% CI = 9.62-14.21).

Stable carbon isotopes ($\delta^{13}C$). $\delta^{13}C$ ranged from -24.64 to -29.42 and was fairly stable from the bottom of the core up to ~650cm (~1931 ± 2 CE), with a mean of -25.35 (95% confidence interval = -26.36 - -24.81) (Figure 8). Above 650cm, $\delta^{13}C$ values became more variable and more depleted on average (mean = - 26.13, 95% confidence interval = -28.50 - -24.92). This is also reflected in the significant correlation between depth and variance (Spearman's rho = -0.72, p-value < 1×10^{-15}). The decline beginning at ~1931 CE is about 34 years earlier than the typical inflection point for $\delta^{13}C$ evident globally, suggesting local influences at Searsville override the global pattern. The most notable decline in $\delta^{13}C$ was found near the top of the core, from ~180-210cm (~2007 ± 0.5 - 2014 ± 0.25 CE), but this was followed by a sharp increase to the top of the core.

Stable nitrogen isotopes ($\delta^{15}N$). $\delta^{15}N$ ranged from 1.81 to 5.08 and declined steadily from the bottom to the top of the core (Spearman's rho = 0.84, p-value < 1×10^{-15}) (Figure 8). Variance also increased through time, but this was driven entirely by a sharp increase after ~300cm (~1999 ± 1 CE): if values above 300 cm are removed, there is no significant relationship between depth and $\delta^{15}N$ variance. This decline generally mirrors the pattern in lake sediments elsewhere (Wolfe et al. 2013).

Inorganic geochemical signals

Relevant trends were noted in nine heavy metals of anthropogenic importance measured in JRBP2018-VC01B. Full ICPMS results can be found in Appendix 11.

Pb. Lead concentration ranged from 11.198 to 31.662 ppm over the core (Figure 9). Values were low and fairly stable from the bottom of the core to ~635 cm (1932 ± 2 CE), varying between 11.198 and 18.738 ppm. From ~635 to ~590cm (1932 ± 2 to 1936 ± 2 CE), Pb concentration increased significantly to the first of two major peaks (maximum = 25.800 ppm, GAM model

peak = 19.47 ppm), at ~570-590cm (1936 ± 2 -1938 ± 2 CE). After a brief decline from ~570 to ~470cm (1938 ± 2 to 1960 ± 0.5 CE), Pb increased again from ~465 to 430cm (1961 ± 0.5 to 1967 ± 1 CE) to the second major peak (maximum = 31.662 ppm, GAM model peak = 20.19 ppm), at ~420-380cm (1971± 1 - 1986 ± 0.5 CE), then declined significantly from ~380 (1986 ± 0.5 CE) to 320cm (1997 ± 0.5 CE), returning to early 1900s values and remaining low to the top of the core (range = 11.313 - 17.684 ppm). This tracks the global pattern.

All sediment samples tested had Pb isotopes with strongly overlapping error bars (Appendix 11). These samples fell in the range of natural background (Ritson et al., 1999), but further Pb isotope analyses are in progress to improve precision.

Hg. The average Hg concentration for Searsville sediments was 91.65 ppb (ng/g) (Figure 9). This represents significant elevation over pre-1860 baseline values of ~47 ppb on average, as evidenced by Hg values from Upper Lake cores (Redondo, 2022). From ~1900 CE, Hg concentration fluctuated through time. Notable peaks and valleys, where values were more than one standard deviation above/below the mean were evident (Figure 1.4). At 783cm (1922 ± 2 CE), Hg concentration was 118.65 ppb. The highest levels were seen in adjacent samples at 428 (201.9 ppb; 1967 ± 2 CE) and 423cm (239.3 ppb, 1970 ± 1 CE). Elevated concentrations were also seen before and after this major peak, from ~383 to ~453cm (~1963 ± 0.5 -1985 ± 0.5 CE). Following this, Hg concentration decreased toward the present, with one rebound at 288cm (129.3ppb; 2000 ± 1 CE). The lowest concentrations recorded for the Searsville core were found at 258cm (66.6 ppb; 2004 ± 0.5 CE) and 933cm (67.55 ppb; 1910 ± 3 CE). See Redondo (2022) and Redondo et al. (in prep) for details.

Other Heavy Metals. Heavy metal concentrations in Searsville core follow a clear sequence of increases throughout the 20th century (Figure 9). Zinc (Z) concentrations increased continuously through the core (pre-1900 to 2018 CE), matching global records of Zn production (Nriagu, 1996; Han et al., 2002). Cadmium (Cd) increased continuously from ~700cm (~1928 +- 2 CE) to the top of the core, later than expected based on annual global production estimates (Han et al., 2002) and concentrations in Greenland ice cores (Candelone et al., 1995; McConnell and Edwards 2008), but on par with Cd measured in Siberian and Chilean alpine ice cores (Eichler et al., 2014; Potocki et al., 2022). Molybdenum (Mo) increased from ~670 cm (~1929 +- 2 CE) to the top of the core, also closely matching the rise in global Mo production (Henckens et al., 2018) and measurements of Mo from alpine ice cores (Arienzo et al. 2021). Cobalt (Co), nickel (Ni), chromium (Cr), and vanadium (V) followed a different pattern, first increasing significantly–beginning at ~850cm (1917+-2 CE) for Co, ~720 cm (1926+- 2 CE) for Ni, ~650cm (1931 +-2 CE) for Cr and V–then declining again–beginning at ~240cm (~2005 CE) for Co, ~250 cm (2004 +- 0.5 CE) for Ni, ~380 cm (1986 +- 0.5 CE) for Cr, and ~400cm (1978+- 1 CE) for V. Increases in Cr and Ni in Searsville closely match the onset of major global production, but the subsequent decline in both elements differs from the global record (Han et al., 2002). The vast majority of Co is produced as a byproduct of other metals including Ni and Cu (Slack et al. 2017) so increases in Co might be expected to track trends in other metals. However, in Searsville, the increase in Co is later than the onset of major global Cu or Ni production (Han et al., 2002). In a study of an alpine ice core, Van de Velde et al. (1999) found that Co, Cr, and Mo all increased in the 1940s, however no samples were analyzed between the 1920s and 1940s. Nevertheless, this suggests that our observed increase in Co in Searsville may reflect global atmospheric increases. Co production declined in the mid 1980s, matching the

timing of our decline in Searsville, though we do not recover the expected increase in the 2000s (Slack et al. 2017). Vanadium (V) in Searsville closely tracks the rise and then fall of V detected in alpine ice cores in Western Europe, linked to petroleum consumption (Arienzo et al., 2021), and V emissions reported since 1950 (Bai et al., 2021).

Biotic Markers

Ostracods, Cladocera, and Diatoms. In total, 402 ostracod valves and 466 ephippia were recovered from core JRBP2018-VC01A (VIteri, 2022; Viteri et al. in prep). Members of the Candonidae family and *Physocypria globula* were the most abundant ostracods (Figure 10). *Cypridopsis vidua* and *Ilyocypris* cf. *gibba* are rare, with *C. vidua* occurring only in youngest levels, and particularly abundant (85.4%) in the top half, especially from 546 to 603cm (1937 ± 2 to 1951 ± 0.25 CE). *Ilyocypris* cf. *gibba* was only in levels older than 1950 CE. All taxa are considered cosmopolitan (Smith and Delorme, 2010). 14.7% of ostracod valves were small juvenile molts (instars), which are typically unidentifiable to the species-level (Smith and Delorme, 2010).

Ephippia from the cladoceran *Daphnia* spp. occur throughout the core. Those from *Ceriodaphnia* spp. make a brief appearance low in the core, at 969-971cm (1909 +- 3 CE), are absent until 601-603cm (1937 ± 2 years), then increase markedly in abundance at 546-548cm depth (1950 +- 0.5 -1951 +- 0.5 CE), above which high abundance is sustained.

Diatoms were rare, highly dissolved, or absent in all JRBP2018-VC01A processed samples. See Supplementary Materials for more details.

Pollen, spores, and non-pollen palynomorphs. Sequoia sempervirens (coast redwood), *Quercus* (oak) sp. and *Pseudotsuga menziesii* (Douglas-fir) each increased over the course of the record, with some fluctuations (Figure 11). Other important and common tree types include *Lithocarpus* (tanoak) and *Pinus* c.f. *radiata* (Monterey pine), *Umbellularia californica* (California Bay), *Aesculus californica* (California buckeye), *Juglans* (walnut), *Acer* (maple), and *Betula* (*pendula* [European white birch] / *occidentalis* [water]). The introduced tree species *Eucalyptus* (blue gum) and *Olea* (olive) are found through the record, while *Ulmus* (*americana* [eastern] / *parviflora* [Chinese] elm) and *Ailanthus altissima* (tree-of-heaven) first appeared at 994-997 (~1907 ± 3 CE) and 558-563cm (~1943 ± 0.5 -1947 ± 0.25 CE) respectively.

Shrub pollen types included *Artemisia* (sagebrush), *Ceanothus* (California lilac), *Chrysolepis* (chinquapin), *Corylus* cf. *cornuta* (hazel), the Ericaceae (probably *Arctostaphylos*) and Rosaceae (rose) families, *Rhus* (lemonade bush) and *Rhamnus* (buckthorn), and others, but were dominated by plants of the Asteraceae (sunflower family). Common herbs are the Poaceae (grass family), with introduced ruderals such as the Amaranthaceae (goosefoot family), *Plantago* (plantain), and *Rumex* (dock), all of which were present at the beginning of the record. Poaceae increased from 883 to 714cm (1917 ± 2 to 1928 ± 2 CE), then declined after 505cm (1960 ± 0.5 CE). Ruderals were also less abundant above ~530cm (~1953 CE). Introduced cereal grains (Cerealia, including species *Secale* (rye) and *Zea* (maize)) occurred regularly below ~560cm (~1946 CE), but were less common above. Additional introduced species include: Apiaceae, *Erodium*, and Fabaceae (first occurrence: 1135-1140cm; 1900 ± 3 CE); Lactuceae (1110-1114cm; 1902 ± 3 CE); Brassicaceae (1086-1090cm; 1903 ± 3 CE); *Galium* (1020-1027cm; 1906 ± 3 CE); *Acacia* (969-977cm; 1908 ± 3 - 1909 ± 3 CE); *Lathyrus* (935-940cm; 1912 ± 2 CE); and *Portulaca* (809-812cm; 1922 ± 2 CE). Ferns were found throughout, but were most abundant below 809cm (1922 ± 2 CE) and from 377 to 415cm (2000 ± 1 to 1993 ± 0.5 CE).

Among the wetland species, *Alnus rhombifolia* (white alder) generally increased from the bottom of the core to 878cm (1917 ± 2 CE), then declined and persisted. *Salix* (willow) peaked in abundance from 810.5 to 617cm (1922 ± 2 to 1936 ± 2 CE), then declined sharply. Cyperaceae (sedge family), *Typha latifolia* (cattail), and the aquatic macrophytes *Sparganium* (bur-reed) and *Isoetes* (quillwort) were all present throughout the record while *Equisetum* (horsetail) and *Azolla* (water fern) were found only sporadically, and *Potamogeton* (pondweed) and *Brasenia shreberi* (watershield) were rare. *Myriophyllum* (watermilfoil), possibly either a native or introduced species, was found only from 687 to 908cm (1930 ± 2 to 1915 ± 2 CE) while native *Polygonum amphibium* (water knotweed) was found from 426 to 532cm (1985 ± 0.5 to 1953 ± 0.5 CE).

Algae were most common below ~549cm (~1950 CE). Notably, *Debarya* had a large peak at 878-883cm (1917 ± 2 CE) and *Pediastrum* peaked three times between 742 and 852cm (1919 ± 2 to 1925 ± 2 CE), but both were uncommon subsequently. In general, algae and rotifers crashed in abundance at ~549 cm (~1950 CE) and subsequently did not recover. Protozoa show a marked decline at the same level (Figure 10).

The dominant NPP was vesicular-arbuscular fungi (cf *Glomus*), and several species of coprophilous fungi were also found.

Discussion

Satisfying Criteria for Defining a GSSP

The Searsville site satisfies all the criteria ideal for defining a GSSP (Supplementary Material). The core we propose for the GSSP (JRBP2018-VC01B) is 944.5 cm long, encompassing 118 years from 1900-2018 CE. The ~50 years prior to our proposed boundary are represented by 575cm of sediment, while the ~50 years following the boundary encompass 364cm. This very thick and continuous sequence means that our GSSP boundary, and the appearance and fluctuations in the primary and auxiliary markers, can be mapped to particular years (and even in some cases within a season) with a high level of confidence. Clear and relevant geochemical and (sub)fossil data can be correlated to other sites globally and regionally. Access for future research, education, and outreach activities is facilitated by the site's location within Stanford University's Jasper Ridge Biological Preserve.

Primary Marker

We propose the primary marker for the Anthropocene GSSP to be the first widespread appearance of Plutonium-239,240 (^{239,240}Pu) in geological deposits. In JRBP2018-VC01B, the first evidence of ^{239,240}Pu occurs at 528cm, which corresponds to the year 1947 CE. This is consistent with the expectation for earliest global deposition, given the history of nuclear detonations and the 1-2 year lag-time between ejection of plutonium into the atmosphere and incorporation globally into geologic deposits (Supplementary Material). Note that we did not use the ^{239,240}Pu profile to help develop our age model. Because of the demonstrated lag time between nuclear explosions and global deposition of radionuclides, appearance of Pu in multiple geological sites around the world by 1947 CE is more likely than appearance in multiple sites by 1945 (three detonations) or 1946 (two detonations), making 1947 (no detonations) a more practical choice for the Anthropocene GSSP and its chronostratigraphic beginning. Therefore, using ^{239,240}Pu as the primary marker and guide, we propose the base of the Anthropocene be set at 1947 CE, and marked at 528cm depth in Searsville Reservoir core JRBP2018-VC01B.

Using Plutonium-239,240 as a primary marker for the Anthropocene is robust both at Searsville and globally. At Searsville, the sediments track the rise in atmospheric ^{239,240}Pu concentrations in the 1950s, with an early peak in 1958/1958 CE, followed by a decline, matching the timing of the 1959 nuclear weapons testing moratorium (Cundy et al., 2021). This temporary low point in Searsville ^{239,2409}Pu concentrations corresponds to 1961 CE, the year that testing resumed (Cundy et al., 2021). Following peak testing in 1962 CE (Cundy et al., 2021), ^{239,240}Pu peaks in the Searsville sediments at 1963 CE. This supports that Searsville sediments, like those from other deposits around the world, document atmospheric fallout from testing with a lag of 1-2 years, on par with the 1.5 +- 0.5 year residence time of Pu in the atmosphere (Hiros and Povinec, 2015). Notably, Searville is located far from nearby sources of ^{239,240}Pu, and ^{240}Pu/^{239}Pu isotopes confirm that our signal is from global nuclear fallout (Wu et al., 2011).

Global Auxiliary Markers

The Searsville cores JRBP2018-VC01B and -VC01A (taken only a few meters from and tightly correlated to VC01B) demonstrate several auxiliary markers that can be used to recognize Anthropocene deposits worldwide.

Radionuclides. ^{137}Cs. The Searsville record exhibits a clear ^{137}Cs signal that is characteristic of deposits worldwide, with earliest detection at levels corresponding to 1954 CE and a peak recognized at 1963 CE. Therefore, we specify the presence of ^{137}Cs as a reliable auxiliary marker for the Anthropocene.

Novel Material Proxies. Spheroidal Carbonaceous Particles (SCPs). The first SCPs in Searsville were deposited in the mid-1930s. Concentrations were variable afterward and counts were low overall, and most likely reflect distant rather than local sources (see Supplementary Materials). The SCP size profile was in the typical range (<50 um) for sites not located in the immediate vicinity of a source (Rose, 2008). In view of this, we regard SCPs in Searsville as reflecting a global rather than local signal. Searsville conforms to other records that indicate the first appearance of SCPs predates the start date of the Anthropocene if its beginning is recognized as mid-20th century: at Searsville, SCPs first appear ~13 year prior to our suggested start date. However, SCPs clearly document a critical, even if time-transgressive, signal of anthropogenic impacts. This signal may become most useful as an auxiliary marker by using abundance patterns in profiles, rather than first appearances. At Searsville, abundance values are consistently low between core depths dated to the 1930s and ~1940s. Values peak in the 1970s, consistent with other sites in North America. Therefore, SCPs can provide an auxiliary marker of the Anthropocene with stratigraphic profiles that document a relatively sudden rise in SCPs after an earlier first appearance, with the sudden rise corresponding approximately to the onset of the Anthropocene, and peak values securely within the Anthropocene.

Persistent Organic Pollutants (PCBs). A single PCB congener makes its appearance in the Searsville record between 1933 and 1959, consistent with the timing of invention and early use of PCBs. Multiple congeners occur in the record in levels dating from 1959 to 2018, with peak abundance in levels between 1962 and 1998, closely following the pattern of increasing use, then declining use as environmental-protection laws took hold. Similar patterns can be expected in other lake deposits; thus, we recognize the presence of multiple congeners of PCBs as an auxiliary marker. PCB sources generally will be local rather than global, but their use was so

pervasive in the late 20th century that many lake and soil deposits can be expected to contain detectable quantities.

Organic Matter Proxies. Stable nitrogen isotopes $\delta^{15}N$). Declines in $\delta^{15}N$ are caused by burning of fossil fuels and synthetic fertilizer production, which increase reactive nitrogen. The effect of fossil fuel burning on $\delta^{15}N$ started in the 1800s, before the accumulation of sediments in Searsville, while production of synthetic fertilizer started in earnest in the 1920s (Waters et al., 2016). We observed the expected steady decline in $\delta^{15}N$ in Searville through time, with a decline in average values of ~1.8 per mil. Precipitation is considered a major source of $\delta^{15}N$ (Talbot, 2001). Because storm systems on the west coast of North America come over the Pacific, the $\delta^{15}N$ in Searsville almost certainly reflects the atmospheric signal. Because global reactive N increase gradually over the last ~200 years (Waters et al., 2016), profiles typically do not show a pronounced inflection point near mid-century. However, we suggest that $\delta^{15}N$ profiles may prove useful as auxiliary Anthropocene markers by recognizing the point at which the $\delta^{15}N$ values decline by at least half over the time period 1900 to 2000 CE. For the Searsville profile, this point is reached at ~1950 CE. This use of an auxiliary marker will be most useful when: 1) diagenesis is not an issue, (which it is not at Searsville), and 2) when the time scale in question spans the 20th century.

Inorganic Geochemical Signals. Lead (Pb). The Pb profiles for Searsville closely mirror the increasing input of Pb into the atmosphere especially from increasing use of leaded gasoline and other fossil fuels that began ~1930, peaked in the 1970s, and then declined as unleaded gasoline became the norm. At Searsville, the highest peaks in Pb occur in levels corresponding to 1961-1986, indicating that peaks in Pb profiles will provide a useful auxiliary marker to identify Anthropocene sediments deposited from at least the 1960s to the 1980s.

Mercury (Hg). Hg concentration in Searsville was roughly double the pre-industrial Hg concentration in Upper Lake (Redondo, 2022; Redondo et al., in prep), suggesting a major increase in Hg deposition over the last century that is consistent with global and North American patterns of Hg production and consumption (Horowitz et al., 2014; Zhang et al., 2016; Streets et al., 2019). The largest Hg signal in the Searsville core occurred from ~1967-1970, coincident with peak Hg mine production (Han et al. 2002) and US Hg consumption patterns (Horowitz et al. 2014). Elevated Hg can therefore be used to identify sediments deposited during the post-industrial time, and peak Hg, corresponding to the late 1960s and early 1970s, can identify deposits as securely in the Anthropocene.

Other heavy metals. Vanadium (V) is the most abundant metal in petroleum (Amorim et al., 2006) and increases in V have been shown to track petroleum consumption (Arienzo et al., 2021). The increase in V in Searsville began around 1931, consistent with the rise in petroleum production and consumption (Hughes and Rudolf, 2011). The Searsville record also tracks Industrial production of chromium (Cr), nickel (Ni), and molybdenum (Mo), which began to increase in the mid-1920s/early 1930s (Henckens et al., 2018; Han et al., 2002). Increased concentrations of these heavy metals are apparent in Searsville sediments dating younger than 1947 (Figure 9). Atmospheric increases in Mo, V, and Cr have all been documented in alpine ice cores and firn and can be expected to be recorded in a wide variety of geological deposits.

Paleoclimate proxies

The seasonally deposited layering in the Searsville sediments provides a first-order climatic proxy, which can be matched in detail with tree-ring records from nearby blue oaks (*Quercus douglassi*), which in turn enable detailed correlation to high-resolution climate proxies that record such critical features as ENSO variations (Supplementary Material). Given patterns of anthropogenic climate change that begin to become apparent in the mid to late 20th century, it is likely that such detailed climatic proxies will prove useful as auxiliary Anthropocene markers.

Regional and Local Auxiliary Markers

Carbon isotopes. Carbon isotope records from ice cores, which reflect the global atmospheric signature (Rubino et al. 2013, 2019), typically show declining $\delta^{13}C$ through the 20th century with an inflection point and steeper decline in the 1960s. At Searsville, we instead see a decline in mean $\delta^{13}C$ starting in the 1930s, possibly caused in part by atmospheric depletion from fossil fuel burning, that is coupled with an increase in the variability. The Searsville record likely differs from ice core records because ice samples the air directly, whereas lake sediments also record the $\delta^{13}C$ of organic material deposited in the lake (Supplementary Material). For this reason, we do not regard carbon isotopes as providing an effective auxiliary marker at Searsville, though $\delta^{13}C$ likely will be useful in other kinds of deposits.

Paleobiologic Proxies. Paleontological evidence that typically characterizes Epoch/Series boundaries include First and Last Appearance Data (FADs and LADs, respectively), range zones (typically defined by the FAD and LAD of a particular taxon), concurrent-range zones (overlapping ranges of multiple species), interval zones (defined on FAD and LAD of different taxa), lineage zones (defined by a specific segment of an evolutionary lineage), and abundance zones (based on varying abundances of taxa).

At Searsville, subfossil paleobiological data analyzed so far include pollen, ostracods, and cladoceran ephippia. As is the case for most sedimentary records younger than ~10,000 years, at Searsville auxiliary markers that rely on FADs of newly evolved species are not evident, given that most species on Earth today originated long before the 20th century. However, FADs of immigrant taxa can be useful regionally (Himson et al. 2021). At Searsville, *Cypridopsis vidua*, which makes its first appearance near the top of the record at 300-302cm (corresponding to 2014 CE) in JRBP2018-VC01A, may provide a useful FAD for recognizing Anthropocene parts of the section. The pollen record documents many non-native plant species, but all were introduced to the area prior to the accumulation of Searsville sediments. Ongoing work to extract sedimentary DNA (*seda*DNA) shows promise for establishing a chronology of introduced invasive species (Supplementary Material).

LADs caused by extinction are not evident in the Searsville record or others of similar age for reasons noted in Supplementary Material. However, Holocene and Anthropocene sediments may be distinguished on the basis of local and regional species disappearances. At Searsville, a useful LAD is the loss of the ostracod *Ilyocypris gibba*, which drops out of the JRBP2018-VC01A record at levels equating to ~1948 CE. This is essentially where we place the Holocene-Anthropocene boundary based on earliest evidence of Pu, as defined above, making the absence of *I. gibba* useful auxiliary marker locally.

Abundance zones may well hold the most promise as auxiliary markers for identifying the position of the Holocene-Anthropocene boundary at Searsville. Beginning at ~1947 (559.5 cm), *Physocypria globula* is at least as abundant as ostracods in family Candonidae, and above ~443cm (~1976), is by far the most abundant species. Raw counts even more strongly support

the replacement of Candonidae species by *P. globula* as marking the Anthropocene-Holocene boundary at Searsville (Supplementary Material). Below ~725cm, ostracod counts are too low to draw meaningful relative abundance conclusions. Also at ~1947 and above, the cladaceran taxa occur at approximately equal relative percentages, whereas below *Daphnia* usually dominates over *Ceriodaphnia*. Both taxa decline in absolute abundance at ~1947 (Supplementary Material). The Holocene-Anthropocene boundary also clearly coincides with the rapid decline of rotifers, algae, and protozoa (Figure 10). Accordingly, we recognize a *P. globula* abundance zone from 558cm (1947 +- 0.25 CE) to the top of the core (characterized by high *P. globula* abundance) as identifying Anthropocene sediments at Searsville. A Rotifer-Algae-Protozoa abundance zone from the bottom of the core to 558 cm (characterized by relatively abundant rotifers, algae, and protozoa) identifies Holocene sediments, and pronounced decline or lack of those taxa above 558cm identify Anthropocene sediments. Relatively equal percentages of *Daphnia* and *Ceriodaphnia* also appear useful in characterizing the post-1947 sediments. While the specific taxa involved in these zones may only apply locally at Searsville, we expect that other deposits exhibit contemporaneous changes in microfossil assemblages as a result of intensifying anthropogenic activities in their watersheds.

The terrestrial pollen record in Searsville also illustrates increasing human resource use at a local scale, mirroring shifts that took place in much the same way regionally and globally. For example, the abundance changes document the rebound of coast redwood (*Sequoia sempervirens*) and Douglas-fir (*Pseudotsuga menziesii*) after cessation of logging and grazing, respectively (Supplementary Material). The usefulness of such changes in the upland vegetation as auxiliary markers for the Anthropocene is limited at Searsville, as they do not coincide with a Holocene-Anthropocene set at the mid-20th century. However, in general, the influence of anthropogenic land-use on vegetation is clearly evident, which is a common finding in most pollen records of the 20th century. Changes to riparian, wetland, and aquatic vegetation, on the other hand, were abrupt and staggered from ~1920s into the ~1940s (Figure 11), in part influenced by construction activities that emplaced a levee or altered the height of the dam (Supplementary Material).

In sum, the paleobiologic proxies at Searsville are useful in locally differentiating proposed Anthropocene layers from underlying Holocene sediments. While the patterns result from local modifications in the Searsville watershed and therefore may not extend regionally, they reflect a general feature of the Great Acceleration: intensification of anthropogenic inputs, which may well be expected in contemporaneous deposits elsewhere.

Searsvillian Stage and Age

The recognition of the Anthropocene GSSP in the Searsville Reservoir deposits would warrant definition of the Searsvillian Stage/Age. This stage/age is named with reference to Searsville Reservoir, in turn named for the historic town of Searsville. The GSSP and primary marker (^{239,240}Pu) and auxiliary markers for the Searsvillian Stage/Age would correspond to those we propose for the Anthropocene GSSP at Searsville. Like the Anthropocene, the Searsvillian Stage/Age would begin at 1947 CE. This boundary accordingly would mark the end of the preceding Meghalayan Stage/Age.

Conclusions

The Searsville Reservoir Site exhibits all the features ideal for recognizing the GSSP for the Anthropocene. The structurally undisturbed sediments are thick with a rapid sedimentation rate,

continuous with no facies changes over the critical interval, dated with high precision (seasonally to annually) throughout the sequence, span the critical interval, and they contain well-studied, clear primary and auxiliary markers.

The best primary marker is the presence of globally deposited ^{239,240}Pu, which has a robust signature at Searsville and first appears in 1947, as early as can be expected for a globally relevant ^{239,240}Pu signal. The Searsville GSSP therefore would place the beginning of the Anthropocene at 1947 CE.

Auxiliary markers in geochemical and sedimentary profiles include the presence of ^{137}Cs; relatively low values of δ^{15}N (nitrogen); and relatively high values of mercury (Hg), lead (Pb), vanadium (V), chromium (Cr), nickel (Ni), molybdenum (Mo), spheroidal carbonaceous particles (SCPs) and polychlorinated biphenyls (PCBs), all of which are consistent with documented global signatures and/or with expectations of sedimentary signatures of the Great Acceleration.

Paleontological auxiliary markers include a very strong local signal of an abrupt relative-abundance shift of various ostracod and cladoceran taxa, and in rotifers, algae, and protozoa, all of which coincide with the proposed Holocene-Anthropocene boundary at Searsville. The abundance shifts in Searsville microfauna reflect the local manifestation of increasing anthropogenic influence in watersheds globally that accelerated in the mid-20th century. Therefore, while the exact species involved may differ in other sites, Holocene-to-Anthropocene abundance shifts in local microfauna species might be expected in many lake deposits worldwide that are adequately sampled. Palynological data reflect anthropogenic transformations of the surrounding area, documenting the long history of local anthropogenic impacts, a general feature of pollen records worldwide, and facilitate correlation to other sites in the region that have produced pollen records.

Correlation potential of Searsville deposits with many other kinds of geological deposits and increment-forming organisms used as paleoclimate proxies is high. Relevant geochemical signals are found in other lakes, peat deposits, marine sediments, corals, speleothems, trees, and ice cores. Paleontological markers (matched through chain of correlation) can apply to marine and freshwater deposits. Linkage of the annually resolved Searsville sediment record with nearby tree-ring records, already underway, can provide high-resolution correlation using detailed paleoclimatic proxies (such as ENSO fluctuations) as well. Additional studies underway that will further aid in correlation include using sedimentary DNA to pinpoint the first arrival of immigrant species, and geochemical and paleontological data to match the Searsville sediments with their marine counterparts in nearby San Francisco Bay.

In addition to the geological and geochemical attributes of the Searsville Site, it is located within Stanford University's Jasper Ridge Biological Preserve, with a long and successful track record of facilitating research, education, and preservation. This ensures continued access of the site by researchers and students, and as a focal point for communication and outreach to the general public. The sediments that have been analyzed so far are duplicated in at least six archival cores, and in the short term, more cores can be obtained with appropriate permissions from Stanford and pertinent regulatory agencies. Future plans to drain the reservoir will likely result in well-exposed outcrops that would even further facilitate access, study, and communication about the Anthropocene, and how it records the most recent transition in the Earth System.

Supplemental Materials

Supplementary. Upper Lake; Geographic and geologic setting of the. Searsville Site; History of Land Use Around Searsville Reservoir; Site Accessibility; Previous Work; Methods: Chronological Controls; Methods: Inorganic geochemical signals; Results: Chronology; Results: Biotic Markers; Discussion: Satisfying Criteria for Defining a GSSP; Discussion: Plutonium-239,240 as a Primary Marker; Discussion: Auxiliary Markers.

Appendices. 1) Searsville and Upper Lake sediment cores; 2) CT intensity and gamma bulk density; 3) Grain size analysis; 4) Lead-210, Cesium-137 and Ra-226; 5) Total organic carbon versus CT intensity and Titanium concentration; 6) Correlation of JRBP2018-VC01A and JRBP2018-VC01B cores; 7) Plutonium methods and sample depths; 8) SCPs; 9) PCBs; 10) Carbon and Nitrogen Analysis; 11) ICPMS Analysis; 12) Mercury Analysis; 13) Analysis of pollen, spores, and non-pollen palynomorphs; 14) Sedimentation rates; 15) Radiocarbon Analysis.

Funding
The authors disclosed receipt of the following financial support for the research, authorship, and/or publication of this article: This work was supported by Haus der Kulturen der Welt, Stanford University, and the United States Geological Survey.

References
Amorim FAC, Welz B, Costa ACS, Lepri FG, Goresti M, Vale R and Ferreira SLC (2007) Determination of vanadium in petroleum and petroleum products using atomic spectrometric techniques. *Talanta* 72(2): 349-359.

Anderson RS, Ejarque A, Rice J, Smith S and Lebow C (2015) Historic and Holocene Environmental Change in the San Antonio Creek Basin, Mid-coastal California. *Quaternary Research* 83: 273-286.

Anderson RS, Stegner MA, Hadly EA, Barnosky AD, La Selle SP and Sherrod B (in prep) Using paleoecology and historical records to determine environmental history in a California natural area.

Appleby PG (2001) Chronostratigraphic techniques in recent sediments. In: Last WM and Smol JP (eds) *Tracking Environmental Change Using Lake Sediments, Vol. 1: Basin Analysis, Coring, and Chronological Techniques*. Dordrecht: Kluwer Academic Publishers, pp. 171-203.

Arienzo MM, Legrand M, Preunkert S, Stohl A, Chellman N, Eckhardt S, Gleason KE and McConnell JR (2021) Alpine ice-core evidence of a large increase in vanadium and molybdenum pollution in Western Europe during the 20th century. *Journal of Geophysical Research: Atmospheres* 126: e2020JD033211

Aris J and Fitzpatrick C (1980) *Biology of the fishes of Searsville Lake*. Biology 194 project, Jasper Ridge Paper, SU Item TECB-867 (Technical Reports), Stanford University, 23p + appendices.

Bai X, Luo L, Tian H, Liu S, Hao Y, Shuang Z, Lin SS, Zhu C, Guo Z and Lv Y (2021) Atmospheric Vanadium emission inventory from both anthropogenic and natural sources in China. *Environmental Science and Technology* 55: 11568-11578.

Bailey H (1980) *Niche utilization in centrarchid fish inhabiting Searsville Lake.* MS Thesis, Stanford University, USA.

Balasubramanian K (1993) *A Comparative Study of Decomposition in Searsville Lake*. Biology 96 project, Jasper Ridge Paper, Stanford University, 8p.

Baldo A(1985a) *A study of the Searsville Lake in the Jasper Ridge Biological Preserve*. Biology 195 project, Jasper Ridge Paper, SU Item TECB-626 (Technical Reports), Stanford University, 8p.

Baldo A (1985b) *Comparison of Searsville and Lagunita*. Biology 44y project, Jasper Ridge Paper, SU Item TECB-625 (Technical Reports), Stanford University, 10p.

Bently GH (1918) *Studies on green freshwater algae: Pediastrum and Coelastrum.* MA Thesis, Stanford University, USA.

Berhe AA, Fries T, Fuller CC, Harden JW and Miller LG (2007) Terrestrial sedimentation and Carbon storage in impoundments: The case of Searsville Reservoir, California. Report of 1998 Coring Results Provided to Jasper Ridge Biological Preserve. JRBP White Paper, 27 pp.

Bigus P, Tobiszewski M and Namiesnik J (2014) Historical records of organic pollutants in sediment cores. *Marine Pollution Bulletin* 78: 26-42. http://dx.doi.org/10.1016/j.marpolbul.2013.11.008

Bocek B and Reese E (1992) Land use history of Jasper Ridge Biological Preserve. *Jasper Ridge Biological Preserve Research Report No. 8,* Stanford University, USA.

Brown E (1998) *The relationship between disturbance, insect diversity, and mosquito abundance*. Independent project paper for Bio 181 (Field Ecology), Department of Biological Sciences, Stanford University.

Candelone J-P, Hong S, Pellone C and Boutron (1995) Post-Industrial Revolution. Changes in large-scale atmospheric pollution of the northern hemisphere by heavy metals as documented in. central Greenland snow and ice. *Journal of Geophysical Research* 100(D8): 16605-16616.

Carter C (1992) *Seasonal variations in environmental conditions of fresh-water ostracode habitat, San Francisco Peninsular, California*. United States Geological Survey Open File Report, 92-253.

Carter C (1991) *Seasonal occurrences of ostracodes in lakes and streams of the San Francisco Peninsula, California.*United States Geological Survey Open File Report, 91-118.

Chesley K (2019) First transcontinental railroad and Stanford forever linked. Stanford News. https://news.stanford.edu/2019/05/08/first-transcontinental-railroad-stanford-forever-linked/

Coleman RG (2004) Geologic nature of the Jasper Ridge Biological Preserve, San Francisco Peninsula, California. *International Geology Review* 46: 629-637.

Comans RNJ, Midddelburg JJ, Zonderhuis J, Woittiez JRW, De Lange GJ, Das HA and Van Der Weijden CH (1989) Mobilization of radiocaesium in pore water of lake sediments. *Nature* 339: 367-369.

Cundy A, Waters C, Hajdas I and Saito Y (2021) Radioactive fallout as a marker for the Anthropocene. Anthropocene Working. Group Essay.

Del Favero B (1988) *Controlling Myriophyllum brasiliense in Searsville Lake*. Biology 196 project, Jasper Ridge Paper, SU Item TECB-870 (Technical Reports), Stanford University, 4p.

DeSante. D (1971) *A breeding bird census of a willow-box elder woodland at Searsville Lake: Research Report #7*. Research Report Stanford University Jasper Ridge Biological Experimental Area, 10p + appendix.

Eichler A, Tobler L, Eyrikh S, Malygina N, Papina T and Schwikowski M (2014) Ice-core based assessment of historical anthropogenic heavy metals (Cd, Cu, Sb, Zn) emissions in the Soviet Union. *Environmental Science and Technology* 48: 2635-2642.

Ejarque A, Anderson RS, Simms AR and Gentry BJ (2015) Prehistoric fires and the shaping of colonial transported landscapes in southern California: a palaeoenvironmental study at Dune Pond, Santa Barbara County. *Quaternary Science Reviews* 112: 181-196.

EPA (1998) Method 8270D (SW-846): Semivolatile Organic Compounds by Gas Chromatography/ Mass Spectrometry (GC/MS). Revision 4. US Environmental Protection Agency.

Fægri K and Iversen J (1989) *Textbook of Pollen Analysis.4th Edition*. Chichester: John Wiley and Sons.

Fay D (1978) *Studies on the insect fauna of a willow woodland near Searsville Lake*. Biology 199 project, Jasper Ridge Paper (JR-78), SU Item TECB-453 (Technical Reports), Stanford University.

Felin F (1940) *The seasonal fluctuation of benthic macrofauna and limnetic plankton in Searsville Lake: a contribution to the biology of fluctuating reservoirs*. PhD Thesis, Stanford University, USA.

Freyberg DL (2001) Maintaining open water at Searsville Lake. Final Project Report, David and Lucile Packard Foundation Grant No. 98-5517, JRBP archives.

Fries T (1998) 12/23/1998 Correspondence to Philippe Cohen, in reference to Fries T. 1998. Analytical Reports: Searsville Lot #D8K030133 (17 Dec 1998) and Lot #D8L170123 (28 Dec 1998) USGS In JRBP archives.

Gamble D, Niell B, Shah R, Chyi L and Behrstock E (1996) *Searsville Watershed Biotic Assessment: Survey of Aquatic Life in Searsville Watershed*. Biology 96 project, Jasper Ridge Paper, Stanford University, 9p.

Goring S, Williams JW, Blois JL, Jackson ST, Paciorek CJ, Booth RK, Marlon JR, Blaauw M and Christen JA (2012) Deposition times in the northeastern United States during the Holocene: establishing valid priors for Bayesian age models. *Quaternary Science Reviews* 48: 54-60.

Han FX, Banin A, Su Y, Monts DL, Plodinec MJ, Kingery WL and Triplett GE (2002) Industrial age anthropogenic inputs of heavy metals into the pedosphere. *Naturwissenschaften* 89:497-504

Hancock GJ, Tims SG, Fifield SK and Webster IT (2014) The release and persistence of radioactive anthropogenic nuclides. In: Waters CN, Zalasiewicz JA, Williams M, Ellis MA, Snelling AM (eds) *A Stratigraphical Basis for the Anthropocene*. London: Geological Society, pp. 265–281.

Haslett J and Parnell A (2008) A simple monotone process with application to radiocarbon-dated depth chronologies. *Journal of the Royal Statistical Society: Series C (Applied Statistics)* 57(4): 399-418.

Henckens MLCM, Driessen PPJ and Worrell E (2018) Molybdenum resources: their depletion and safeguarding for future generations. *Resources, Conservation, and Recycling* 134: 61-69.

Heppner C and Loague K (2008) A dam problem: simulated upstream impacts for a Searsville-like watershed. *Ecohydrology* 1(4): 408-424.

Heppner CS (2007) A dam problem: characterizing the upstream hydrologic and geomorphologic impacts of dams. PhD Thesis, Stanford University, USA.

Himson S, Williams M, McGann M, Rose N, Wilkinson I, Zalasiewicz J and Waters C (2021) A biostratigraphic record of Anthropocene ecological change in one of the world's most invaded aquatic ecosystems, San Francisco, CA. *EGU General Assembly* EGU21-15133. https://doi.org/10.5194/egusphere-egu21-15133.

Hirose K and Povinec (2015) Sources of plutonium in the atmosphere and stratosphere-troposphere mixing. *Scientific Reports* 5:15707. DOI: 10.1038/srep15707

Holland M and Schultheiss P (2014) Comparison of methane mass balance and X-ray computed tomographic methods for calculation of gas hydrate content of pressure cores. *Marine and Petroleum Geology* 58: 168-177.

Horne DJ and Siveter DJ (2016). Collecting and processing fossil ostracods. *Journal of Crustacean Biology* 36, 841–848.

Horowitz HM, Jacob DJ, Amos HM, *et al.* 2014. Historical mercury releases from commercial products: Global environmental implications. *Environ Sci Technol* **48**: 10242–50.

Howarth CL (1981) *A history of sedimentation: Searsville Lake*. Geology 1 project, Jasper Ridge Paper, SU Item TECB-804 (Technical Reports), Stanford University, 19p.

Hughes L and Rudolph J (2011) Future world oil production: growth, plateau, or peak? *Current Opinion in Environmental Sustainability* 3: 225-234. DOI 10.1016/j.cosust.2011.05.001

Inoue J, Tomozawa A and Okudaira (2013) The Use of Size Distributions of Spheroidal Carbonaceous Particles in Swimming Pool Deposits for Evaluating Atmospheric Particle Behaviour. *Water, Air, & Soil Pollution* 224: 1580.

JRBP (2018) Jasper Ridge Strategic Plan. Available at: https://jrbp.stanford.edu/sites/default/files/lores_stratplan.pdf

Jasper Ridge Biological Preserve, Stanford University (2022a). Davis Instruments Vantage Pro, 5-minute logging interval (2013-2022). https://jrbp.stanford.edu/research/weather

Jasper Ridge Biological Preserve, Stanford University (2022b). Tycon Systems ProWeatherStation, 5-minute logging interval (2018-2022). https://jrbp.stanford.edu/research/weather

Keller J and Margolis M (1989) *The depths of Searsville Lake*. Biology 96 project, Jasper Ridge Paper, SU Item TECB-882 (Technical Report), Stanford University, 10p. + appendices.

Kirsher B (1984) *About lichens*. Biology 195 project, Jasper Ridge Paper, SU Item TECB-632 (Technical Reports), Stanford University, 4p.

Kittleson G, Hecht B and Holmes DO (1996) *Sedimentation and channel dynamics of the Searsville Lake watershed and Jasper Ridge Biological Preserve, San Mateo County, California.* Balance Hydrologics Project Assessment 9536.07

Koweek DA, García-Sánchez C, Brodrick PG, Gassett P and Caldeira K (2020) Evaluating hypoxia alleviation through induced downwelling. *Science of the Total Environment* 719: 137334. https://doi.org/10.1016/j.scitotenv.2020.137334

Krall JA (2013) *Towards understanding sediment transport and deposition in a heavily sediment-impacted reservoir and on its upstream alluvial surface*. PhD Thesis, Stanford University, USA.

Kulp T, Miller L, Braiotta F, Webb S, Kocar B, Blum J and Oremland R (2014) Microbial reduction of Sb(V) in anoxic freshwater sediments. Environmental Science and technology 48(1): 218-226.

La Selle SM, Stegner MA, Nasr BM, Barnosky AD, Hadly EA and Sherrod B (2022) Core logs, computed tomography scans, photographs, X-ray fluorescence, and grain size data from Searsville Reservoir, Jasper Ridge Biological Preserve, Stanford, CA. *U.S. Geological Survey data release.* https://doi.org/xx.xxxx/xxxxx

Lerner A (1998) *The effects of sedimentation on riparian plant diversity, density, and richness at Searsville Lake.* Independent project paper for Bio 181 (Field Ecology), Department of Biological Sciences, Stanford University.

Lu F and Collier J (1990) *Short survey of Searsville Lake*. Biology 96 project, Jasper Ridge Paper, SU Item TECB-892 (Technical Reports), Stanford University, 8p.

Lu F (1992) *Foraging behavior of American Coots (*Fulica americana*) at Searsville Lake*. Jasper Ridge Paper, Stanford University, 7p.

Lund N and Gullard P (2003) Life on the San Andreas Faults: A history of Portola Valley. San Francisco: Scottwall Associates.

McAndrews JH, Berti AA and Norris G (1973) *Key to the Quaternary Pollen and Spores of the Great Lakes Region.* Royal Ontario Museum Life Sciences Miscellaneous Publication, Toronto.

McConnell JR and Edwards R (2008) Coal burning leaves toxic heavy metal legacy in the Arctic. *PNAS* 105(34): 12140-12144.

McGraw J (1977) *A water bird census of Searsville Lake winter: 1976-1977*. Biology 195 project, Jasper Ridge Paper (JR-77), SU Item TECB-481 (Technical Reports), Stanford University,18p.

Meece E (1993). *Wood Ducks and Ring-necked Ducks at Searsville Lake.* Views (Lake Issue), Fall 1993:10 (5 p).

Menne MJ, Durre I, Vose RS, Gleason BE and Houston TG (2012a) An Overview of the Global Historical Climatology Network-Daily Database. *J. Atmos. Oceanic Technol.* 29: 897-910. doi:10.1175/JTECH-D-11-00103.1.

Menne MJ, Durre I, Korzeniewski B, McNeill S, Thomas K, Yin X, Anthony S, Ray R, Vose RS, Gleason BE and Houston TG (2012b) Global Historical Climatology Network - Daily (GHCN-Daily), Version 3. Station USC00049792 (WOODSIDE FIRE STATION 1, CA US). NOAA National Climatic Data Center. doi:10.7289/V5D21VHZ [Accessed February 24, 2022].

Miller LG, Baesman SM, Kirshtein J, Voytek MA and Oremland RS. (2013) A biogeochemical and genetic survey of acetylene fermentation by environmental samples and bacterial isolates. *Geomicrobiology Journal* 30(6): 501-516.

Moore PD, Webb JA and Collinson ME (1991) *Pollen Analysis, 2nd Edition*. Oxford: Blackwell Scientific Publications.

Mullen LK (1982) *Siltation in Searsville Lake*. Geology 1 project, Jasper Ridge Paper, SU Item TECB-806 (Technical Reports), Stanford University, 7p + appendices.

Nriagu JO (1996) A history of global metal pollution. *Science* 272: 223-224

Page S(1996) *Rescuing our urban streams: Dam lowering as an approach to environmental restoration*. Undergraduate Honors Thesis, Stanford University, USA.

Pampeyan EH (1993) Geologic map of the Palo Alto and part of the Redwood Point 7-1/2' quadrangles, San Mateo and Santa Clara counties, California. United States Geological Survey https://doi.org/10.3133/i2371

Penuelas J, Gamon J, Griffin K and Field CB (1993) Assessing community type, plant biomass, pigment composition, and photosynthetic efficiency of aquatic vegetation from spectral reflectance. Remote Sensing of the Environment 46(2): 110-118.

Poinar GO, Jr. (1979) *Mermithids infecting mosquitos,* Romanomermis culicivorax *Ross & Smith, field trials, Searsville Lake*. In: Poinar GO, Jr., *Nematodes for Biological Control of Mosquitoes*. CRC Press, pp.31-34.

Potocki M, Dixon DA, Kurbatov AV, et al. (2022) Trace metal emission history captured in a Chilean ice core. *Atmospheric Environment* 276: 119002.

R Core Team (2021) *R: A language and environment for statistical computing.* Vienna: R Foundation for Statistical Computing. URL https://www.R-project.org/.

Radoslovich JA (1989) *Looking into the depths of Searsville Lake-An examination of nitrogen input into Searsville Lake*. Biology 96, Jasper Ridge Paper, SU Item TECB-883 (Technical Reports), Stanford University, 3p + appendices.

Redondo S (2022) *Signals of an Insidious Pollutant: Temporal, Spatial, and Biotic Interplay of Anthropogenic Mercury in a Terrestrial Ecosystem.* PhD thesis, Stanford University.

Redondo SA, Stegner MA, LaSelle SP, Sherrod B, Barnosky AD, Anderson RS, Fernandez LE and Hadly EA (in prep) Over 250 years of mercury dynamics revealed by laminated sediments from Santa Cruz Moutains, California, USA.

Regnery D (1991) *The history of Jasper Ridge: From Searsville pioneers to Stanford scientists.* Stanford: Stanford Historical Society.

Reille M (1992) *Pollen et spores d'Europe et d'Afrique du nord.* Marseille: Laboratoire de Botanique historique et Palynologie, Universite d'Aix-Marseille III.

Reimer PJ, Austin WE, Bard E, Bayliss A, Blackwell PG, Ramsey CB, Butzin M, Cheng H, Edwards RL, Friedrich M and Grootes PM (2020) The IntCal20 Northern Hemisphere radiocarbon age calibration curve (0–55 cal kBP). *Radiocarbon 62*(4): 725-757.

Ritson PI, Bouse RM, Flegal AR and Luoma SN (1999) Stable lead isotopoc analyses of historic and contemporary lead contamination of San Francisco Bay estuary. *Marine Chemistry* 64: 71-83.

Rose NL (1994) A note on further refinements to a procedure for the extraction of carbonaceous fly-ash particles from sediments. *Journal of Paleolimnology* 11: 201-204.

Rose NL (2008) Quality control in the analysis of lake sediments for spheroidal carbonaceous particles. *Limnology and Oceanography: Methods* 6: 172-179.

Rose NL (2015) Spheroidal carbonaceous fly-ash particles provide a globally synchronous stratigraphic marker for the Anthropocene. *Environmental Science and Technology* 49 (7): 4155-4162.

Rubino M, Etheridge DM, Thornton DP et al. (2019) Revised records of atmospheric trace gases CO_2, CH_4, N_2O, and $d^{13}C$-CO_2 over the last 2000 years from Law Dome, Antarctica. *Earth Systems Science Data* 11: 473-492.

Rubino M, Etheridge DM, Trudinger CM, Allison CE, Battle MO, Langenfelds RL, teele LP, Curran M, Bender M, White JWC, Jenk TM, Blunier T and Francey RJ (2013) A revised 1000 year atmospheric record from Law Dome and South Pole, Antarctica. *Journal of Geophysical Research: Atmosphere* 118: 1-18. doi:10.1002/jgrd.50668

Ruhl C (1992) *Testing seems to support theories of Daphnia and diel vertical migration in Searsville lake.* Biology 44y project, Jasper Ridge Paper, Stanford University, 7p.

Schnurrenberger D, Russell J and Kelts K (2003) Classification of lacustrine sediments based on sedimentary components. *Journal of Paleolimnology 29*(2): 141–154. https://doi.org/10.1023/A:1023270324800

Scott FM (1925) Introduction to the limnology of Searsville Lake. PhD thesis, Stanford University, USA.

Scott FM (1927) Introduction to the Limnology of Searsville Lake. *Stanford University Publications, University Series, Biological Sciences* V(1).

Searsville Alternatives Study (2015) Searsville alternatives study steering committee recommendations. Stanford University. Available at: https://news.stanford.edu/searsville/Searsville_Steering_Committee_Recommendations_April_2015.pdf

Searsville Project Team (2022) Searsville Watershed Restoration Project. Available at: https://searsville.stanford.edu/

Shieh J (1991) *Measurements of methane emissions from the Searsville lake area*. Biology 96 project, Jasper Ridge Paper, Stanford University, 4p

Sigman D (1989) *Sediments of creeks draining into Searsville Lake*. Biology 96 project, Jasper Ridge Paper, SU Item TECB-884 (Technical Reports), Stanford University, 7p + appendices.

Simpson G (2022) _gratia: Graceful ggplot-Based Graphics and Other Functions for GAMs Fitted using mgcv_. R package version 0.7.3, <URL: https://gavinsimpson.github.io/gratia/>.

Slack JF, Kimball BE and Shedd KB (2017) Cobalt. In: Schulz KJ, DeYoung JH, Jr., Seal RR, II, and Bradley DC (eds) *Critical Mineral Resources of the United States—Economic and Environmental Geology and Prospects for Future Supply.* United States Geological Survey Professional Paper 1802–F

Smith AJ and Delorme LD (2010) *Ostracoda*. In: Thorpe JH and Covich AP (eds) *Ecology and classification of North American freshwater invertebrates*. Cambridge: Academic Press, pp. 725-771.

Smith RL and Oremland RS (1983) Anaerobic oxalate degradation: widespread natural occurrence in aquatic sediments. *Applied and Environmental Microbiology* 46: 106-113.

Smith FW, Jr. (1963) *A comparison of the fish species composition of Searsville Reservoir, 1950-51 and 1957-58*. MA thesis, Stanford University, USA.

Smith J (1992) *A species richness analysis of Searsville Lake at different depths*. Biology 44y project, Jasper Ridge Paper, Stanford University, 10p.

Streets DG, Horowitz HM, Lu Z, *et al.* (2019) Five hundred years of anthropogenic mercury: Spatial and temporal release profiles. *Environ Res Lett* 14: 084004.

Talbot MR (2001) Nitrogen isotopes in palaeolimnology. In: eds Last WM and Smol JP (eds) *Tracking Environmental Change Using Luke Sediments. Volume 2: Physical and Geochemical Methods.* Dordrecht: Kluwer Academic Publishers.

Tanaka A, Nakano T and Ikehara K (2011) X-ray computerized tomography analysis and density estimation using a sediment core from the Challenger Mound area in the Porcupine Seabight, off Western Ireland. *Earth, planets and space* 63.2: 103-110.

Tolia N (1992) *Searsville Lake: Species diversity and distribution*. Biology 44y project, Jasper Ridge Paper, Stanford University, 14p.

Trilling B et al. (1981) The Searsville Site Guide. Jasper Ridge Biological Preserve, Stanford University, 62p.

Troels-Smith J (1955) Karakterisering af lose jordater (Characterisation of Unconsolidated Sediments). *Danmarks Geologiske Undersogelse* 3: 39-73.

Van de Velde K, Ferrari C, Barbante C, Moret I, Bellomi T, Hong S and Boutron C (1999) A 200 year record of atmospheric Cobal, Chromium, Molybdenum, and Antimony in high altitude alpine firn and ice. *Environmental Science and Technology* 33(20): 3495-3501.

van Geel B (2001) Non-pollen palynomorphs. In: Smol JP et al. (eds) *Tracking Environmental Change Using Lake Sediments, vol. 3.* Dordrecht : Kluwer Academic Publishers, pp. 99-119.

van Hoeve ML and Hendrikse M (eds) (1998) *A study of non-pollen objects in pollen slides; the Types as described by Dr Bas van Geel and colleagues*. Utrecht: Private printing.

Vandekerkhove J, Declerck S, Vanhove M, et al. (2004) Use of ephippial morphology to assess richness of anomopods: potentials and pitfalls. *Journal of Limnology* 63: 75. doi: 10.4081/jlimnol.2004.s1.75.

Viteri M (2022) Exhuming the dead to save the living: Fingerprints of the Anthropocene on California's faunal communities. PhD Thesis, Stanford University, USA.

Viteri M, Stegner MA, La Selle SP, Barnosky AD and Hadly EA (in prep) Using microcrustaceans from a high-resolution lake core to track a century of human impacts in Woodside, CA.

Wade JM (1995) *Siltation sources flowing into Searsville Lake*. Biology 96 project, Jasper Ridge Paper, Stanford University, 6p.

Warner M (1987) *An investigation of the antibiotic resistance of Coliform bacteria in Lake Searsville and its Tributaries.* Bio 44y project, Jasper Ridge Paper, SU Item TECB-652 (Technical Reports), Stanford University, 18pp.

Waters CN, Zalasiewicz J, Summerhays C, Barnosky AD, Poirier C, Galuska A, Cearreta A, Edgeworth M, Ellis EC, Ellis M, Jeandel C, Leinfelder R, McNeill JR, Richter J deB, Steffer W, Syvitski J, Vidas D, Wagreich M, Williams M, Zhisheng A, Grinvald J, Odada E, Oreskes N and Wolfe AP (2016) The Anthropocne is functionally and stratigraphically distinct from the Holocene. *Science* 351 (6269): aad2622-1. DOI: 10.1126/science.aad2622

Wilcox A (1995) *Reservoir sedimentation and the prospects for dam removal: A case study of Searsville Dam, Jasper Ridge Biological Preserve, Stanford University*. Landscape Architecture 222 Term Paper, Jasper Ridge Paper, University of California at Berkeley, 19p.

Wolfe AP, Hobbs WO, Birks HH, Briner JP, Holmgren SU, Ingolfsson O, Kaushal SS, Miller GH, Pagani M, Saros JE and Vinebrooke RD (2013) Stratigraphic expression of the Holocene-Anthropocene transition revealed in sediments from remote lakes. *Earth-Science Reviews* 116: 17-34. https://doi.org/10.1016/j.earscirev.2012.11.001

Wood SN (2011) Fast stable restricted maximum likelihood and marginal likelihood estimation of semiparametric generalized linear models. *Journal of the Royal Statistical Society (B)* 73(1): 3-36

Wood SN (2017) *Generalized Additive Models: An Introduction with R (2nd edition).* Chapman and Hall/CRC.

Wu F, Zheng J, Liao H, Yamada M and Wan G (2011) Anomalous Plutonium Isotopic Ratios in Sediments of Lake Qinghai from the Qinghai-Tibetan Plateau, China. *Environmental Science and Technology* 45: 9188–9194.

Yang K (1993). *Parrot's Feather in Searsville Lake.* Views (Lake Issue), Fall 1993:4 (3 p).

Zhang Y, Jacob DJ, Horowitz HM, *et al.* 2016. Observed decrease in atmospheric mercury explained by global decline in anthropogenic emissions. *Proc Natl Acad Sci* **113**.

Tables:

Table 1. Chronologic controls for JRBP2018-VC01B.

Tie point	Year CE	Depth (cm)
Core top	2018	158.5
Cu peak (earliest)	1943	540.5-542.5
Cu peak (second)	1952	511.5-512.5
Cu peak (last)	1953	503.5
1906 earthquake	1906	1013
1984 earthquake	1984	386
1989 earthquake	1989	376.5
1998 core top	1998	309
Cesium-137 peak	1963	447.5-453
Flood year (Winter 1954-1955)	1955	487-502
Flood year (Winter 1997-1998)	1998	352-305
Flood year (Winter 2004-2005)	2005	260-234

Figures:

Figure 1. Map of Searsville Reservoir and the San Francisquito Creek Watershed. Green line (a) = extent of Searsville in 1892; A = coring location for JRBP2018-VC01A; B = coring location for JRBP2018-VC01B. blue shading (b) = San Francisquito watershed; green polygon = JRBP; blue lines = creeks. (Map prepared by Trevor Hébert, JRBP).

Figure 2. Precipitation and wind direction in the Searsville area. a) Average monthly precipitation for Woodside, CA and JRBP (1973-2015, from NOAA Station USC00049792 Woodside Fire Station 1; 2015-2022 from JRBP, latitude 37.407128 N, longitude 122.241492 W and latitude 37.405428 N, longitude 122.241492 W) (Data from JRBP, 2022a,b; Menne et al. 2012a,b). b) Wind direction at Searsville dam (August 2018 - May 2022, latitude 37.407128 N, longitude 122.241492 W) (Data from JRBP, 2022b). Red star indicates the location of JRBP.

Figure 3. Timeline of social/cultural and land use change in the Searsville region from the mid 1600s to present. Vertical black line indicates the construction of Searsville Dam; shaded region shows the time period not captured by Searsville sediments. Red dashed vertical line indicates the proposed GSSP at 1947 CE

Figure 4. Searsville core JRBP2018-VC01B CT, XRF, ^{137}Cs, and age model. From left to right: CT scan; linescan; average CT intensity; XRF Ti, Cu, and Ca; ^{137}Cs; and age-depth model. Red dashed horizontal line indicates the proposed GSSP depth at 1947 CE

Figure 5. Searsville core JRBP2018-VC01B grain size. Color indicates CT intensity at the depths associated with each grain size sample. Each line represents the weight % grain size of a single sample.

Figure 6. Searsville core JRBP2018-VC01B ^{239,240}Pu concentration. Red dashed horizontal line indicates the proposed GSSP depth at 1947CE

Figure 7. Searsville core JRBP2018-VC01B Spheroidal Carbonaceous Particle concentrations. Red horizontal line indicates the proposed GSSP depth at 1947CE

Figure 8. Searsville core JRBP2018-VC01B organic matter proxies. From left to right: total organic carbon (TOC), total nitrogen (TN), Carbon/Nitrogen ratio (C/N), $d^{13}C$, and $d^{15}N$. Gray shading shows the GAM model 95% confidence interval. Solid blue/red line shows GAM significant increase/decrease. Red dashed horizontal line indicates the proposed GSSP depth at 1947 CE

Figure 9. Searsville core JRBP2018-VC01B heavy metals. From left to right: Zinc (Zn), Cadmium (Cd), Molybdenum (Mo), Cobalt (Co), Nickel (Ni), Chromium (Cr), Vanadium (V), Lead (Pb), and Mercury (Hg). Gray shading shows the GAM model 95% confidence interval. Solid blue/red line shows GAM significant increase/decrease. Red dashed horizontal line indicates the proposed GSSP depth at 1947 CE Two extreme Zn values (507 cm, 638.95 ppm; 192 cm, 744.412 ppm) were removed for scale.

Figure 10. Searsville core JRBP2018-VC01A Plankton. a) Relative abundance of Ostracods and Cladocera ephippia; b) Counts of rotifers, algae, and protozoa. Red dashed horizontal line indicates the proposed GSSP year, 1947 CE

Figure 11. Searsville core JRBP2018-VC01A dominant taxa and major pollen groups. Red dashed horizontal line indicates the proposed GSSP at 1947 CE

Figure 12. Selected Searsville Reservoir global (^{239,240}Pu, ^{137}Cs), global/regional (Pb, SCPs, Hg), and local (plankton zones) signals. Red dashed horizontal line indicates the proposed GSSP year at 1947 CE High abundance zones for Candonidae (1), rotifers (7), algae (8), and protozoa (9); High abundance and persistence zones for *P. globula* (2) and *Ceriodaphnia* (6); First occurrence of *C. vidua* (3); occurrence sone for *I. gibba* (4) and *Daphnia* (5).

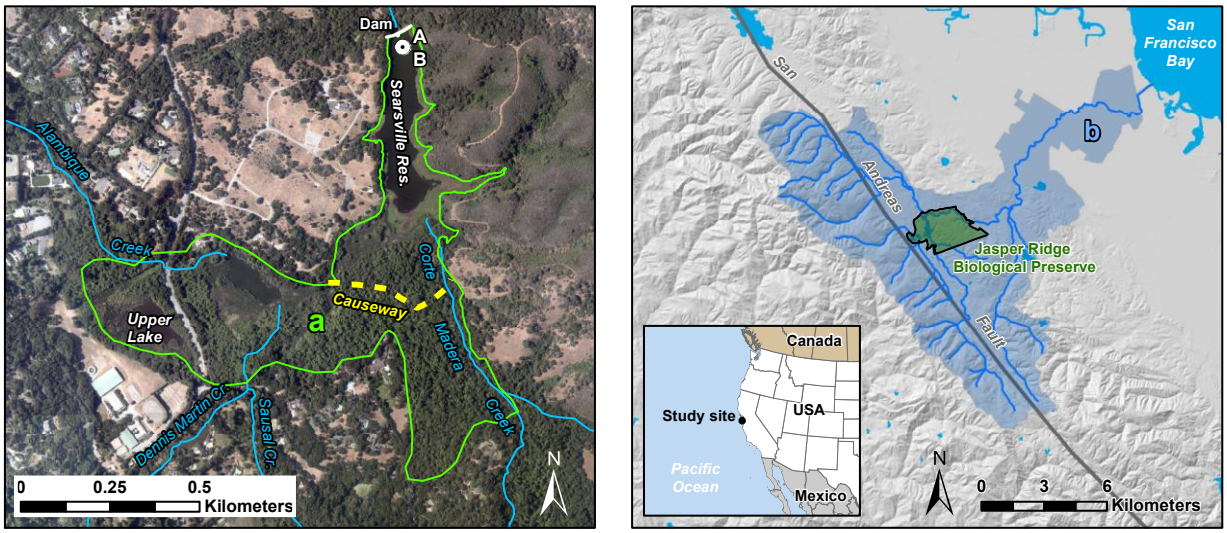
Dam
A
B
Searsville Res.
Alambique
Creek
Upper
Lake
Causeway
a
Corte
Madera
Creek
Dennis Martin Cr.
Sausal Cr.
0
0.25
0.5
Kilometers
N
San
Andreas
Fault
San
Francisco
Bay
b
Jasper Ridge
Biological Preserve
Canada
USA
Study site
Pacific
Ocean
Mexico
N
0
3
6
Kilometers

Figure 1.

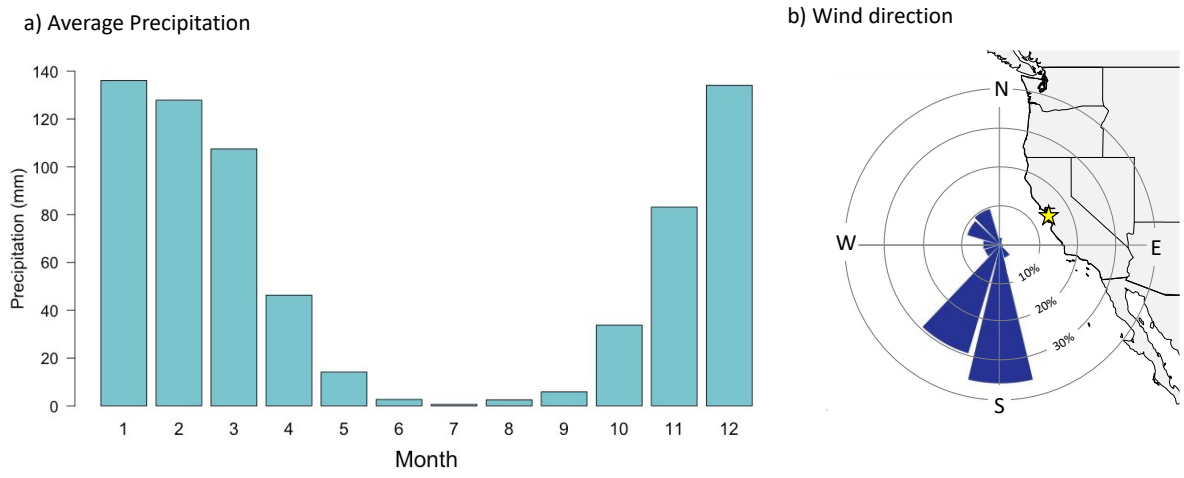
a) Average Precipitation
Precipitation (mm)
0
20
40
60
80
100
120
140
1
2
3
4
5
6
7
8
9
10
11
12
Month
b) Wind direction
N
W
E
S
10%
20%
30%

Figure 2.

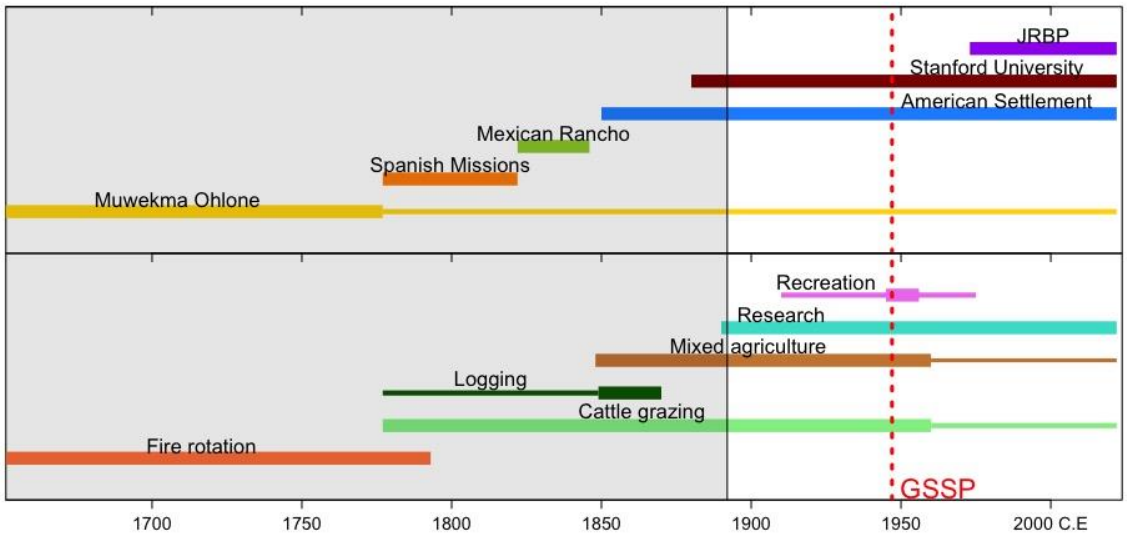
JRBP
Stanford University
American Settlement
Mexican Rancho
Spanish Missions
Muwekma Ohlone
Recreation
Research
Mixed agriculture
Logging
Cattle grazing
Fire rotation
GSSP
1700
1750
1800
1850
1900
1950
2000 C.E

Figure 3.

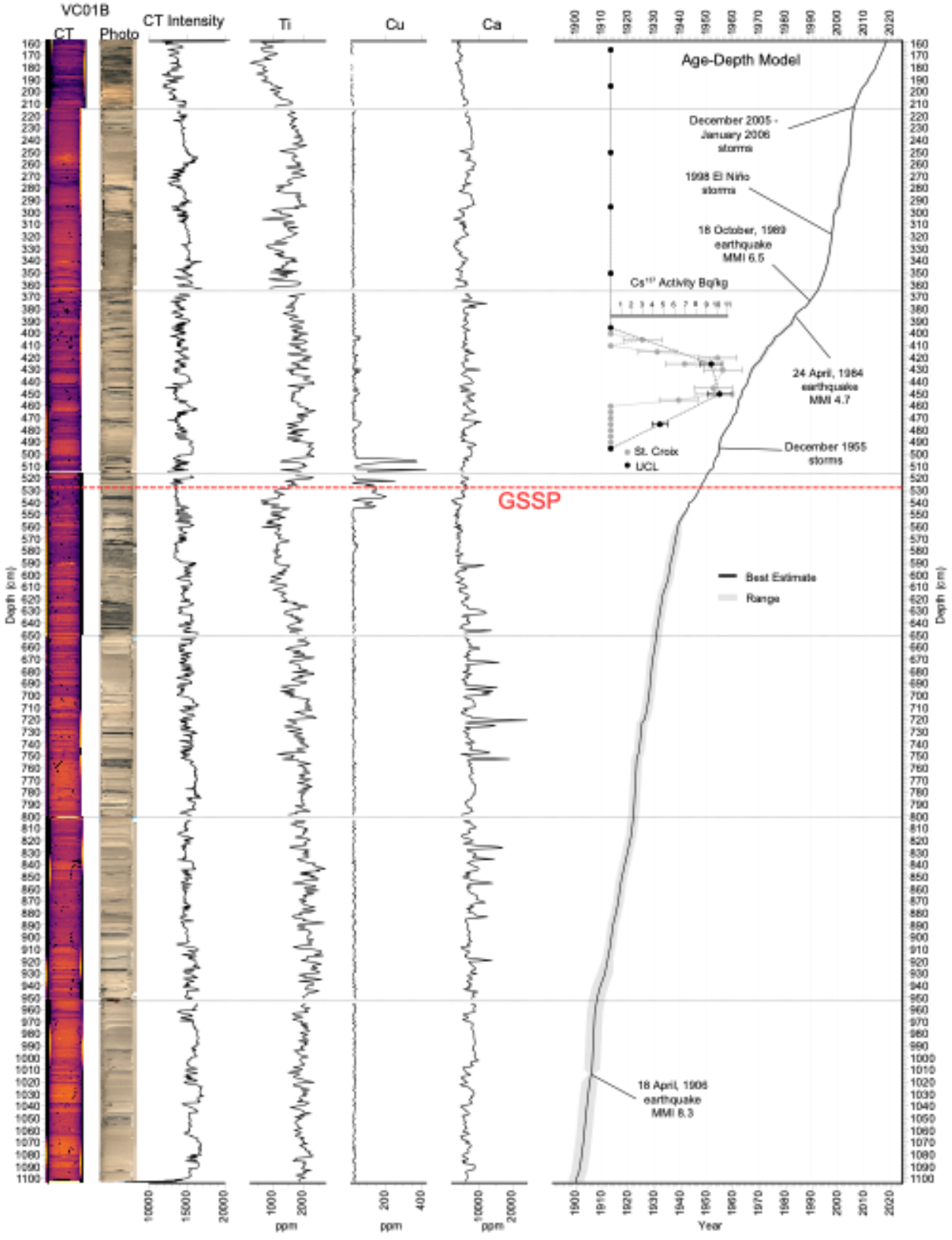
VC01B
CT
Photo
CT Intensity
Ti
Cu
Ca
Age-Depth Model
December 2005 - January 2006 storms
1998 El Niño storms
18 October, 1989 earthquake MMI 6.5
Cs137 Activity Bq/kg
24 April, 1984 earthquake MMI 4.7
St. Croix
UCL
December 1955 storms
GSSP
Best Estimate
Range
18 April, 1906 earthquake MMI 8.3
Depth (cm)
ppm
Year

Figure 4.

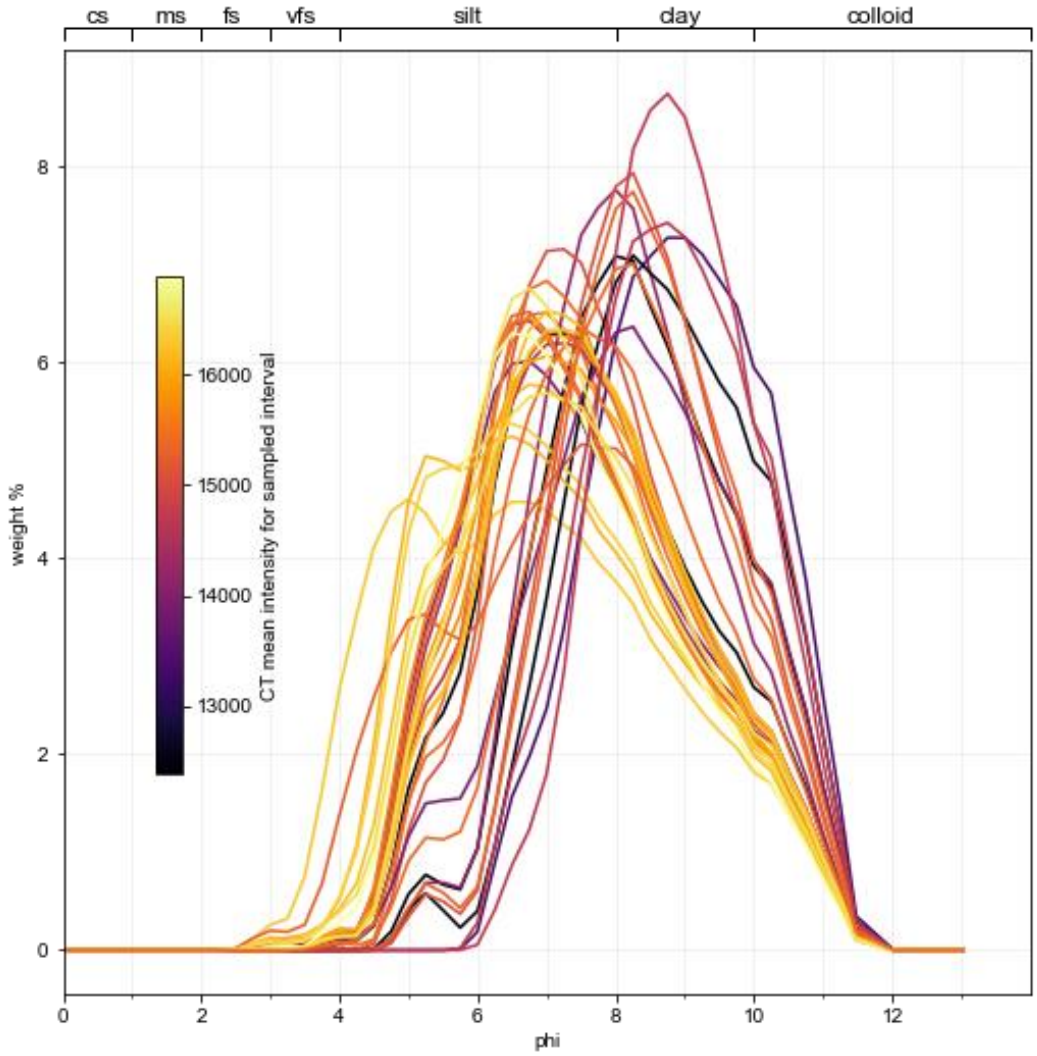
cs
ms
fs
vfs
silt
clay
colloid
weight %
phi
CT mean intensity for sampled interval
16000
15000
14000
13000
0
2
4
6
8
10
12

Figure 5.

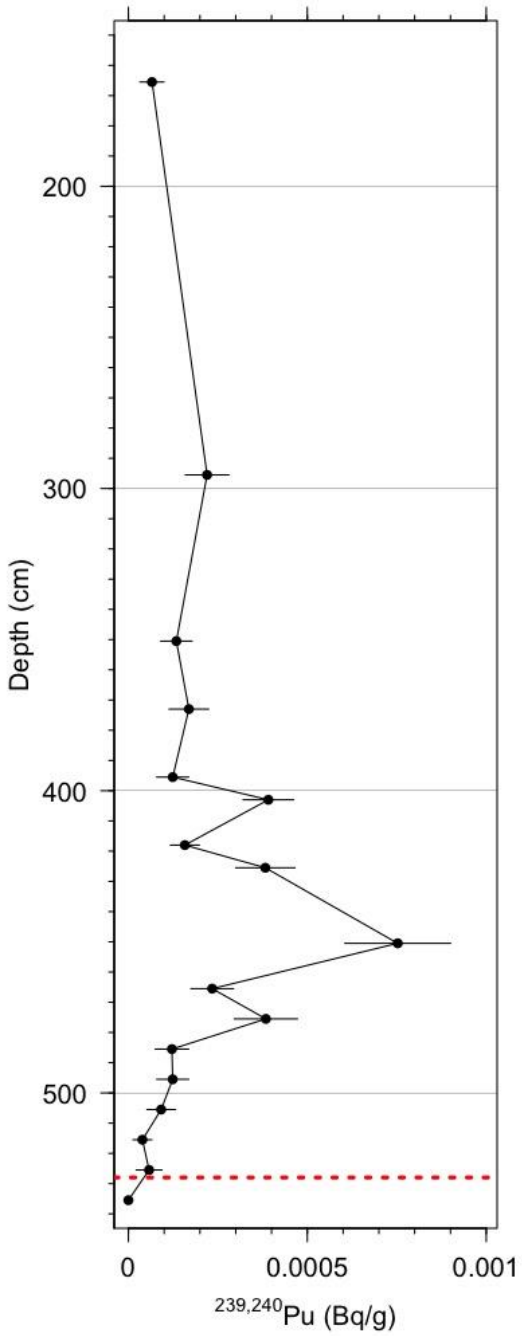

Figure 6.

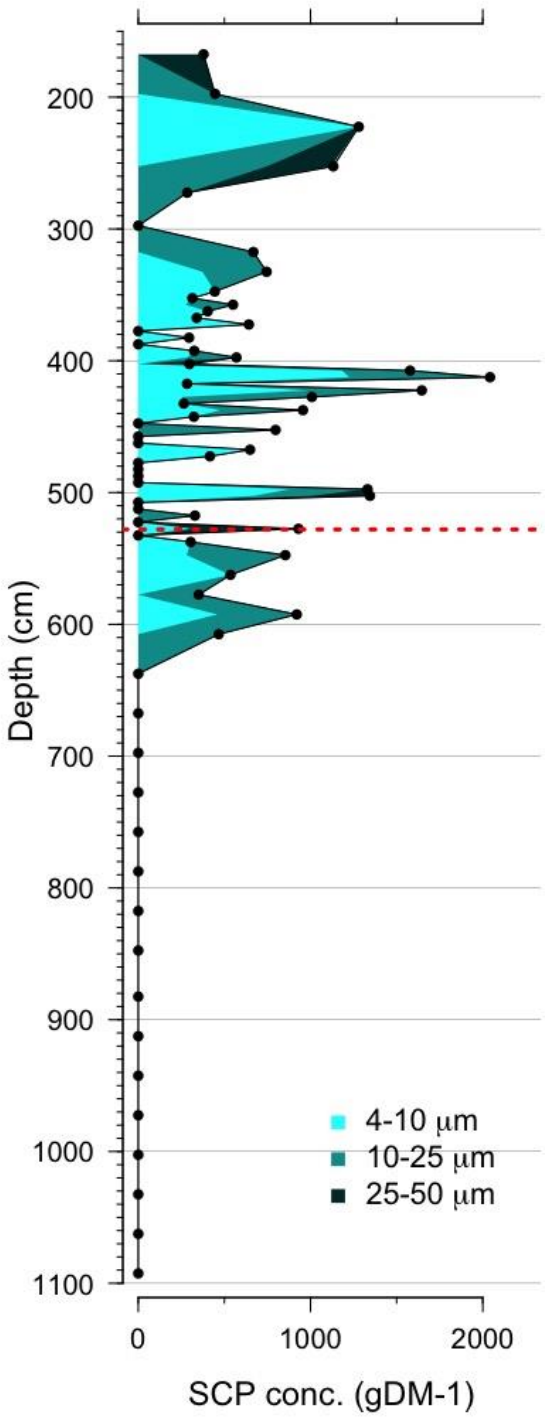
200
300
400
500
600
700
800
900
1000
1100
Depth (cm)
0
1000
2000
SCP conc. (gDM-1)
4-10 μm
10-25 μm
25-50 μm

Figure 7.

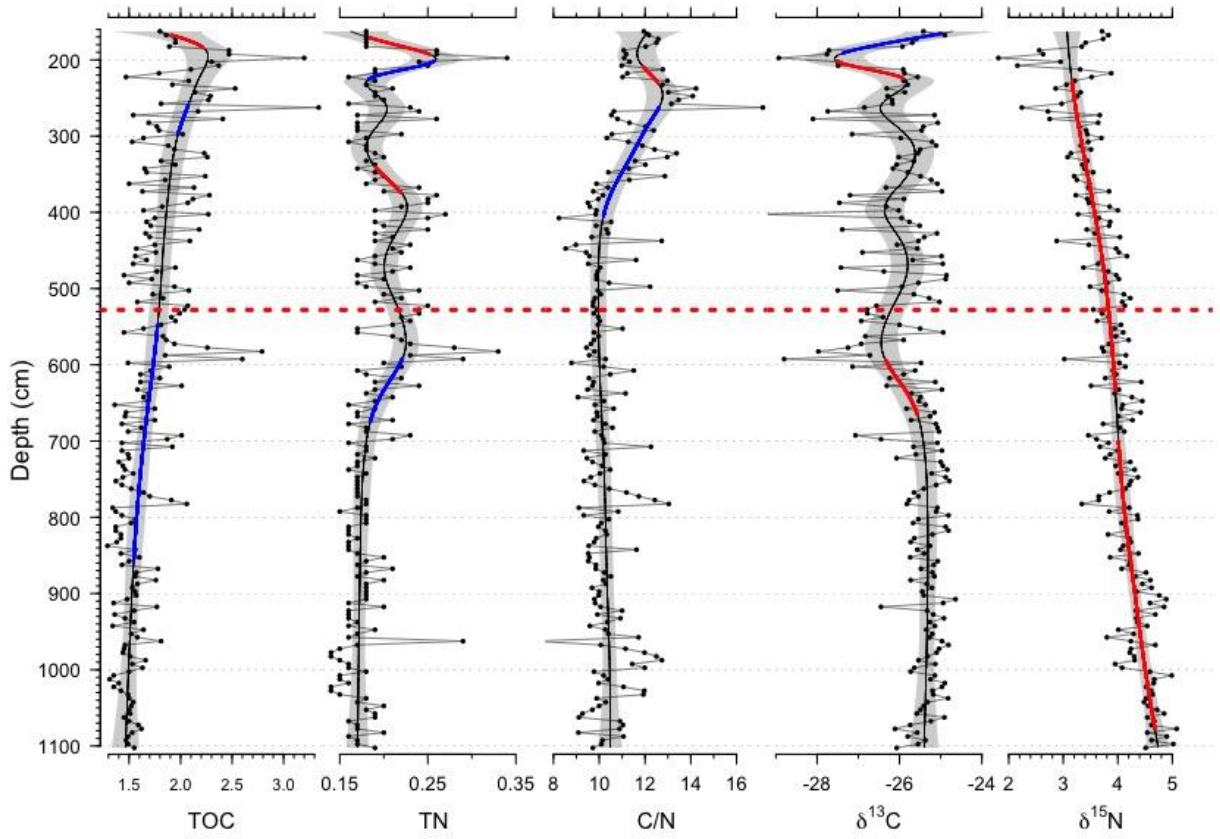
Depth (cm)
200
300
400
500
600
700
800
900
1000
1100
1.5
2.0
2.5
3.0
TOC
0.15
0.25
0.35
TN
8
10
12
14
16
C/N
-28
-26
-24
$\delta^{13}C$
2
3
4
5
$\delta^{15}N$

Figure 8.

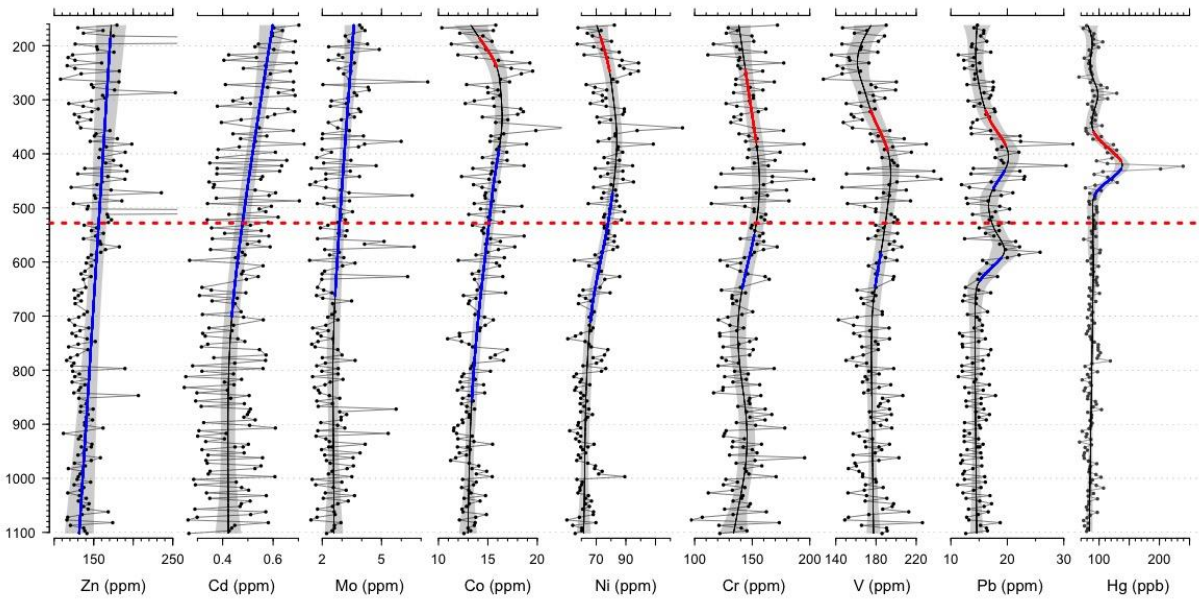
200
300
400
500
600
700
800
900
1000
1100
150
250
Zn (ppm)
0.4
0.6
Cd (ppm)
2
5
Mo (ppm)
10
15
20
Co (ppm)
70
90
Ni (ppm)
100
150
200
Cr (ppm)
140
180
220
V (ppm)
10
20
30
Pb (ppm)
100
200
Hg (ppb)

Figure 9.

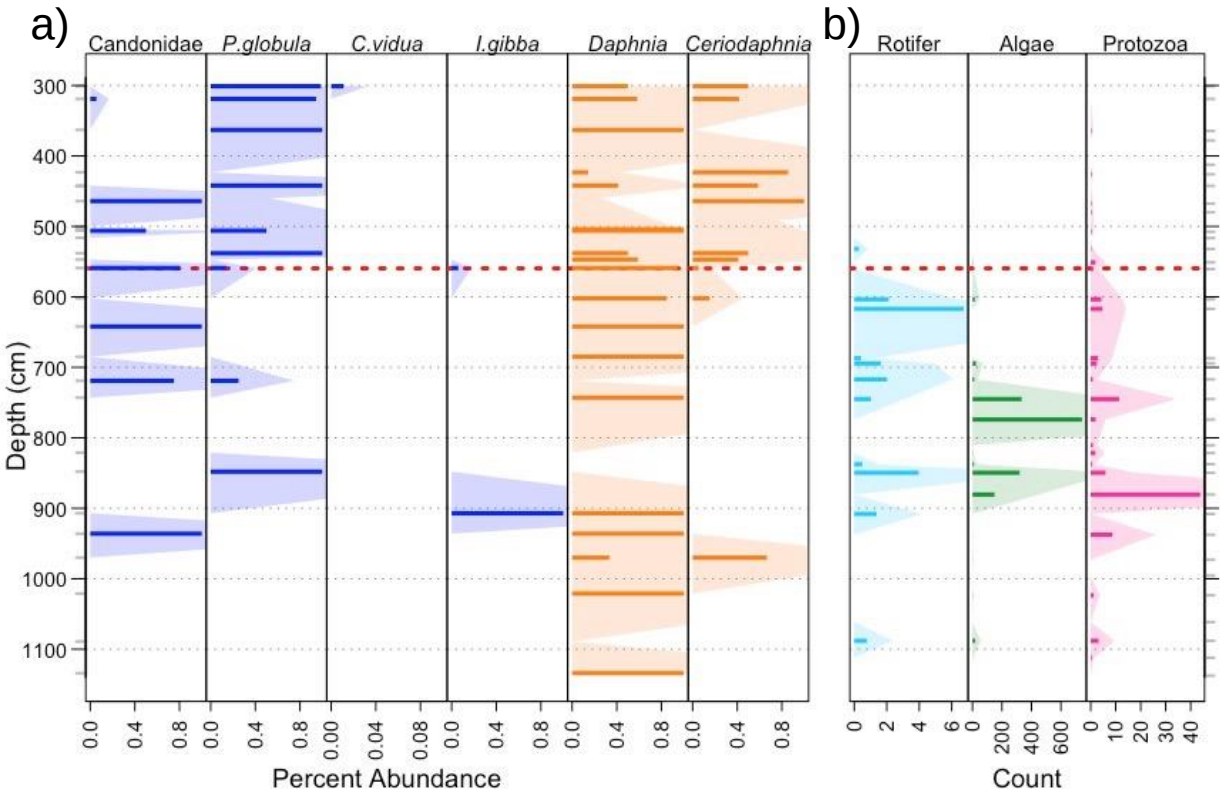
a)
Candonidae
P.globula
C.vidua
I.gibba
Daphnia
Ceriodaphnia
b)
Rotifer
Algae
Protozoa
Depth (cm)
300
400
500
600
700
800
900
1000
1100
0.0
0.4
0.8
0.00
0.04
0.08
0
2
4
6
200
400
600
10
20
30
40
Percent Abundance
Count

Figure 10.

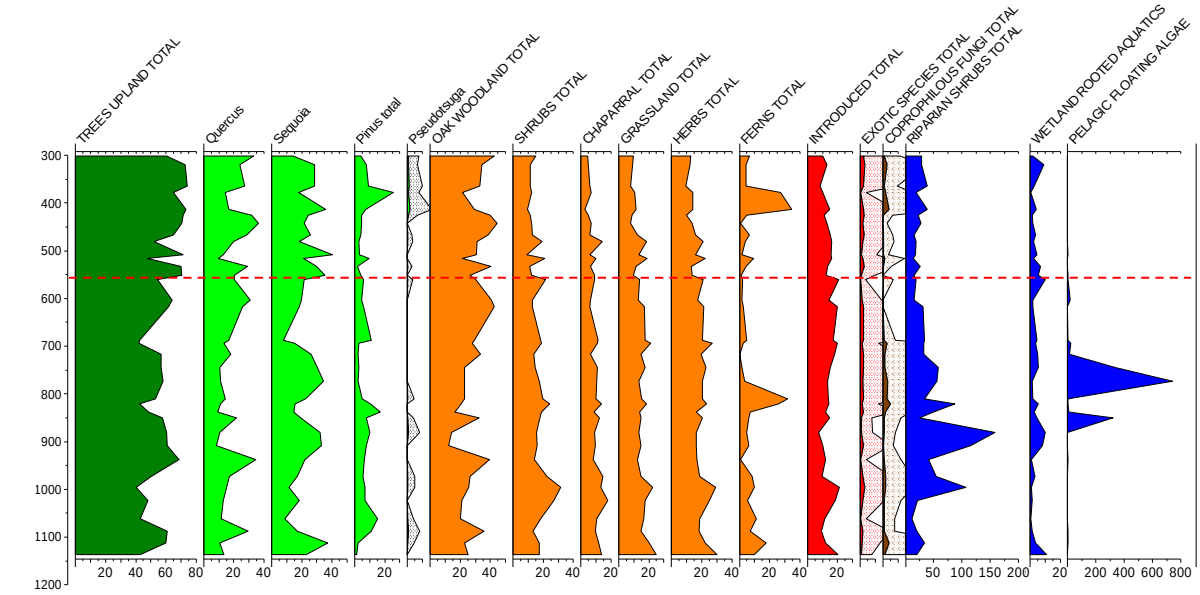
TREES UPLAND TOTAL
Quercus
Sequoia
Pinus total
Pseudotsuga
OAK WOODLAND TOTAL
SHRUBS TOTAL
CHAPARRAL TOTAL
GRASSLAND TOTAL
HERBS TOTAL
FERNS TOTAL
INTRODUCED TOTAL
EXOTIC SPECIES TOTAL
COPROPHILOUS FUNGI TOTAL
RIPARIAN SHRUBS TOTAL
WETLAND ROOTED AQUATICS
PELAGIC FLOATING ALGAE
300
400
500
600
700
800
900
1000
1100
1200
20 40 60 80
20 40
20 40
20
20 40
20 40
20 40
20 20
20 40
20 40
20
20 40
20
50 100 150 200
20
200 400 600 800

Figure 11.

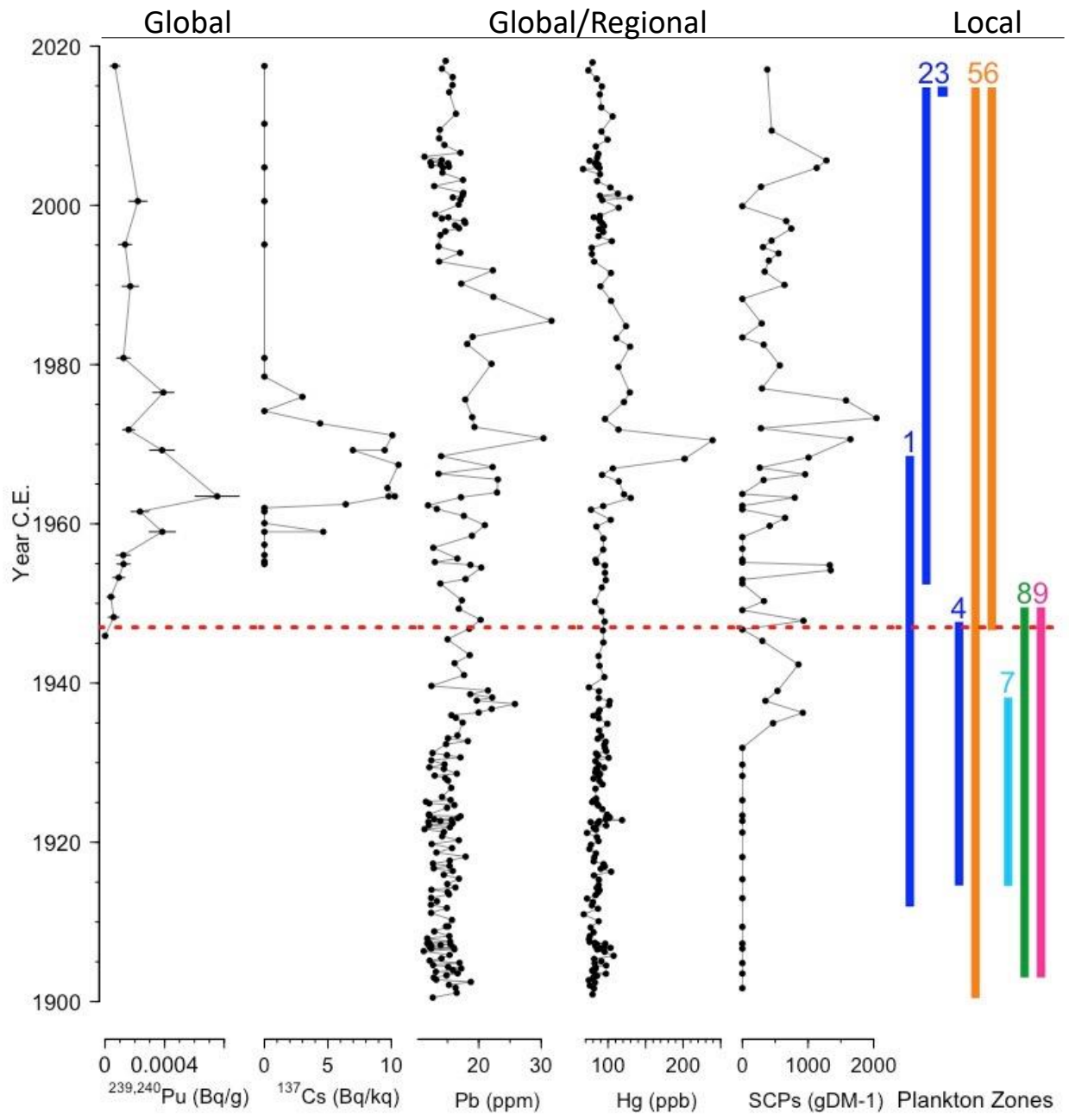
Global
Global/Regional
Local
2020
2000
1980
1960
1940
1920
1900
Year C.E.
23
56
1
4
89
7
0 0.0004
239,240Pu (Bq/g)
0 5 10
137Cs (Bq/kq)
20 30
Pb (ppm)
100 200
Hg (ppb)
0 1000 2000
SCPs (gDM-1)
Plankton Zones

Figure 12.

SUPPLEMENTARY MATERIAL

Upper Lake

Upper Lake is a sag pond on the San Andreas Fault, i.e., a natural lake rather than one created by Searsville Dam. It has a sedimentary record that extends back several hundred years and possibly more (Anderson et al., in prep; Redondo et al., in prep). The top portion correlates with the ~130-year Searsville Reservoir record; the oldest radiocarbon dates are about ~1300 yr BP. Palynology and mercury in Upper Lake cores have been studied comprehensively back to 1700 C.E. and will be reported elsewhere (Anderson et al., in prep, Redondo et al., in prep).

Geographic and Geologic Setting of the Searsville Site

Searsville Reservoir is embedded in a land-use matrix including cattle ranches and horse farms, suburban/rural development, and, in the upper reaches of the watershed, relatively undeveloped forested environments. Immediately to the east are Stanford University lands and Silicon Valley, a highly urbanized global center for technology innovation on the edge of San Francisco Bay. The reservoir is fed by five major creeks–Alambique, Dennis Martin, Sausal, Westridge, and Corte Madera. Corte Madera is the primary source of sediment (Kittleson et al., 1996). These creeks bring sediments derived from Quaternary alluvium; Plio-Pleistocene Santa Clara Formation conglomerates and sandstone; Middle Miocene Ladera sandstone and mudstone; Eocene Whisky Hill Formation consisting of turbiditic sandstone, conglomerate, and clastic debris; and Jurassic to Cretaceous Franciscan Complex greenstone, blueschist, chert, graywacke, and serpentine (Pampeyan, 1993; Kittleson et al., 1996; Coleman, 2004).

History of Land Use Around Searsville Reservoir

In addition to its high-resolution sedimentary record with clear evidence of geologically significant anthropogenic signals, the geographic location of Searsville Reservoir and its richly documented history and prehistory contribute to its value as a GSSP site. Archaeological sites near Searsville Reservoir and elsewhere in the South San Francisco Bay document regional and local anthropogenic influences from pre-European, early occupation by the ancestors of the indigenous Ohlone, who still live in this region today Native Americans (Bocek, 1990; Severson, 2022). The records are enriched by continued interaction with the living members of the Muwekma Ohlone, to whom the Searsville area remains important and, in some areas, sacred. Historical archives of European arrival document that the landscape was transformed throughout the region by increasingly intense logging, agriculture, industrialization, and urbanization (Bocek and Reese, 1992). During WWI, JRBP housed soldiers from Camp Fremont, while also hosting botany field expeditions and scouting trips. Stanford University acquired the lake and surrounding land in 1919 (Kittleson et al., 1996), but even before then, it was used for education and research by Stanford students and faculty, with nearly continuous academic studies since the 1890s (JRBPa, 2022). With formal acquisition by Stanford, those uses increased. For five decades, Searsville Reservoir was also a recreational facility, dubbed Searsville Park, where visitation included thousands of people per summer and activities included fishing, swimming, boating, sunbathing on beaches constructed with sand hauled in from the nearby beach town of Santa Cruz, horseback riding, motorcycle racing, and so on (Bocek and Reese, 1992). In 1973, the educational and research uses were deemed incompatible with wholesale recreational use. The Stanford Board of Trustees designated the lake and surrounding areas as Jasper Ridge

Biological Preserve, and by 1976, access by the public was restricted to docent-led tours, which continue to the present day.

Site Accessibility

Researchers, educators, and students can readily access the site through established protocols (JRBP, 2022a), and the general public is welcomed on docent-led tours (JRBP, 2022b). Each year the preserve sees thousands of visits geared towards education about Earth and biotic systems for students, researchers, and members of the general public (JRBP Staff, 2022).

Previous Work

For the 1998 cores, among the analyses carried out were bulk density profiles, magnetic susceptibility, porosity, sediment description and photographs, ^{137}Cs, ^{210}Pb, total Carbon (C), inorganic and total organic carbon, total Nitrogen (N), $d^{13}C$, $d^{15}N$, chlorinated pesticides and herbicides, organophosphorus pesticides PCBs, and Lead concentrations (Berhe et al., 2007). These analyses established that a core taken near our proposed GSSP core (JRBP2018-VC01B) recovered the entire sedimentary column from the pre-lake surface in 1892 to 1998, that a ^{137}Cs spike was evident to help calibrate the age model, that the sedimentary details of the core allowed for secure correlations between cores, and that features characteristic of what would later come to be recognized as Anthropocene indicators, such as ^{137}Cs, $d^{13}C$, and pesticide/herbicide compounds, were present. This all served to highlight the potential of Searsville Reservoir as a candidate GSSP site.

Archival materials document changes in the lake pertinent to interpreting its sedimentary history. When first constructed, the spillway elevation was 101.52 m (333.07 ft). The spillway level was raised in 1894 by 2.90 m (9.5ft) and again in 1920 by 1.79 m (5.87 ft), bringing it to the current elevation of 104.17m (341.76 ft) (Kittleson et al., 1996). A riparian woodland began to form where Sausal and Corte Madera Creeks entered the lake. In 1929, a levee (called The Causeway) was constructed to trap silt in Middle Lake before it entered the main body of the Reservoir (Bocek and Reese, 1992; Kittleson et al., 1996) (Figure 1).

These alterations, combined with continued sedimentation and development of a delta, influenced both the size of the reservoir and sediment inputs. Because of increasing issues with upstream flooding of neighboring properties, the causeway was breached in 1970 to allow Corte Madera Creek to flow directly into the Reservoir. At that time, Middle Lake had silted in considerably and little sediment was being captured by the levee. The bathymetry of Searsville Reservoir was mapped at various points through time and subsequent analyses (especially our age model, detailed below) have shown that sediment accumulated rapidly from 1892 to 1929 (change in depth behind the dam = ~10.5 m) (Kittleson et al., 1996). After the construction of the levee, sedimentation rates declined: water depth behind the dam decreased by only ~3m from 1929 to 1996 (Kittleson et al., 1996).

Methods: Chronological Controls

First, an approximate age model was constructed for VCO1B by counting inferred seasonal layers downcore from the top of the core, with the youngest layer regarded as October, 2018, when the core was taken. These inferred seasonal layers consist of relatively coarse sediments typically deposited during wet-season rainstorms (usually November through April), and much finer, more organic layers typical of the dry-season deposition (May through October), when

aquatic plant and algae proliferate and settle to the bottom of the lake. Thus, most of the coarse-fine couplets likely correspond to one year.

Counting the couplets was facilitated by first obtaining CT scans of the cores and color-enhancing the images so that less dense, dry-season, organic-rich sediments showed up as bright purple bands, and denser, wet-season, low-organic sediments showed up as bright orange or yellow bands. The colors generally correspond to sediment density and grain size. This initial step of couplet-counting suggested the bottom of the core dates to 1897-98±3 years. Later, matching the bottom of JRBP2018-VC01B to the equivalent portion of the 1998 USGS core that unequivocally bottomed out on the pre-lake soils with redwood detritus confirmed that the bottom of JRBP2018-VC01B fell near 1897. Further confirming that the couplet-counting method was reliable were sediments indicative of extreme precipitation events recorded historically, which were evident at expected years. For example, the couplet counts placed three years with notable flooding–2005, 1998, and 1955–at thick wet season deposits.

Uncertainty from using layer counts alone arises from the likelihood that the inferred seasonal layers do not always have an exact one-to-one correspondence with years. The complication is that episodic rains can also wash in thin couplets, the bottoms of which are graded coarser material, and the tops fining into more organic sediments derived from vegetation that washed in during the rain. For some thin couplets, then, subjectivity comes into play in deciding which of the thin couplets represents a wet-dry cycle that records a low-precipitation year, and which couplets represent episodic rainstorms in higher-precipitation years that had frequent, intense storms.

Therefore, to further resolve the initial chronology that was developed solely by counting couplets, we identified chronological anchor points that could be tied with precision to particular years, and accordingly adjusted the ages of the inferred seasonal layers to match with those anchors. The chronological anchors included the top of the core (October 2018), sedimentary features indicative of the 1989 Loma Prieta and 1906 San Francisco earthquakes (evident as disturbed layers in otherwise regularly-layered sediments), the 1963 ^{137}Cs spike, several historical events that were recorded and would have predictable influences on lake sediments or geochemistry, and confirming and refining seasonal layer-counts by matching them with detailed XRF profiles of Titanium, which increases with increasing precipitation run-off into the lake (Stegner et al., in prep.).

The location of the ^{137}Cs spike in JRBP2018-VC01B was determined by analyzing freeze-dried sediment samples by direct gamma assay in the Environmental Radiometric Facility at University College London, using ORTEC HPGe GWL series well-type coaxial low background intrinsic germanium detector. Some adjacent samples were combined to increase sample sizes. Because these samples were discontinuous, an additional 19 samples collected in continuous 5cm thick (~3.5 g dry weight) units from 493-398 cm were analyzed for ^{137}Cs by direct gamma assay at the University of Minnesota St. Croix Watershed Research Station to refine the location of the ^{137}Cs peak. Two of these samples were subsequently excluded from our study because they were from a flood deposit which would have been deposited over only a few days and so had anomalously low Cesium concentrations. We also applied the same methodology for assaying ^{210}Pb, ^{226}Ra, and ^{241}Am (Appendix 4). Of these, only ^{137}Cs provided a signal useful as chronological tiepoint, with the 1963 peak clearly evident at 447.5 cm depth in JRBP2018-VC01B (see Results: Chronology for more detail).

Historic events useful in establishing the age model included the use of algaecides to clear the water in the years the reservoir was a popular swimming destination. Copper sulfate

($CuSO_4$) was used from 1943-1947 at a rate of 300 lbs per week beginning in the spring each year (Erwin, 1947a; Jones, 2021). In 1952 and 1953, 10 tons of copper sulfate were applied to the lake (JRBP Archives, 1952-1953). XRF peaks in copper (Cu) are evident in both JRBP2018-VC01B and JRBP2018-VC01A at depths of the cores that the layer counting had identified as near (but not exactly) 1943, 1952, and 1953. We therefore adjusted the layer-count ages accordingly to place those years at layers/depths containing the onset of the Cu peaks (considered to be 1943 C.E.) and two final distinct peaks (1952 C.E. and 1953 C.E. respectively) (Figure 4). Chloride of lime, or calcium hypochlorite ($Ca(ClO)_2$), was also used to control algae from as early as the 1930s (Felin 1940) and through the 1940s (Erwin, 1947b; Jones, 2021). Therefore, we used the Ca peaks that occur from ~590-920 cm to refine the ages of the wet-dry couplets from the 1910s to the 1930s (Figure 4).

To further refine the age model for JRBP2018-VC01B, we used the Ti XRF profile to increase the precision of distinguishing wet-season from dry-season layers (Stegner et al., in prep; Figure 4). Previous studies on sediment cores have demonstrated a strong relationship between Ti and rainfall (Hendy et al. 2015). We confirmed this to be the case in Searsville Reservoir by XRF analyses of filtered water samples collected at frequent intervals from 1996-2008 C.E. (unpublished data), with collection dates matched to local precipitation and stream runoff records for the area. In the core, layers consisting of relatively coarse, high-density sediments show high Ti content, consistent with the sedimentological -evidence they were deposited during wet-season rainstorms (usually November through April). Lower-density layers with more organic content show lower Ti content: these are typical of dry-season deposition (May through October) (Appendix 5). Thus, the Ti profile provides a highly-resolved, continuous record of yearly wet-season/dry-season couplets throughout the core, independent of the visual observations derived from the CT scans. The wet-dry couplets recognized from the Ti profile were then compared with the layer-counts derived from visual analysis of the CT density scans, and used to make minor adjustments in intervals where the CT data had been less conclusive.

JRBP2018-VC01A was then correlated to JRBP2018-VC01B by matching distinctive seasonal-layer patterns evident in the CT scans and distinctive features of the XRF scans.

Methods: Inorganic geochemical signals

We subsampled the freeze-dried sediment samples used for C and N analyses. Aliquots of each sample were freeze-dried and elemental concentrations are based on dry sample weight. After drying, all preparation and dilution steps took place in the Stanford SIGMA clean lab facility. The facility is equipped with a class 100 metal free clean lab and work was performed in class 10 workstations. Approximately 100 mg of material was digested in Optima® grade concentrated hydrofluoric acid and nitric acid at elevated temperatures and pressures in a CEM MARS5 microwave digestion system. Digested sample solutions were clear with no undissolved material or precipitates. A gravimetric fraction of the digested solution was used for elemental concentration determination. Diluted samples prepared in a 2% nitric acid matrix were analyzed on an Agilent 8900 ICPMS operated in single quad mode with He as the reaction gas. A synthetic standard mixed to mirror the composition of soil (CRM-soil-A) was used to monitor data quality. External reproducibility is estimated by repeated analysis of the USGS BHVO2 standard dissolved in parallel with the samples

Results: Chronology

^{210}Pb dating. Total ^{210}Pb activities were almost in equilibrium with supported ^{210}Pb in all the measured samples from 162.5 to 495.5 cm of JRBP2018-VC01B (Appendix 4). Unsupported ^{210}Pb activities, calculated by subtracting supported ^{210}Pb activity from total ^{210}Pb activity, were less than the relevant counting errors in all the counted samples above 453 cm. The relatively high counting errors rendered the unsupported ^{210}Pb dating impossible. However, some higher unsupported ^{210}Pb activities than the relevant counting errors in 472.5 - 475.5 and 492.5 - 495.5cm samples imply that the counted sediments were formed within the last hundred years or so, consistent with the known age of the reservoir.

137Cs. Cesium-137 had low concentrations in JRBP2018-VC01B (2.99-10.57 Bq/kq)–average ^{137}Cs activities in sediment cores from the Northern Hemisphere are typically at least twice as high as observed in Searsville (Foucher et al. 2021)–but nevertheless the profile at Searsville shows the typical global pattern.

Error bars in the lower part of the core. Between 1929 and 1906, fewer independent tie points were available to independently support couplet-count ages than higher in the core. Further contributing to potential error in this part of the core is the fact that sedimentation rates were much higher before 1929 when construction of the causeway began to slow down sediment deposition in the deeper part of the reservoir, making it harder to distinguish wet/dry seasons from individual storm events. To help refine ages in this in this lower region of the core, Ca peaks in the XRF helped to identify true dry season deposition versus multiple storms within the wet season,, because chloride of lime was only used between May and September (Felin, 1940; Bocek and Reese, 1992). Nevertheless, to be conservative we assigned error bars of ±2-3 years in this lower region of the core.

Carbon-14 dating. Dates ranged from 3,362 ± 22 ^{14}C YBP (3,499-3,682 calendar YBP) to 16,463 ± 62 ^{14}C YBP (19,614-20,083 calendar YBP). d^{13}C isotopes for these samples ranged between -23.6 and -28.5, indicating that the source of dated carbon is dissolved organic matter rather than limestone, precluding the possibility of the "hard water effect." These anomalous dates likely result from the presence of organic material older than the range of radiocarbon dating and with no remaining ^{14}C ("old carbon"). Most likely the old carbon comes from lignite which is known to occur in small pockets throughout the Santa Cruz Mountains, including in the general vicinity of Jasper Ridge (Stoffer, 2002). Within the catchment area of Searsville Reservoir is Coal Mine Ridge, where lignite was actively mined. and so this is a likely source of contamination. The catchment of Searsville has not burned significantly in 150 years, and no charcoal was detected in the cores.

Results: Biotic Markers

Subfossil remains all came from core JRBP VC01A; note that in comparing core-depths to JRBP VC01A, years correspond to different depths in the two cores because of different total length of cores and compaction during the coring process.

Ostracods and Cladocera. Shifts in the ostracod assemblages were primarily driven by Candonidae and *Physocypria globula* (Figure 10). Ostracods were absent from samples at 422-424.5 (1987 ± 0.5 - 1989 ± 0.5 CE), 499-501 (1960 ± 0.5 - 1961 ± 0.5 C.E.), 501-503 (1960 ± 0.5 - 1961 ± 0.5 C.E.), 503-505 (1960 ± 0.5 C.E.), 515-517 (1955 ± 0.5 - 1956 ± 0.5 C.E.), 533-

535 (1953 ± 0.25 C.E.), 546-548 (1950 ± 0.25 - 1951 ± 0.25 C.E.), 684-686 (1930 ± 2 C.E.), 820-822 (1922 ± 2 C.E.), and below 969 cm (before 1909 ± 3 C.E.). The oldest sample with ostracods (935-937 cm, 1912 ± 2 C.E.) contained only individuals of Candonidae. Candonidae was then replaced by *Ilyocypris* cf. *gibba* at 906-908 cm (1915 ± 2 C.E.), but this taxon then disappeared with only one recurrence at 558-560 cm (1946 ± 0.25 - 1946 ± 0.25 C.E.) which included 3 valves. Candonidae dominated from about 550 to 950 cm (1911 ± 3 to 1949 ± 0.25 C.E.). *Physocypria globula* first appeared at 847-849 cm (1919 ± 2 C.E.) and was sporadically present afterward, but became the dominant taxon above ~420 cm (~1991 C.E.). In the top sample (300-302 cm; 2014 ± 0.25 C.E.) *P. globula* was joined by *Cypridopsis vidua*, the only occurrence of this species, represented by 2 valves. Overall ostracod abundance was much higher above ~422 cm (~1989 C.E.), composing 70.4% of the ostracod valves in the core.

Ephippia from the cladocerans *Daphnia* spp. and *Ceriopdaphnia* spp. were found in many levels of the core, but were particularly abundant (85.4%) in the top half, especially from 546 to 603 cm (1937 ± 2 to 1951 ± 0.25 C.E.). Neither ostracods nor epphippia were recovered from 499 to 535 cm (1953 ± 0.25 to 1961 ± 0.5 C.E.), except a small recovery at 505-507 cm (1959 ± 0.5 - 1960 ± 0.5). See Viteri (2022) and Viteri et al. (in prep) for details.

Diatoms. Sparse diatoms, primarily benthic in habitat preference, were detected on the slide from 298-304 cm (2013 ± 0.5 - 2015 ± 0.25 C.E.). Further down core, evidence of diatom dissolution was present at depths 465-470 cm (1966 ± 0.75 - 1967 ±1 C.E.) and 588-594 cm (1939 ±1.3 - 1938 ± 1.75 C.E.). Only the central areas of highly silicified large benthic genera (i.e., *Gyrosigma*) were readily evident at those depths. Low diatom abundance and poor preservation are likely a result of physical and chemical processes within the lake and catchment, whereby either the diatom signal is being diluted by more allochthonous than autochthonous material being delivered to the basin and/or lake chemistry has resulted in the dissolution of diatom frustules.

Pollen, spores, and non-pollen palynomorphs. Thirty-five of the forty pollen samples from JRBP2018-VC01A contained countable assemblages. The average pollen count was 326 +/- 38 grains/sample. . The richness of the palynomorph assemblage was high: 144 palynomorph types included 72 terrestrial pollen types, 9 aquatic and/or wetland types, 8 algal types, 20 ferns and allies, and 35 non-pollen palynomorphs (NPPs). See Anderson et al. (in prep) for further details

Discussion: Satisfying Criteria for Defining a GSSP

Multiple cores (three archived) verify that deposition over the required time interval is continuous and that the depositional history is replicated throughout the lake basin. Sedimentation has been essentially continuous on an annual scale. Lithofacies are uniform throughout the sequence, without any major reworking, hiatuses, or unconformities. CT scans demonstrate that the sediment layers in Searsville are unaffected by bioturbation or reworking– layers less than 1mm thick are found preserved with sharp boundaries throughout cores that have been analyzed, likely because the bottom waters are seasonally hypoxic (Koweek et al., 2020).

Koweek et al. (2020) found that, because there are no stream inputs or flow over the dam in the dry season, the lake has essentially no current and becomes stagnant, causing the bottom waters of Searsville to be seasonally hypoxic, which possibly contributes to the lack of bioturbation. The rapid sedimentation rate may also play a key role in limiting bioturbation. Any hiatuses in our record would be negligible. Minor hiatuses (less than a year) conceivably could

be caused by wet seasons during which very little or no rain fell, but summer autochthonous deposition would mitigate this effect, and there are no consecutive years without rainfall. In any case, the possibility of the <1-year hiatuses is accounted for by the error bars in our age model. Although the wet season deposition in Searsville is driven by storms and the material is often associated with landslides in the upper reaches of the watershed, mass flow of sediment does not reach the lake, nor is there evidence of turbidites in the cores. Sediment layers associated with earthquakes remain discrete from neighboring layers, and are confined to less than a year's sediment input. Notable earthquake disturbance of sediments does not occur near the proposed GSSP boundary. The sediments are free of diagenetic alterations or metamorphism, and are not depositional and geochemical signals within them are not overprinted by later events.

The chronology is resolved to at least the annual level (and to the seasonal level in most portions of the core) and is supported by multiple lines of evidence, including geochemical (Cu, Ca, Ti), sedimentological (sediment density, earthquakes), and radiometric data (Cs-137). Some of these chronological tie points are directly dated to year (Cs-137) and even month (Cu, earthquakes) while others track seasonal fluctuations and facilitate counting of annual layers (Ti, Ca, density). We have established a strong link between wet/dry seasons and fluctuation in both Titanium and CT intensity which allowed us to count annual layers and to confidently identify the season of deposition for most of the core regardless of the age error bars. From ~1939 to 2018 C.E., age error was less than a year, and was less than three years prior to that. From 1943-1963 C.E. specifically, the time period spanning the proposed GSSP, the error is between 0.25 and 0.5 years, accounting for variation in the onset and conclusion of the wet season each year. Sedimentation rates ranged between 1 and 47.5 cm/year, providing enough thickness to associate samples with season, and for certain years it would be possible to collect multiple samples throughout a year to track intra-annual trends.

Discussion: Plutonium-239,240 as a Primary Marker

The first appearance of plutonium in Searsville in 1947 is consistent with expectations of earliest incorporation of ^{239,240}Pu into geological deposits globally, although the first local or regional appearance of ^{239,240}Pu theoretically could occur as early as 1945 in some deposits. Three detonations took place that year: on July 16, August 6, and August 9. Two more took place in 1946, on July 1 and 22. None took place in 1947.

Because Pu ejected into the troposphere and larger particles in the stratosphere (1-10 micrometers) wash out within a few weeks to a few months, Pu can be expected to appear in some deposits within a few hundred miles downwind of explosions as early as late 1945 (New Mexico, USA and in Japan) or 1946 (Bikini Atoll), but to our knowledge, the earliest Pu. For more distant sites, lag times between ejection of Pu into the atmosphere and settling into the geologic column are likely greater. Particles of Pu are thought to remain in the stratosphere for as long as 2.5 to five years (Alvarado et al, 2014; Hirose and Povinec 2015), but more typically 1.5±0.5 years (Waters et al., 2015; Hirose and Povinec 2015). More generally, deposition of radionuclides into deposits globally have been shown to lag explosions by about a year. Moreover, the probability of ^{239,240}Pu finding its way into the geological record globally increases with the frequency and the increasing geographic distribution of nuclear detonations: hence the globally recognized peak of ^{239,240}Pu and ^{137}Cs in 1963, one year after the peak of nuclear weapons testing.

Discussion: Auxiliary Markers

Burning of fossil fuels is a key driver of the changes associated with the Anthropocene, including climate change, and profiles of SCPs, $d^{13}C$, and $d^{15}N$ are known to document these changes globally, generally with clear inflection points in the mid-20th century.

SCPs. Potential local sources of SCPs in the Bay Area are not present upwind of Searsville and we see no signal of increasing SCPs in relation to potential local sources. For example, SCPs declined after 1955, when Interstate 280, which passes less than 2km from Searsville, was constructed. We also see no increase in SCPs when major power plants, e.g. Moss Landing Power Plant and Metcalf Energy Center, came on line in the region (PSE, 2022).

Stable nitrogen isotopes $d^{15}N$). Although previous research has shown seasonal changes in $d^{15}N$ of algae of ~5 per mil (Francois et al. 1996), the magnitude of decline in Searsville is on par with that observed in other sediment cores (Wolfe et al. 2013). Small-scale agriculture has been a part of the watershed since before the Reservoir, but there are no major sources of fertilizer runoff which is expected to increase $d^{15}N$ rather than decrease (Meyers and Teranes 2001), as we observe in Searsville.

Carbon isotopes. The $d^{13}C$ signature at Searsville integrates the C isotope fractionation of different organisms, as well as the relative proportion of organic matter derived from those different sources. This local and regional organic input likely explains why total organic carbon in the Searsville record began increasing in the 1920s, coincident with the first major presence of algae and *Sparganium* (bur-reed) documented in the pollen record. At the same time, a delta colonized by dense willow forest began to form at the southern end of the lake as recorded historically (Kittleson et al., 1996, Bocek and Reese, 1992). Increases in the relative proportion of aquatic plants contributing to the organic material would be consistent with a depleting $d^{13}C$ at about that time.butOverall, the range of $d^{13}C$ values in the core (-24.6 - -29.42 per mil) is consistent with influences by aquatic plants (Chappuis et al., 2013), terrestrial C3 plants, algae (Schidlowski, 2001), some combination of all three, and/or possibly additional groups. The overall trend suggests that until the late 1970s, the C/N ratio reflected higher aquatic plant/algae organic inputs (Talbot, 2001). C/N then increased slightly suggesting either a modest increase in terrestrial organics. Preferential diagenetic loss of N in the older sediments has also been suggested as a possibility (Talbot, 2001; Meyers and Teranes, 2001), but we found no evidence of this.

Climate proxies. In the Searsville sediments, thickness of dense (wet-season) layers reflect high-precipitation and/or flood years that can be correlated with historic records. This record is currently being linked to high-resolution tree-ring climatic proxies obtained from blue oaks (*Quercus douglasii*) less than a km from the lake. Blue oaks are exquisitely sensitive to cool-season precipitation and are common in the foothills surrounding the California Central Valley (Stahle et al., 2013). To date, more than thirty blue oak chronologies have been developed, are publicly available, and have been used to skillfully reconstruct regional winter precipitation and drought (Meko et al., 2011; Griffin and Anchukaitis, 2014), streamflow (Meko et al., 2001), strength of the North Pacific High that guides the onshore storm track (Black et al. 2014), and even San Francisco Bay salinity due to its dependency on freshwater inputs (Stahle et al. 2011). Old-growth blue oak stands occur within JRBP and already are in the process of being analyzed to develop site-specific growth and climate histories. Indeed, blue oaks are the “gold standard”

for cool-season precipitation reconstruction, and enable correlation of the Searsville climate record not only with regional climate, but also broader global-scale patterns given the influence of such teleconnected processes as the El Nino Southern Oscillation (ENSO) on winter precipitation (Stahle et al., 2013; Black et al., 2014). Work so far identifies general correspondence between the sediment layers in the core and tree-ring reconstructed precipitation, although the temporal scales captured by each proxy likely differ: cores appear to reflect event-scale processes, such as floods, to seasonal averages while blue oak ring width strongly reflects average cool-season precipitation. Ultimately these blue oak and sediment cores will be tightly correlated, combining their complementary perspectives to yield a more comprehensive record of environmental history than either could provide on its own.

Paleobiologic Proxies. Preliminary work on sedimentary DNA shows promise for identifying First Appearance Data (FAD) for late Holocene and Anthropocene immigrants, particularly mosquitofish (*Gambusia*), wild turkeys (*Meleagris gallopavo*), American bullfrogs (*Lithobates catesbeianus*), and parrot-feather (*Myriophyllum brasiliensis*). All are found in Searsville Reservoir today, and historic records document their first appearances in the early 20th century. Preliminary analyses are promising and have found nonnative species including brown bullhead (*Ameiurus nebulosus*) and European carp (*Cyprinus carpio*) introduced to California waterways at the turn of the century; wild boar (*Sus scrofa*), introduced to California in the 1700s by the Spanish but are not yet physically present in JRBP, but in the drainage (Ruiz, 2022); and common house mosquitos (*Culex pipiens*), present in the Americas well before 1924 (Freeborn, 1924).

Last Appearance Data (LAD) caused by extinction so far have limited utility in 20th and 201st century geological deposits. Although extinction rates clearly have accelerated during that time, the species that have gone extinct so far were not cosmopolitan enough to leave abundant fossil remains in most geological deposits or lived in habitats with low fossilization potential.

Abundance Zones at Searsville are underpinned by anthropogenic impacts on the lake. At Searsville, a zone from ~499 to 535 cm (~1953-1961 CE) in JRBP2018-VC01A (encompassing the Holocene-Anthropocene boundary in this core) almost completely lacks adult ostracod and cladocera microfossils. This zone corresponds with massive amounts of algaecides and herbicides applied to the lake which apparently killed these organisms (Smith, 1963). Above 558 cm, the ostracods and cladocerans re-appear, but in notably different abundances than were evident below. This relationship is particularly clear in plotting raw counts of microfauna through time (Figure S1).

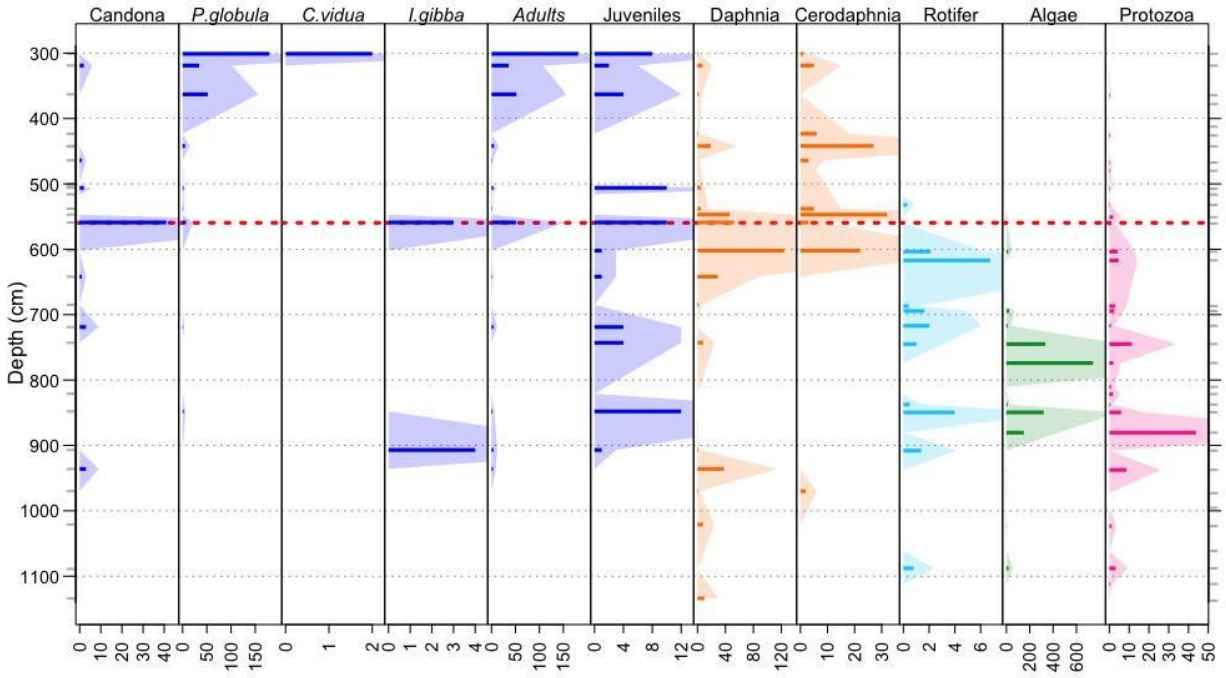

Figure S1. Raw counts of microfauna remains recovered from Core JRBP2018-VC01A.

Palynology: Intensive logging in the 1880s impacted much of the California Coast Range (Rood, 1975; Bocek and Reese, 1992), accounting for fluctuations in coast redwood (*Sequoia sempervirens*) and Douglas-fir (*Pseudotsuga menziesii*). Oaks (*Quercus*) (Oaks) and oak woodland clearly expanded after the 1930s, likely stimulated by the cessation of cattle grazing, as evidenced by historic research on oaks and canopy expansion at JRBP and neighboring lands (Franco, 1976; Herwitz et al., 2000).

The construction of the dam created far more habitat for aquatic species which fluctuated in abundance with changes in the lake depth and extent of the delta, most of which persist to this day. On a broader scale, such fluctuations in aquatic vegetation related to dam construction are probably a widespread signal in reservoir sites and other lakes affected by damming rivers and creeks. Dam construction is a global signal of the Anthropocene. Although the timing of peak dam construction differs slightly by continent (1960s in North America, Oceania, and Europe; 1980s in Africa and Asia, and 2010s in South America), an acceleration is seen in the 1950s across all continents (Zhang et al., 2018), and on a global scale (Steffen et al. 2015).

References:

Alvarado JA, Steinmann P, Estier S, Bochud F, Haldimann M and Froidevaux P (2014) Anthropogenic radionuclides in atmospheric air over Switzerland during the last few decades. *Nature Communications* 5: 3030. doi: 10.1038/ncomms4030 (2014).

Anderson RS, Stegner MA, Hadly EA, Barnosky AD, La Selle SP and Sherrod B (in prep) Using paleoecology and historical records to determine environmental history in a California natural area.

Berhe AA, Fries T, Fuller CC, Harden JW and Miller LG (2007) Terrestrial sedimentation and Carbon storage in impoundments: The case of Searsville Reservoir, California. Report of 1998 Coring Results Provided to Jasper Ridge Biological Preserve. JRBP White Paper, 27 pp.

Black BA, Sydeman WJ, Frank DC et al. (2014) Six centuries of variability and extremes in a coupled marine-terrestrial ecosystem. *Science* 345: 1498-1502.

Bocek B and Reese E (1992) Land use history of Jasper Ridge Biological Preserve. *Jasper Ridge Biological Preserve Research Report No. 8,* Stanford University, USA.

Bocek B, Chiariello N, Ehrlich PR, Mooney HA, Thomas JH and Vitousek PM (1990) *Jasper Ridge - A Stanford Sanctuary.* Stanford Alumni Association, Stanford, California, 174 pp.

PSE (2022) California Power Map. Available at: https://www.psehealthyenergy.org/california-power-map/

Chappuis E, Seriñá V, Martí E, Ballesteros E and Gacia E (2017) Decrypting stable-isotope (d13C and d15N) variability in aquatic plants. *Freshwater Biology* 62: 1807-1818. DOI: 10.1111/fwb.12996

Coleman RG (2004) Geologic nature of the Jasper Ridge Biological Preserve, San Francisco Peninsula, California. *International Geology Review* 46: 629-637.

Erwin (1947a) Memo. Stanford University Archives.

Erwin (1947b) Memo. Stanford University Archives.

Felin F (1940) *The seasonal fluctuation of benthic macrofauna and limnetic plankton in Searsville Lake: a contribution to the biology of fluctuating reservoirs*. PhD Thesis, Stanford University, USA.

Foucher A, Chaboche P-A, Sabatier P and Evrard O (2021) A worldwide meta-analysis (1977-2020) of sediment dating using fallout radionuclides includings 137Cs and 210Pbxs. *Earth Syst. Sci. Data* 13: 4951-4966. https://doi.org/10.5194/essd-13-4951-2021

Franco GMM (1976) *Grazing effects on oak distribution in Jasper Ridge and adjacent areas*. MA Thesis, Stanford University, USA.

François R, Altabet MA and LH Burckle (1992) Glacial to interglacial changes in surface nitrate utilization in the Indian sector of the Southern Ocean as recorded by sediment. *Paleoceanography* 7: 589–606.

Freeborn SB (1924) *The mosquitoes of California*. PhD Thesis, University of Massachusetts, Amherst, USA.

Griffin D and Anchukaitis KJ (2014) How unusual is the 2012-2014 California drought? *Geophysical Research Letters* 41: 9017-9023.

Hendy IL, Napier TJ and Schimmelmann A (2015) From extreme rainfall to drought: 250 years of annually resolved sediment deposition in Santa Barbara Basin, California. *Quaternary International* 387: 3-12. http://dx.doi.org/10.1016/j.quaint.2015.01.026

Herwitz SR, Sandler B and Slye RE (2000) Twenty-one years of crown area change in the Jasper Ridge BiologicalPreserve based on georeferenced multitemporal aerial photographs. *International Journal of Remote Sensing* 21(1): 45-60.

Hirose K and Povinec (2015) Sources of plutonium in the atmosphere and stratosphere-troposphere mixing. *Scientific Reports* 5:15707. DOI: 10.1038/srep15707

Jones L (2021) *Memo: Some Historical Mentions of Chemical Treatment at Searsville Reservoir.* Stanford University Business Office Records. Private collection held by Land, Buildings and Real Estate, Stanford University.

JRBP (2022a) Jasper Ridge Biological Preserve Research Overview. Available at: https://jrbp.stanford.edu/research (accessed 27 June 2022)

JRBP (2022b) Jasper Ridge Biological Preserve: Visiting the preserve. Available at: https://jrbp.stanford.edu/visit

JRBP Archives (1952-1953) Note on copper sulfate and benechlor, 1952-1953. JRBP archives.

JRBP Staff (2022) Jasper Ridge Annual Reports. Available at: https://jrbp.stanford.edu/about/what-we-do/reports

Kittleson G, Hecht B and Holmes DO (1996) *Sedimentation and channel dynamics of the Searsville Lake watershed and Jasper Ridge Biological Preserve, San Mateo County, California.* Balance Hydrologics Project Assessment 9536.07

Koweek DA, García-Sánchez C, Brodrick PG, Gassett P and Caldeira K (2020) Evaluating hypoxia alleviation through induced downwelling. *Science of the Total Environment* 719: 137334. https://doi.org/10.1016/j.scitotenv.2020.137334

Meko DM, Therrell MD, Baisan CH and Hughes MK (2001) Sacramento River flow reconstructed to A.D. 869 from tree rings. *J. Amer. Water Resour. Assoc*. 37: 1029–1039.

Meko DM, Stahle DW, Griffin D and Knight TA (2011) Inferring precipitation-anomaly gradients from tree rings. *Quat. Int*. 235: 89–100.

Meyers PA and Teranes JL (2001) Sediment organic matter. In: Last WM and Smol JP (eds) *Tracking Environmental Change Using Lake Sediments. Volume 2: Physical and Geochemical Methods.* Dordrecht: Kluwer Academic Publishers.

Pampeyan EH (1993) Geologic map of the Palo Alto and part of the Redwood Point 7-1/2' quadrangles, San Mateo and Santa Clara counties, California. United States Geological Survey https://doi.org/10.3133/i2371

Redondo S (2022) *Signals of an Insidious Pollutant: Temporal, Spatial, and Biotic Interplay of Anthropogenic Mercury in a Terrestrial Ecosystem.* PhD thesis, Stanford University.

Redondo SA, Stegner MA, LaSelle SP, Sherrod B, Barnosky AD, Anderson RS, Fernandez LE and Hadly EA (in prep) Over 250 years of mercury dynamics revealed by laminated sediments from Santa Cruz Moutains, California, USA.

Rood RC (1975) *The Historical geography and environmental impact of the lumber industry of the Santa Cruz Mountains*. PhD thesis, University of California, Santa Cruz, USA.

Ruiz AM (2022) Resource Management Policies: Midpeninsula Regional Open Space District. Available at: https://www.openspace.org/sites/default/files/Resource_Management_Policies.pdf

Schidlowski M (2001) Carbon isotopes as biogeochemical recorders of life over 3.8 Ga of Earth history: evolution of a concept. *Precambrian Research* 106: 117-134.

Severson AL, Byrd BF, Mallott EK et al. (2022) Ancient and modern genomic of the Ohlone Indigenous population of California. *PNAS* 119(13):e21115333119.

Smith FW, Jr. (1963) *A comparison of the fish species composition of Searsville Reservoir, 1950-51 and 1957-58*. MA thesis, Stanford University, USA.

Stahle DW, Griffin RD, Cleaveland MK, et al (2011) A tree-ring reconstruction of the salinity gradient in the northern estuary of San Francisco Bay. San Francisco Estuary and Watershed Science Rep. 9-1, 22 pp. Available at: http://www.escholarship.org/uc/item/5cz3q8v4.

Stahle DW, Griffin RD, Meko DM et al. (2013) The ancient blue oak woodlands of California: longevity and hydro-climatic history. *Earth Interactions* 17: 1-12.

Steffen W, Broadgate W, Deutsch L, Gaffney O and Ludwig C (2015) The trajectory of the Anthropocene: The Great Acceleration. *The Anthropocene Review* 2(1): 81-98. DOI: 10.1177/2053019614564785

Stegner MA, Black BA, LaSelle SP, Hadly EA and Barnosky AD (in prep) Fitanium as an indicator of stream flow.

Stoffer P (2002) *Rocks and Geology in the San Francisco Bay Region*. USGS Bulletin 2195, 58pp.

Talbot MR (2001) Nitrogen isotopes in palaeolimnology. In: eds Last WM and Smol JP (eds) *Tracking Environmental Change Using Luke Sediments. Volume 2: Physical and Geochemical Methods.* Dordrecht: Kluwer Academic Publishers.

Viteri M (2022) Exhuming the dead to save the living: Fingerprints of the Anthropocene on California's faunal communities. PhD Thesis, Stanford University, USA.

Viteri M, Stegner MA, La Selle SP, Barnosky AD and Hadly EA (in prep) Using microcrustaceans from a high-resolution lake core to track a century of human impacts in Woodside, CA.

Waters CN, Syvitski JPM, Gałuszka A, Hancock GJ, Zalasiewicz J, Cearreta A, Grinevald J, Jeandel C, McNeill JR, Summerhayes C and Barnosky A (2015) Can nuclear weapons fallout mark the beginning of the Anthropocene Epoch? *Bulletin of the Atomic Scientists* 71(3): 46-57. DOI: 10.1177/0096340215581357

Wolfe AP, Hobbs WO, Birks HH, Briner JP, Holmgren SU, Ingolfsson O, Kaushal SS, Miller GH, Pagani M, Saros JE and Vinebrooke RD (2013) Stratigraphic expression of the Holocene-Anthropocene transition revealed in sediments from remote lakes. *Earth-Science Reviews* 116: 17-34. https://doi.org/10.1016/j.earscirev.2012.11.001

Zhang AT, Urpelainen J and Schlenker W (2018) Power of the River: Introducing the Global Dam Tracker (GDAT). Available at: https://www.energypolicy.columbia.edu/sites/default/files/pictures/GlobalDams_CGEP_2018.pdf

Appendices

Appendix 1. Searsville and Upper Lake sediment cores

Table S1.1 Searsville and Upper Lake cores collected in 2018 and 2020. Core name, date of collection, latitude/longitude, compaction, drive depth, core length, core top and bottom depths, and present status (split, scanned). SV = Searsville, UL = Upper Lake.

Site	Core ID	Date Collected	Lat	Long	Comp-action %	Drive Depth (cm)	Core length (cm)	Core top (cm)	Core Bottom (cm)	Status
SV	JRBP2018-VC01A	10/29/18	37.40683	-122.23784	24%	1140	851	289	1140	split, CT, XRF
SV	JRBP2018-VC01B	10/29/18	37.40684	-122.23788	15%	1103	944.5	158.5	1103	split, CT, XRF
SV	JRBP2018-VC02	10/30/18	37.40496	-122.23793	20%	1008	815.5	192.5	1008	split, CT
SV	JRBP2018-VC03	10/30/18	37.40328	-122.23766	29%	1041	751.5	289.5	1041	split, CT
SV	JRBP2020-VC01C	2/19/20	37.40688	-122.23789	12.70%	869.5	754.5	115	869.5	archive
SV	JRBP2020-VC01D	2/19/20	37.4069	-122.23786	14.40%	883.5	754	129.5	883.5	archive
SV	JRBP2020-VC02B	2/19/20	37.40499	-122.23801	11%	1039	927	112	1039	archive
SV	JRBP2020-VC03B	2/19/20	37.40325	-122.23763	13.40%	1036	900	136	1036	split, XRF
UL	JRUL2020-VC01A	2/20/20	37.4009	-122.24664	15.30%	410.5	351	59.5	410.5	split, CT, XRF
UL	JRUL2020-VC02	2/20/20	37.40078	-122.24683	19.60%	454	365	89	454	split, CT, XRF
UL	JRUL2020-VC03	2/20/20	37.40094	-122.24654	12.50%	373	326	47	373	split, CT, XRF

Appendix 2. CT intensity and gamma bulk density

CT intensity and Gamma bulk density (g/cc) are significantly correlated with one another. CT intensities collected at 104 micron resolution were averaged to match the depths of gamma bulk density measurements, at 1 cm resolution.

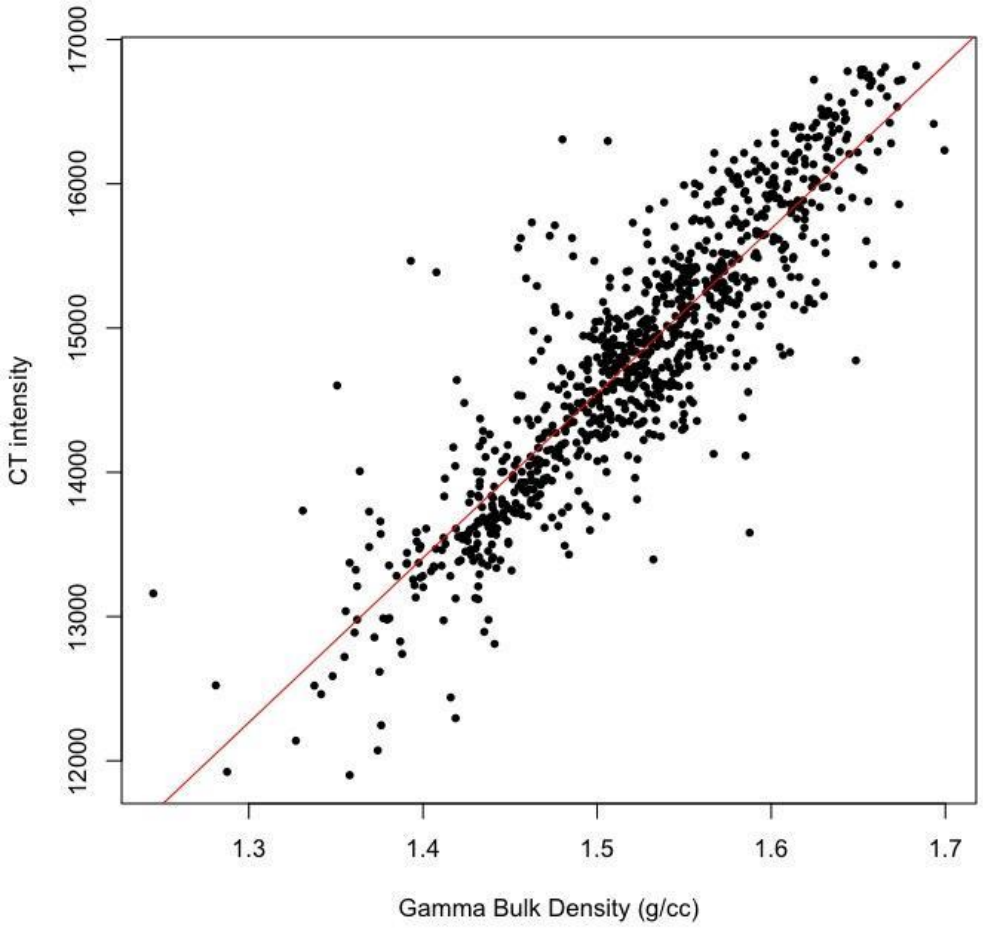

Figure S2.1 Correlation between CT intensity and gamma bulk density in Searsville core JRBP2018-VC01B. Red line is a linear regression model (Adjusted R squared = 0.78, p value < 1x10-14).

Appendix 3. Grain size analysis

Grain-size analyses were performed at the US Geological Survey Pacific Coastal and Marine Science Center. Samples were treated with hydrogen peroxide solution to remove organic materials and placed in an ultrasonic bath to liberate fine fractions. Samples were then wet-sieved through 2.0 mm and 0.063 mm sieves and separated as gravel (>2.0 mm), sand (0.063 to 2.0 mm) and mud (<0.063 mm). The sand and mud fractions were analyzed using a Beckman Coulter LS 13-320 laser diffraction particle size analyzer (Beckman Coulter Inc., Brea, CA, USA) at ¼-phi size intervals. Statistical parameters of the grain-size distribution (for example, mean grain size, Φ10, Φ 90, median, mode, standard deviation, kurtosis and skewness) of the samples are calculated using the graphic methods of Folk and Ward (1957) using pcSDSZ and GradiStat software (Blott and Pye, 2001).

Table S3.1 Grain size in Searsville core JRBP2018-VC01B. F-W = Folk and Ward

Sample Depth (cm)	D10 Phi	D50 Phi	D90 Phi	F-W Median	F-W Mean	F-W Sorting	F-W Skewness	F-W Kurtosis
160.25-161.25	6.568	8.214	10.138	8.214228	8.291326	1.373142	0.071039	0.914023
161.25-162.2	5.712	7.526	9.836	7.526075	7.659573	1.583785	0.11191	0.945605
162.25-163.25	5.35	7.208	9.712	7.207939	7.367986	1.666702	0.146243	0.907258
163.25-164.25	5.422	7.179	9.657	7.179444	7.356022	1.617399	0.166461	0.933296
254.5-255.5	4.304	6.596	9.432	6.595719	6.690065	1.969112	0.100877	0.851662
340.5-341.5	5.096	7.078	9.514	7.077596	7.168781	1.691215	0.101998	0.930636
351.5-352.5	5.481	7.262	9.59	7.261974	7.395495	1.568315	0.132302	0.966456
352.5-353.5	5.533	7.435	9.712	7.435057	7.535446	1.594803	0.089489	0.960094
353.5-354.5	7.224	8.838	10.408	8.837887	8.838968	1.232521	-0.0209	0.899954
354.5-355.5	6.553	8.044	9.912	8.044155	8.130122	1.291073	0.106116	0.959145
355.5-356.5	5.923	7.494	9.704	7.494186	7.64504	1.462444	0.150049	0.989526
356.5-357.5	5.389	7.134	9.604	7.134	7.307836	1.608897	0.168682	0.945458
357.5-358.5	5.355	7.114	9.6	7.114142	7.286208	1.618501	0.168551	0.943109
358.5-359.5	5.741	7.391	9.707	7.390628	7.553248	1.522792	0.157513	0.958395
445.5-446	6.913	8.556	10.312	8.555981	8.596818	1.314008	0.026414	0.891558
463-464	4.88	6.855	9.58	6.854606	7.011627	1.80373	0.152322	0.866928
590-591	4.712	7.294	9.672	7.293653	7.203975	1.902954	-0.04277	0.89888
783-784	4.926	6.886	9.539	6.885582	7.029455	1.771621	0.144098	0.880028
959.25-960.25	5.517	7.383	9.608	7.382603	7.470797	1.563208	0.089534	0.962906
960.75-961.75	6.133	8.173	10.143	8.173121	8.178786	1.559587	-0.03263	0.966952
993.75-994.75	5.455	7.328	9.6	7.327583	7.420849	1.586271	0.097989	0.936114
1013.25-1014.25	6.76	8.272	10.036	8.271549	8.336726	1.260649	0.07315	0.954924
1015.75-1016.75	5.813	7.693	9.833	7.693454	7.764916	1.550986	0.055042	0.964885

1017.75-1018.75	5.608	7.456	9.712	7.455843	7.563695	1.569993	0.096769	0.964731
1019.75-1020.75	7.426	8.758	10.25	8.757681	8.800322	1.094426	0.050287	0.940589
1030.75-1031.75	5.216	7.008	9.449	7.007537	7.153664	1.618331	0.153631	0.94382
1045.75-1046.75	6.757	8.322	10.105	8.321745	8.382297	1.288605	0.057675	0.950564
1061.75-1062.75	7.11	8.7	10.318	8.700272	8.71687	1.237515	0.003967	0.912056
1077.75-1078.75	5.484	7.183	9.649	7.182744	7.373667	1.590458	0.17854	0.955573
1088.75-1089.75	5.174	7.192	9.573	7.191676	7.264368	1.682445	0.083268	0.9253
1091.75-1092.7	6.31	8.116	10	8.116036	8.144942	1.436316	0.007013	0.983793

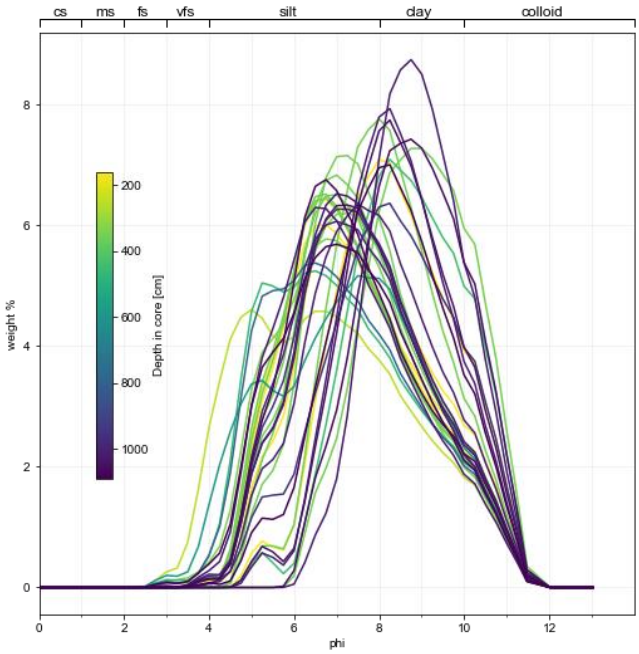

Figure S3.1 JRBP2018-VC01B grain size versus depth.

References:

Blott SJ and Pye K (2001) GRADISTAT: a grain size distribution and statistics package for the analysis of unconsolidated sediments. *Earth Surf. Proc. Land.* 26: 1237–1248.

Folk RL and Ward WC (1957) Brazos River bar: a study in the significance of grain size parameters. J. *Sediment. Petrol.* 27: 3–26.

Appendix 4. Lead-210, Cesium-137 and Ra-226

Lead-210 was determined via its gamma emissions at 46.5keV, and ^{226}Ra by the 295keV and 352keV gamma rays emitted by its daughter isotope ^{214}Pb following 3 weeks storage in sealed containers to allow radioactive equilibration. Cesium-137 and ^{241}Am were measured by their emissions at 662kev and 59.5kev (Appleby et al., 1986). The absolute efficiencies of the detector were determined using calibrated sources and sediment samples of known activity. Corrections were made for the effect of self-absorption of low energy gamma rays within the sample (Appleby et al., 1992).

Table S4.1 Lead-210 concentrations in Searsville core JRBP2018-VC01B.

		Pb-210						Cum Unsupported	
		Total		Supported		Unsupp		Pb-210	
Depth (cm)	Dry Mass (g cm^{-2})	Bq Kg^{-1}	±	Bq Kg^{-1}	±	Bq Kg^{-1}	±	Bq m^{-2}	±
162.5-163, 167.5-168	5.1823	62.08	6.82	65	2	-2.92	7.11	-49.4	260.5
192.5-193, 197.5-198	23.2078	60.87	6.34	59.11	1.81	1.76	6.59	-153.9	1033.1
247.5-248, 252.5-253	59.3759	45.81	7.03	55.16	1.86	-9.35	7.27	-1526.5	2374.9
292.5-293, 297.5-298	90.4706	59.18	5.65	60.44	1.63	-1.26	5.88	-3176.1	3276.4
347.5-348, 352.5-353	132.1913	60.58	6.03	55.01	1.63	5.57	6.25	-2277	4022.7
392.5-393, 397.5-398	164.6794	53.96	7.9	58.88	2.22	-4.92	8.21	-2171.4	4651.1
422.5-423, 427.5-428	185.8085	61.3	6.14	55.65	2.05	5.65	6.47	-2094.3	5016.3
447.5-448, 452.5-453	205.1932	59.9	8.24	64.68	2.25	-4.78	8.54	-2010	5205.8
472.5-473, 477.5-478	222.9123	62.23	6.73	50.5	1.96	11.73	7.01	-1394.2	5414.1
492.5-493, 497.5-498	237.5906	66.3	5.78	58.12	1.63	8.18	6.01	51.4	5515.1

Table S4.2 Cesium-137 concentrations in Searsville core JRBP2018-VC01B.

Depth (cm)	Cs-137 (Bq/kg)	+-	Lab
162.5-163, 167.5-168	0	0	UCL

192.5-193, 197.5-198	0	0	UCL
247.5-248, 252.5-253	0	0	UCL
292.5-293, 297.5-298	0	0	UCL
347.5-348, 352.5-353	0	0	UCL
392.5-393, 397.5-398	0	0	UCL
422.5-423, 427.5-428	9.48	1.08	UCL
447.5-448, 452.5-453	10.28	1.19	UCL
472.5-473, 477.5-478	4.64	0.78	UCL
492.5-493, 497.5-498	0	0	UCL
398-403	0		St.Croix
403-408	2.99327486	1.85	St.Croix
408-413	0		St.Croix
413-418	4.38731578	1.85	St.Croix
418-423	10.088215	1.85	St.Croix
423-428	6.97171778	1.85	St.Croix
428-433	10.5713925	1.85	St.Croix
433-438	0*		St.Croix
438-443	3.50571663*	1.85	St.Croix
443-448	9.69802528	1.85	St.Croix
448-453	9.79378463	1.85	St.Croix
453-458	6.40774823	1.85	St.Croix
458-463	0		St.Croix
463-468	0		St.Croix
468-473	0		St.Croix
473-478	0		St.Croix
478-483	0		St.Croix
483-488	0		St.Croix
488-493	0		St.Croix

* Sample was located in a storm deposit and was removed.

References

Appleby PG, Richardson N and Nolan P J (1992) Self-absorption corrections for well-type germanium detectors. *Nucl. Inst. & Methods B* 71: 228-233.

Appleby PG, Nolan PJ, Gifford DW, Godfrey MJ, Oldfield F, Anderson NJ and Battarbee RW (1986) 210Pb dating by low background gamma counting. *Hydrobiologia* 141: 21-27.

Appendix 5. Total organic carbon versus CT intensity and Titanium concentration

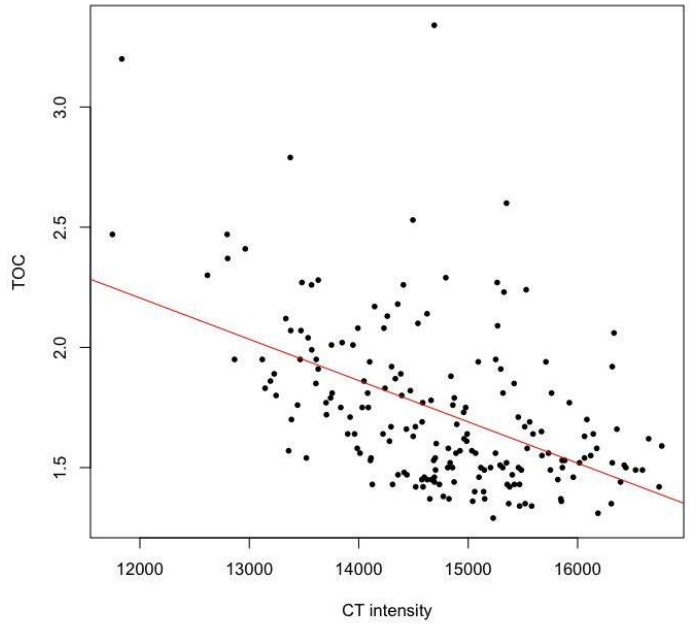

Figure S5.1 Correlation of total organic carbon (TOC) and CT intensity in Searsville core JRBP2018-VC01B. Red line shows a linear regression model (Adjusted R squared = 0.24, p-value < $1x10^{-12}$)

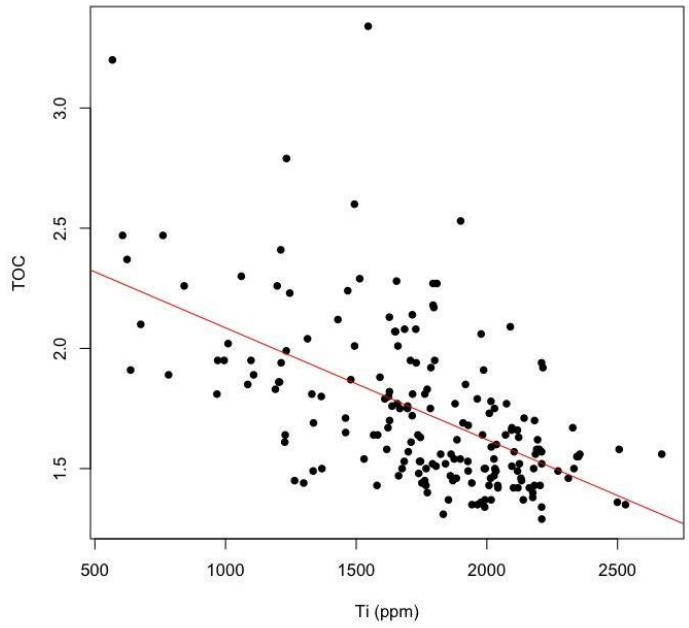

Figure S5.2. Correlation of total organic carbon (TOC) and Titanium (Ti) concentration in Searsville core JRBP2018-VC01B. Red line shows a linear regression model (Adjusted R squared = 0.32, p-value < $1x10^{-15}$)

Appendix 6. Correlation of JRBP2018-VC01A and JRBP2018-VC01B cores

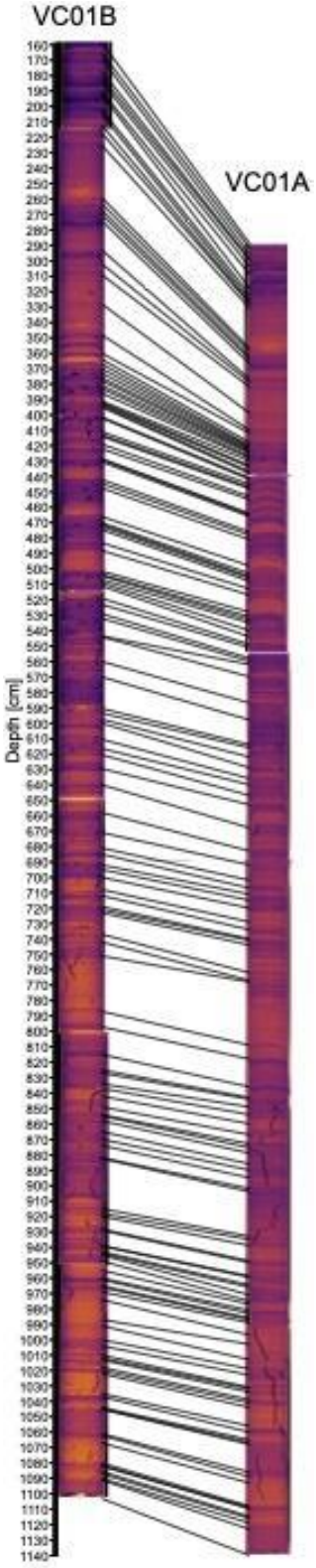

Figure S6.1. Correlation of JRBP2018-VC01A and JRBP2018-VC01B

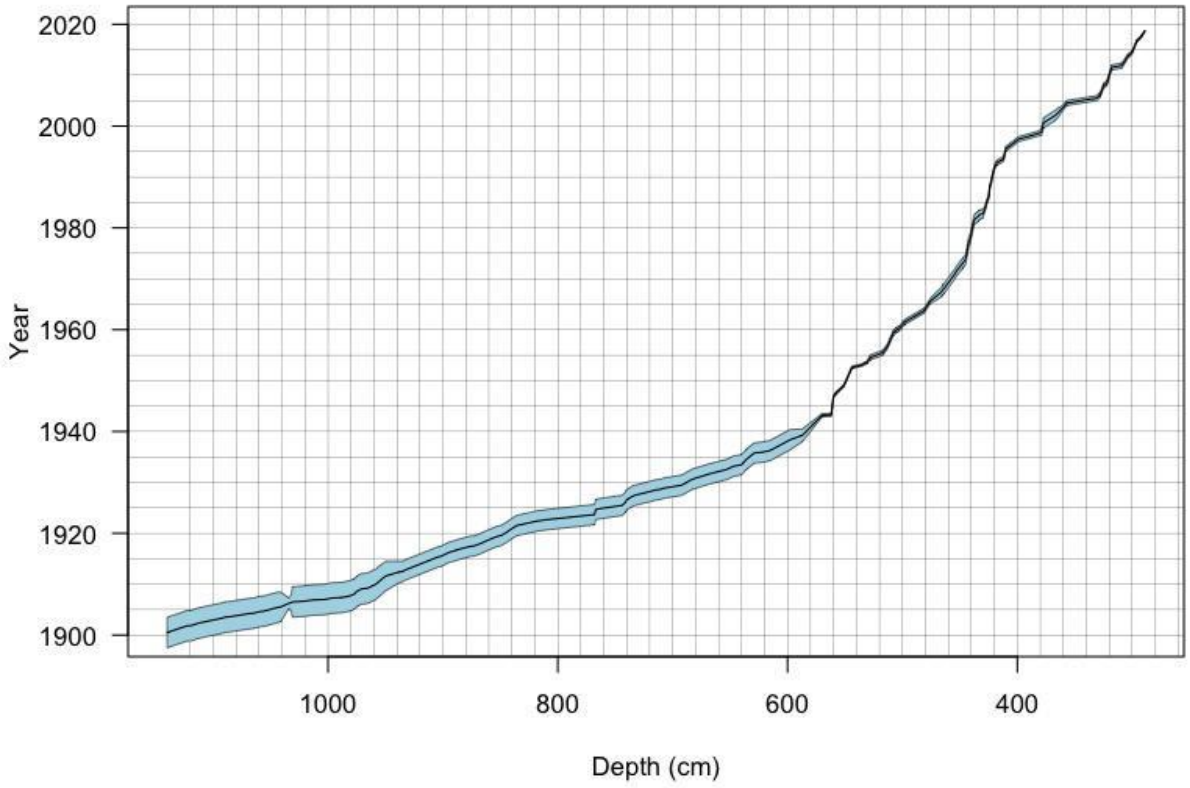

Figure S6.2. Age-Depth model for JRBP2018-VC01A.

Appendix 7. Plutonium methods and sample depths

Dry sediment samples were transferred to glass beakers and ignited at 450°C to remove organic matter present in the samples. The remaining inorganic fraction was spiked with ^{242}Pu chemical recovery tracer, mixed with lithium metaborate flux and fused at 1100°C to achieve a homogenous melt. The obtained liquid glass was quenched in deionised water and the resulting solidified glass was dissolved in 8M HNO_3 at 90°C (overnight). The resulting solution was cooled to room temperature and the precipitated boric acid, resulting from the added flux, was filtered off using a GF/A filter paper. Pu was pre-concentrated from the sample solution by means of co-precipitation with $Fe(OH)_3$ at pH 5-6. The precipitate was separated by centrifuging and re-dissolved in 9M HCl.

The 9M HCl solutions were transferred to anion exchange columns (1x8, chloride form, 5cm high, 0.9cm internal diameter), previously pre-conditioned with 9M HCl. Pu was retained on the columns and was purified by sequential washes with 9M HCl (30ml), 8M HNO_3 (50ml) and again with 9M HCl (10ml). Finally, the Pu fraction was eluted to pre-cleaned beakers using 40ml of 0.1M NH_4I/9M HCl solution. The solution was evaporated to dryness with 5ml of conc. HNO_3 added to remove excess iodine present and thin alpha spectrometric sources were prepared by electrodeposition.

Each source was then counted using Octete (Ortec/Amtek) alpha spectrometers equipped with PIPS detectors. The resulting spectra were analyzed using Maestro spectral analysis software. Following counting, $^{240}Pu/^{239}Pu$ ratios were determined using a Thermo Scientific Neptune Plus MC-ICP-MS after radiochemical re-purification of the Pu alpha spectrometry discs, following Lokas et al. (2022).

Table S7.1 Plutonium concentrations and ratios in Searsville core JRBP2018-VC01B.

GAU IDs	Depths (cm)	$^{239,240}Pu$ (Bq/g)	+/-	^{238}Pu (Bq/g)	+/-	$^{238}Pu/^{239,240}Pu$	+/-	$^{240}Pu/^{239}Pu$	Pu 2σ error
GAU4200/3-1 + GAU4200/3-2	162.5-163, 167.5-168	0.0000659	$3.39x10^{-05}$	$3.15x10^{-05}$	$2.13x10^{-05}$	0.47827684	0.81186165		
GAU4200/3-7 + GAU4200/3-8	292.5-293, 297.5-298	0.00021992	$6.10x10^{-05}$	$6.59x10^{-05}$	$4.16x10^{-05}$	0.29975336	0.41322112		
GAU4200/3-9 + GAU4200/3-10	347.5-348, 352.5-353	0.00013406	$4.41x10^{-05}$	$4.95x10^{-05}$	$3.21x10^{-05}$	0.36940081	0.53651493		
GAU4200/3-11 + GAU4200/3-12	367.5-368, 377.5-378	0.00016906	$5.56x10^{-05}$	$7.28x10^{-05}$					
GAU4200/3-13 + GAU4200/3-14	392.5-393, 397.5-398	0.00012391	$4.50x10^{-05}$	$7.58x10^{-05}$	$3.48x10^{-05}$	0.6119367	0.71582222		
GAU4200/3-15	402.5-403	0.0003911	$7.08x10^{-05}$	0.00010737	$4.39x10^{-05}$				
GAU4200/3-16 + GAU4200/3-17	407.5-408, 412.5-413	NA	NA	NA					
GAU4200/3-18	417.5-418	0.00015775	$4.08x10^{-05}$	$5.49x10^{-05}$					
GAU4200/3-19 + GAU4200/3-20	422.5-423, 427.5-428	0.00038264	$8.31x10^{-05}$	$5.32x10^{-05}$	$3.44x10^{-05}$	0.13894893	0.18980142	0.223	0.007

GAU4200/3-433	432.5-433	0.00049863	0.00010039	9.42x10^{-05}	4.61x10^{-05}	0.18900355	0.19987817	0.189	0.038
GAU4200/3-22 + GAU4200/3-23	437.5-438, 442.5-443	0.00019218	5.23x10^{-05}	2.49x10^{-05}	1.68x10^{-05}	0.129818	0.1888408	0.187	0.011
GAU4200/3-24 + GAU4200/3-25	447.5-448, 452.5-453	0.0007526	0.00014807	9.99x10^{-05}				0.186	0.005
GAU4200/3-27 + GAU4200/3-28	462.5-463, 467.5-468	0.00023412	5.99x10^{-05}	4.70x10^{-05}				0.191	0.01
GAU4200/3-29 + GAU4200/3-30	472.5-473, 477.5-478	0.00038416	8.86x10^{-05}	5.34x10^{-05}	NA			0.204	0.008
GAU4200/3-31 + GAU4200/3-32	483.5-483, 487.5-488	0.00012167	4.69x10^{-05}	7.07x10^{-05}	NA				
GAU4200/3-33 + GAU4200/3-34	492.5-493, 497.5-498	0.00012381	4.50x10^{-05}	6.06x10^{-05}	3.10x10^{-05}	0.48960229	0.61356134		
GAU4200/3-35 + GAU4200/3-36	502.5-503, 507.5-508	9.16x10^{-05}	4.02x10^{-05}	6.37x10^{-05}	NA				
GAU4200/3-37 + GAU4200/3-38	512.5-513, 517.5-518	3.92x10^{-05}	2.65x10^{-05}	5.89x10^{-05}	NA				
GAU4200/3-39 + GAU4200/3-40	522.5-523, 527.5-528	5.78x10^{-05}	3.62x10^{-05}	7.35x10^{-05}	NA				
GAU4200/3-41 + GAU4200/3-42	532.5-533, 537.5-538	0	NA	8.49x10^{-05}	NA				

Appendix 8. SCPs

Dried sediment was subjected to sequential chemical attack by mineral acids to remove unwanted fractions leaving a suspension of mainly carbonaceous material and a few persistent minerals in water. SCPs are composed mostly of elemental carbon and are chemically robust. The use of concentrated nitric acid (to remove organic material), hydrofluoric acid (siliceous material) and hydrochloric acid (carbonates and bicarbonates) therefore does them no damage. A known fraction of the final suspension was evaporated onto a coverslip and mounted onto a microscope slide. The number of SCPs on the coverslip were counted using a light microscope at x450 magnification and the sediment concentration calculated in units of 'number of particles per gram dry mass of sediment' (gDM^{-1}).

The criteria for SCP identification under the light microscope followed Rose (2008). The detection limit for the technique is typically c. 100 gDM^{-1} and concentrations have an accuracy of c. ± 45 gDM^{-1} (Rose 2008) although detection limits were higher in JRBP2018-VC01B (typically 250 - 450 gDM^{-1}). Analytical blanks and SCP reference material were included in duplicate and triplicate respectively. Reference concentrations agreed closely with expected values (6005 ± 70 gDM^{-1}) while no SCPs were observed in the blanks.

Table S8.1 SCP counts and concentrations in Searsville core JRBP2018-VC01B.

Depth (cm)	SCP count	SCP conc (gDM-1)	Upper 90% C.L. (gDM-1)	Lower 90% (gDM-1)	Dry weight (fraction)	Wet density (g/cm^3)	Dry Bulk Density (g/cm^3)
167.5-168	1	379	750	8	0.48	1.4838	0.7122
197.5-198	1	446	883	9	0.3405	1.374	0.4678
222.5-223	3	1280	2005	556	0.5075	1.5145	0.7686
252.5-253	3	1132	1773	492	0.5326	1.5738	0.8382
272.5-273	1	284	562	6	0.435	1.4485	0.6301
297.5-298	0	0	0	0	0.3967	1.4575	0.5782
317.5-318	2	668	1130	205	0.5052	1.484	0.7497
332.5-333	2	745	1261	229	0.5282	1.5283	0.8072
347.5-348	1	444	879	9	0.4703	1.5853	0.7456
352.5-353	1	314	622	6	0.5123	1.5526	0.7954
357.5-358	2	550	930	169	0.5402	1.5698	0.8481
362.5-363	1	403	797	8	0.5339	1.5664	0.8363
367.5-368	1	339	670	7	0.4706	1.4777	0.6954
372.5-373	2	642	1086	197	0.5365	1.4759	0.7918
377.5-378	0	0	0	0	0.474	1.4398	0.6824
382.5-383	1	295	583	6	0.427	1.3614	0.5813

387.5-388	0	0	0	0	0.4632	1.4261	0.6605
392.5-393	1	325	643	6	0.4911	1.4724	0.7231
397.5-398	2	570	965	175	0.4759	1.4525	0.6913
402.5-403	1	297	588	6	0.3801	1.4046	0.5339
407.5-408	4	1578	2351	805	0.4518	1.4651	0.6619
412.5-413	5	2042	2938	1147	0.5517	1.495	0.8248
417.5-418	1	283	560	6	0.5122	1.4518	0.7436
422.5-423	5	1646	2367	924	0.4393	1.4669	0.6444
427.5-428	4	1008	1501	514	0.5121	1.4981	0.7671
432.5-433	1	264	522	5	0.4386	1.4217	0.6236
437.5-438	4	956	1425	488	0.563	1.5687	0.8832
442.5-443	1	323	640	6	0.4338	1.449	0.6286
447.5-448	0	0	0	0	0.4463	1.4066	0.6278
452.5-453	2	797	1349	245	0.4472	1.4244	0.637
457.5-458	0	0	0	0	0.4973	1.4761	0.734
462.5-463	0	0	0	0	0.6009	1.6192	0.9729
467.5-468	2	649	1098	199	0.4857	1.4948	0.726
472.5-473	1	416	823	8	0.441	1.2451	0.5491
477.5-478	0	0	0	0	0.4737	1.4492	0.6865
482.5-483	0	0	0	0	0.492	1.5467	0.7609
487.5-488	0	0	0	0	0.4772	1.4621	0.6977
492.5-493	0	0	0	0	0.5573	1.5804	0.8807
497.5-498	3	1331	2084	578	0.5604	1.5826	0.887
502.5-503	4	1345	2004	686	0.4463	1.4623	0.6527
507.5-508	0	0	0	0	0.455	1.484	0.6752
512.5-513	0	0	0	0	0.4663	1.4741	0.6874
517.5-518	1	329	650	7	0.5393	1.4862	0.8015
522.5-523	0	0	0	0	0.4712	1.4777	0.6963
527.5-528	3	930	1457	404	0.4611	1.4257	0.6574
532.5-533	0	0	0	0	0.4603	1.4189	0.6531
537.5-538	1	304	601	6	0.4731	1.4394	0.681

547.5-548	3	854	1338	371	0.4375	1.331	0.5823
562.5-563	1	535	1059	11	0.4787	1.4794	0.7082
577.5-578	1	351	696	7	0.4419	1.4202	0.6276
592.5-593	2	920	1558	283	0.5276	1.4592	0.7699
607.5-608	1	467	924	9	0.5663	1.5813	0.8955
637.5-638	0	0	0	0	0.5641	1.5912	0.8976
667.5-668	0	0	0	0	0.5676	1.5772	0.8952
697.5-698	0	0	0	0	0.4731	1.4706	0.6957
727.5-728	0	0	0	0	0.5333	1.549	0.8261
757.5-758	0	0	0	0	0.5889	1.5651	0.9217
787.5-788	0	0	0	0	0.5899	1.572	0.9273
817.5-818	0	0	0	0	0.5663	1.4077	0.7972
847.5-848	0	0	0	0	0.5337	1.4634	0.781
882.5-883	0	0	0	0	0.4948	1.4917	0.7381
912.5-913	0	0	0	0	0.5661	1.5559	0.8808
942.5-943	0	0	0	0	0.6056	1.5673	0.9492
972.5-973	0	0	0	0	0.5805	1.5867	0.9211
1002.5-1003	0	0	0	0	0.544	1.5496	0.843
1032.5-1033	0	0	0	0	0.6139	1.6429	1.0086
1062.5-1063	0	0	0	0	0.5185	1.5289	0.7927
1092.5-1093	0	0	0	0	0.5625	1.5528	0.8735

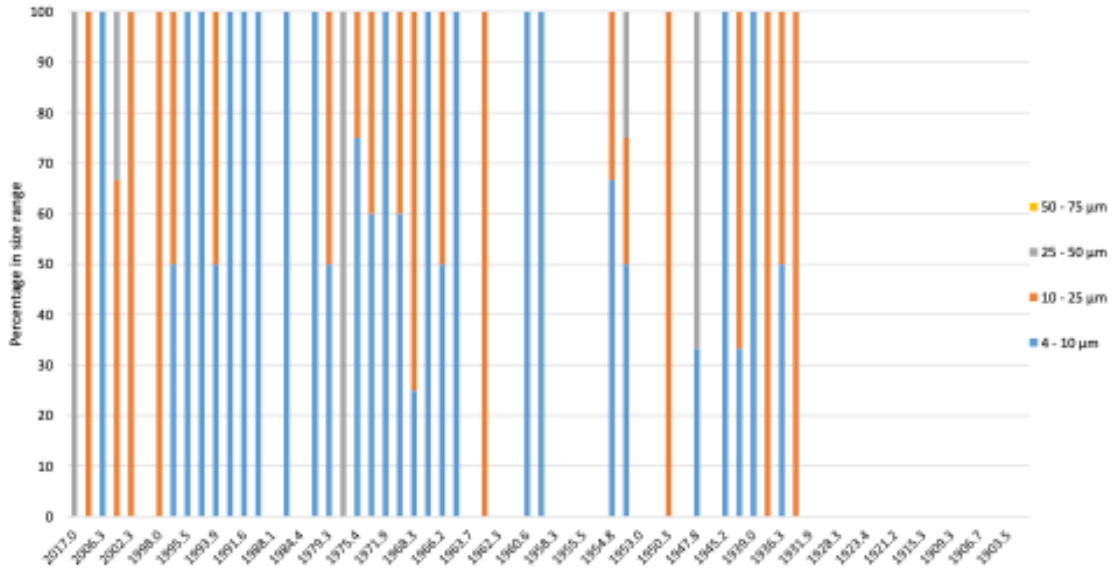

Figure S8.1 JRBP2018-VC01B SCP size distribution.

Appendix 9. PCBs

Table S9.1 Combined PCB samples and number of congeners detected in Searsville core JRBP2018-VC01B.

Depth (cm)	N congeners detected
160-159	2
172-171	
188-187	
204-203	
220-219	
236-235	
252-251	
268-267	
284-283	
300-299	
316-315	7
332-331	
348-347	
364-363	
380-379	
396-395	
412-411	
428-427	
444-443	
460-459	
476-475	1
492-491	

508-507	
524-523	
540-539	
556-555	
572-571	
588-587	
604-603	
620-619	
636-635	0
652-651	
668-667	
684-683	
700-699	
716-715	
732-731	
748-747	
764-763	
780-779	
796-795	0
812-811	
828-827	
844-843	
860-859	
876-875	
892-891	
908-907	

924-923	
940-939	
956-955	0
972-971	
988-987	
1004-1003	
1020-1019	
1036-1035	
1052-1051	
1068-1067	
1084-1083	
1100-1099	

Appendix 10. Carbon and Nitrogen Analysis

Freeze dried sediment samples were crushed and loaded into tin (for N analysis) and silver (for C analysis) capsules. To remove carbonates ($CaCO_3$), C samples were acidified with 6% H_2SO_3 solution (Verardo et al. 1990). Acidification can remove some of the N components, so samples for N analysis were run without acid treatment (Moy et al. 2008). L-glutamic acid (USGS-40) and caffeine (IAEA-600) were used as standards. Samples were analyzed using a Carlo Erba NA1500 Series 2 elemental analyzer coupled to a Finnigan Delta Plus isotope ratio mass spectrometer via a Finnigan Conflo II open split interface. We use standard delta notation, reporting $\delta^{13}C$ relative to the Vienna Pee Dee Belemnite (VPDB) carbonate standard and $\delta^{15}N$ relative to air. Weight % N, % total organic carbon (TOC), and C:N ratio were calculated from the acidified runs. Weight % inorganic carbon (IC) and % $CaCO_3$ were calculated as the difference between total carbon from the un-acidified runs minus TOC from the acidified runs.

Table S10.1 Carbon and Nitrogen total percent weight and stable isotopes in Searsville core JRBP2018-VC01B. TOC = Total organic Carbon; IC = inorganic Carbon.

Depth (cm)	Wt. % N	Wt. % TOC	$d^{15}N$	$d^{13}C$	C:N	Est Wt%IC	Est. %$CaCO_3$
162-162.5	0.18	1.8	3.71	-25.42	11.95	0.1	0.837
167-167.5	0.18	1.86	3.83	-24.9	12.17	0.156	1.303
172-172.5	0.18	1.95	3.73	-25.59	12.58	0.204	1.697
177-177.5	0.18	1.95	3.41	-25.69	12.5	0.195	1.627
182-182.5	0.18	1.89	3.34	-25.93	12.03	0.215	1.795
187-187.5	0.26	2.47	2.56	-27.71	11.07	0.068	0.563
192-192.5	0.26	2.47	2.63	-27.76	11.18	0.201	1.678
197-197.5	0.34	3.2	1.81	-28.93	11.09	0.594	4.95
202-202.5	0.24	2.3	2.95	-27.5	11.33	0.132	1.101
207-207.5	0.25	2.37	2.16	-27.49	10.98	0.229	1.911
212-212.5	0.19	2.1	3.31	-25.91	12.78	0.111	0.927
217-217.5	0.19	1.79	3.88	-25.88	11.23	0.166	1.381
222-222.5	0.16	1.47	3.52	-25.56	11.02	0.158	1.317
227-227.5	0.19	2.08	3.21	-25.9	12.98	0.156	1.303
232-232.5	0.18	1.92	3.06	-25.8	12.76	0.211	1.756
237-237.5	0.21	2.53	2.86	-26.31	14.23	0.011	0.091
242-242.5	0.19	2.14	3.32	-25.87	13.02	0.104	0.865
247-247.5	0.19	2.29	3.26	-26.29	14.09	0.062	0.516

252-252.5	0.2	2.27	3.2	-26.18	13.47	0.078	0.652
257-257.5	0.16	1.81	2.97	-26.17	13.15	0.099	0.826
262-262.5	0.23	3.34	2.24	-26.85	17.15	0.141	1.175
267-267.5	0.24	2.17	2.72	-27.74	10.64	-0.213	-1.773
272-272.5	0.17	1.54	3.67	-25.15	10.53	0.148	1.234
277-277.5	0.26	2.41	2.75	-28.1	10.8	0.38	3.17
282-282.5	0.17	1.69	3.64	-25.07	11.32	0.166	1.379
287-287.5	0.17	1.77	3.29	-25.42	12.02	0.189	1.578
292-292.5	0.17	1.79	3.42	-25.46	12.38	0.265	2.209
297-297.5	0.22	2.02	3.44	-27.15	10.56	0.167	1.396
302-302.5	0.18	1.64	3.7	-25.97	10.33	0.032	0.266
307-307.5	0.16	1.53	3.46	-25.21	11.27	0.19	1.585
312-312.5	0.18	1.88	3.32	-25.11	11.88	0.174	1.453
317-317.5	0.18	1.94	3.51	-25.5	12.42	0.213	1.773
322-322.5	0.19	2.23	3.14	-25.55	13.38	0.341	2.84
327-327.5	0.2	2.26	3.08	-26.02	12.97	0.156	1.301
332-332.5	0.18	1.81	3.44	-25.65	11.56	0.205	1.708
337-337.5	0.19	1.95	3.35	-26.07	12.02	0.136	1.132
342-342.5	0.17	1.65	3.39	-26.16	11.29	0.118	0.979
347-347.5	0.19	1.67	3.55	-25.8	10.4	0.035	0.292
352-352.5	0.2	2.24	3.2	-25.49	12.87	-0.228	-1.9
357-357.5	0.19	1.85	3.25	-25.23	11.32	0.029	0.241
362-362.5	0.18	1.5	3.48	-25.08	9.88	0.059	0.488
367-367.5	0.24	2.13	3.46	-26.33	10.39	0.188	1.564
372-372.5	0.2	1.63	3.84	-24.97	9.74	0.029	0.244
377-377.5	0.26	2.28	3.23	-27.2	10.17	0.181	1.509
382-382.5	0.25	2.12	3.44	-25.89	9.96	0.117	0.973
387-387.5	0.25	2.07	3.47	-27.46	9.5	0.237	1.977
392-392.5	0.22	1.82	3.85	-26.32	9.59	-0.164	-1.366
397-397.5	0.19	1.64	4	-26.02	9.88	0.058	0.482
402-402.5	0.27	2.27	3.27	-29.42	9.85	0.216	1.8

407-407.5	0.25	1.75	3.65	-25.95	8.24	0.017	0.138
412-412.5	0.19	1.67	3.86	-25.76	10.52	0.099	0.826
417-417.5	0.2	1.71	3.84	-25.51	9.86	0.071	0.592
422-422.5	0.25	2.18	3.43	-27.39	10.32	0.285	2.374
427-427.5	0.19	1.66	3.58	-25.09	10.39	0.059	0.491
432-432.5	0.21	1.7	4.04	-25.4	9.67	0.032	0.269
437-437.5	0.19	2.09	2.88	-25.54	12.73	0.101	0.84
442-442.5	0.23	1.75	3.47	-26.06	8.98	0.057	0.474
447-447.5	0.21	1.57	3.97	-25.57	8.53	0.088	0.73
452-452.5	0.22	1.76	4.02	-26.9	9.43	0.225	1.875
457-457.5	0.19	1.56	4.17	-24.98	9.57	0.043	0.355
462-462.5	0.17	1.67	3.71	-25.68	11.61	0.18	1.501
467-467.5	0.19	1.54	3.64	-24.95	9.52	0.148	1.23
472-472.5	0.23	1.95	3.37	-27.42	10.04	0.505	4.207
477-477.5	0.21	1.77	3.82	-26.38	9.93	0.237	1.977
482-482.5	0.17	1.45	3.97	-24.86	9.88	0.13	1.086
487-487.5	0.2	1.72	4.02	-24.88	9.88	-0.017	-0.142
492-492.5	0.17	1.5	3.81	-25.54	10.43	0.069	0.574
497-497.5	0.18	1.94	3.49	-25.94	12.22	0.096	0.801
502-502.5	0.24	2.08	3.71	-27.5	9.94	0.263	2.192
507-507.5	0.2	1.73	4.11	-25.65	10.07	0.023	0.194
512-512.5	0.22	1.83	4.23	-25.28	9.81	0.035	0.293
517-517.5	0.19	1.58	4.08	-25.03	9.74	0.04	0.333
522-522.5	0.25	2.07	4.13	-26.56	9.73	0.146	1.217
527-527.5	0.24	2.04	3.55	-26.79	9.9	0.182	1.519
532-532.5	0.24	1.99	3.71	-26.78	9.76	0.186	1.552
537-537.5	0.22	1.91	3.84	-26.4	9.96	0.178	1.487
542-542.5	0.23	1.95	3.62	-26.93	10.03	0.106	0.88
547-547.5	0.21	1.81	4.06	-26	9.94	0.109	0.907
552-552.5	0.17	1.64	3.94	-25.5	11.02	0.149	1.243
557-557.5	0.17	1.45	4.1	-24.94	9.77	0.061	0.512

562-562.5	0.21	1.83	3.96	-26.83	9.98	0.233	1.944
567-567.5	0.22	1.86	4.2	-25.9	9.77	0.053	0.441
572-572.5	0.23	1.94	3.84	-26.93	9.64	0.243	2.021
577-577.5	0.28	2.26	3.71	-27.25	9.44	-0.079	-0.657
582-582.5	0.33	2.79	3.74	-27.97	9.8	-0.425	-3.538
587-587.5	0.23	1.85	4.15	-26.72	9.56	-0.011	-0.09
592-592.5	0.29	2.6	3.02	-28.8	10.28	0.367	3.056
597-597.5	0.2	1.49	4.03	-25.48	8.79	-0.023	-0.19
602-602.5	0.22	1.89	4.14	-27.14	10.19	0.109	0.906
607-607.5	0.17	1.71	3.91	-25.62	11.51	0.213	1.771
612-612.5	0.18	1.61	3.97	-25.9	10.48	0.012	0.104
617-617.5	0.22	1.8	3.77	-26.24	9.55	0.219	1.821
622-622.5	0.19	1.61	4.43	-25.13	9.75	-0.099	-0.825
627-627.5	0.24	2.01	3.51	-26.31	9.7	0.271	2.255
632-632.5	0.19	1.58	4.02	-24.97	9.49	-0.043	-0.359
637-637.5	0.18	1.69	3.94	-25.71	11.15	0.127	1.061
642-642.5	0.21	1.64	4.26	-25.49	9.07	-0.052	-0.433
647-647.5	0.19	1.68	4.45	-25.53	10.21	-0.094	-0.787
652-652.5	0.16	1.36	4.09	-25.37	9.81	0.042	0.347
657-657.5	0.19	1.75	4.07	-25.83	10.63	0.073	0.605
662-662.5	0.17	1.47	4.42	-25.15	9.89	0.196	1.633
667-667.5	0.17	1.46	4.01	-25.26	9.93	-0.025	-0.209
672-672.5	0.21	1.75	4.27	-25.72	9.75	0.265	2.204
677-677.5	0.16	1.43	3.73	-25.12	10.27	0.138	1.153
682-682.5	0.18	1.62	4.04	-25.08	10.58	0.063	0.526
687-687.5	0.18	1.49	4.12	-25.04	9.8	0.017	0.145
692-692.5	0.23	2.01	3.46	-27.07	10.11	1.188	9.901
697-697.5	0.21	1.87	3.61	-26.45	10.18	0.73	6.083
702-702.5	0.16	1.43	3.83	-25.08	10.22	0.094	0.78
707-707.5	0.18	1.92	3.67	-25.66	12.26	0.114	0.954
712-712.5	0.18	1.43	4	-24.97	9.32	-0.006	-0.052

717-717.5	0.17	1.49	3.86	-25.6	10.28	0.089	0.742
722-722.5	0.19	1.5	3.77	-26.07	9.46	0.26	2.163
727-727.5	0.17	1.4	4.23	-25	9.71	0.234	1.95
732-732.5	0.17	1.44	3.96	-24.95	10.13	0.208	1.73
737-737.5	0.16	1.46	4.31	-24.84	10.48	0.254	2.119
742-742.5	0.18	1.54	4.01	-25.22	10.04	0.311	2.59
747-747.5	0.17	1.44	4.37	-24.88	9.63	0.144	1.204
752-752.5	0.17	1.37	4.24	-24.79	9.33	0.118	0.982
757-757.5	0.17	1.43	4.21	-25.11	9.81	0.157	1.312
762-762.5	0.17	1.52	4.14	-25.41	10.44	0.212	1.771
767-767.5	0.17	1.64	3.85	-25.65	11.19	0.209	1.74
772-772.5	0.17	1.7	3.65	-25.54	11.73	0.317	2.642
777-777.5	0.18	1.91	3.65	-25.77	12.43	0.278	2.319
782-782.5	0.18	2.06	3.34	-25.82	13.04	0.253	2.107
787-787.5	0.17	1.34	4.21	-25.08	9.11	0.058	0.487
792-792.5	0.15	1.37	3.84	-25.11	10.83	0.316	2.635
797-797.5	0.18	1.43	4.36	-24.81	9.32	0.259	2.161
802-802.5	0.18	1.56	4.37	-25.54	10.42	0.13	1.086
807-807.5	0.18	1.52	4.07	-25.67	10.09	0.374	3.119
812-812.5	0.16	1.37	4.15	-24.88	9.96	0.332	2.766
817-817.5	0.16	1.37	4.16	-24.81	10.27	0.193	1.609
822-822.5	0.16	1.42	3.82	-25.2	10.33	0.2	1.669
827-827.5	0.17	1.42	4.21	-25.64	9.87	0.17	1.415
832-832.5	0.16	1.38	4.24	-25.73	9.78	0.347	2.889
837-837.5	0.16	1.29	4.1	-25.26	9.54	0.112	0.932
842-842.5	0.16	1.56	4.05	-25.57	11.63	0.391	3.259
847-847.5	0.17	1.42	4.38	-25.4	9.52	0.046	0.385
852-852.5	0.2	1.6	3.86	-25.74	9.57	0.24	2
857-857.5	0.18	1.5	4.23	-25.07	9.52	0.066	0.553
862-862.5	0.17	1.43	4.21	-25.17	9.86	0.323	2.689
867-867.5	0.21	1.78	4.07	-25.48	9.85	0.475	3.962

872-872.5	0.18	1.57	4.52	-25.2	10.22	0.233	1.942
877-877.5	0.17	1.56	4.32	-25.15	10.51	0.214	1.784
882-882.5	0.2	1.76	4.6	-25.73	10.18	0.643	5.36
887-887.5	0.18	1.58	4.45	-25.34	10.29	0.27	2.251
892-892.5	0.18	1.53	4.62	-25.21	9.68	0.285	2.379
897-897.5	0.18	1.56	4.34	-25.45	10	0.31	2.581
902-902.5	0.18	1.57	4.76	-25.41	9.98	0.296	2.467
907-907.5	0.18	1.48	4.89	-24.64	9.79	0.103	0.858
912-912.5	0.16	1.35	4.59	-24.94	9.82	0.137	1.144
917-917.5	0.2	1.77	4.85	-26.45	10.06	1.425	11.876
922-922.5	0.16	1.55	4.33	-25.33	11	0.228	1.898
927-927.5	0.16	1.36	4.69	-25.18	9.92	0.28	2.335
932-932.5	0.16	1.46	4.34	-24.92	10.93	0.284	2.365
937-937.5	0.17	1.55	4.36	-25.26	10.36	0.207	1.728
942-942.5	0.16	1.34	4.54	-25.14	9.59	0.152	1.265
947-947.5	0.19	1.64	4.01	-25.35	10.27	0.439	3.66
952.5-953	0.17	1.52	4.29	-25.2	10.4	0.3	2.504
957-957.5	0.16	1.58	3.8	-25.27	11.72	0.411	3.428
962-962.5	0.29	1.81	4.24	-24.97	7.23	-0.042	-0.349
967-967.5	0.17	1.46	4.69	-24.81	10.07	0.064	0.53
972-972.5	0.15	1.45	4.24	-25.04	11.15	0.297	2.478
977-977.5	0.14	1.44	4.22	-25.1	11.98	0.329	2.746
982-982.5	0.14	1.51	4.3	-25.32	12.5	0.385	3.209
987-987.5	0.15	1.66	4.31	-25.54	12.74	0.318	2.65
992-992.5	0.16	1.53	3.95	-25.13	11.44	0.372	3.096
997-997.5	0.16	1.63	4.08	-25.64	11.99	0.428	3.57
1002-1002.5	0.18	1.5	4.59	-25.73	9.77	0.407	3.389
1007-1007.5	0.15	1.35	4.99	-25.14	10.19	0.158	1.314
1012-1012.5	0.15	1.31	4.67	-25.25	10.39	0.461	3.842
1017-1017.5	0.16	1.4	4.66	-24.9	9.97	0.165	1.374
1022-1022.5	0.14	1.35	4.52	-24.97	11.06	0.309	2.573

1027-1027.5	0.14	1.42	4.61	-25.2	11.97	0.315	2.624
1032-1032.5	0.15	1.49	4.64	-25.18	11.93	0.4	3.335
1037-1037.5	0.18	1.5	4.52	-24.82	9.89	0.189	1.572
1042-1042.5	0.17	1.54	4.48	-25.32	10.29	0.181	1.51
1047-1047.5	0.2	1.52	4.56	-25.41	10	0.312	2.597
1052-1052.5	0.18	1.5	4.72	-25.49	9.7	0.209	1.739
1057-1057.5	0.19	1.51	4.85	-25.58	9.27	0.198	1.649
1062-1062.5	0.19	1.45	4.54	-24.91	9.11	0.087	0.722
1067-1067.5	0.16	1.5	4.67	-25.24	10.91	0.339	2.825
1072-1072.5	0.17	1.59	4.62	-25.74	11.04	0.157	1.311
1077-1077.5	0.17	1.62	5.08	-26.11	10.89	0.043	0.361
1082-1082.5	0.2	1.53	4.54	-25.57	9.09	0.081	0.678
1087-1087.5	0.16	1.49	4.9	-25.8	11.06	0.446	3.72
1092-1092.5	0.17	1.47	4.62	-25.37	10.14	0.267	2.228
1097-1097.5	0.17	1.49	5.02	-25.55	10.1	0.278	2.318
1102-1102.5	0.19	1.55	4.51	-26.07	9.72	0.181	1.505

Appendix 11. ICPMS Analysis

Major and trace element concentrations in Searsville core JRBP2018-VC01B. See file Appendix11-JRBP2018-VC01B_ICPMS.csv

Lead isotope ratios in Searsville core JRBP2018-VC01B.

Table S11.1 Pb isotope ratios in Searsville core JRBP2018-VC01B.

Depth (cm)	$^{206}Pb/^{208}Pb$	$^{206}Pb/^{207}Pb$	$^{206}Pb/^{204}Pb$
222-222.5	0.46105275	1.21615757	19.1103576
262-262.5	0.46016331	1.20575405	18.8192576
312-312.5	0.46094583	1.2109642	18.9300822
337-337.5	0.46065551	1.21247569	18.9526656
352-352.5	0.46133072	1.21323855	18.9521852
427-427.5	0.46041607	1.2084735	18.9242038
462-462.5	0.4612485	1.21567054	19.0704954
517-517.5	0.46030681	1.21062081	19.017403
557-557.5	0.46146167	1.21705238	19.1257929
617-617.5	0.46003133	1.20917446	18.8919814
672-672.5	0.46064854	1.21610456	19.059463
727-727.5	0.46023629	1.21643808	19.0504648
772-772.5	0.45958068	1.21654092	19.1472861
812-812.5	0.46031876	1.21674605	19.0514471
867-867.5	0.46071769	1.21656079	19.0785163
922-922.5	0.46048293	1.21812272	19.1168719
972-972.5	0.46069192	1.21917956	19.1859995
1022-1022.5	0.46005251	1.21505209	19.0571517

1072-1072.5	0.4514032	1.17382973	18.4431819
1102-1102.5	0.46064092	1.21652523	19.1047414

Appendix 12. Mercury Analysis

For Mercury (Hg) analysis, samples (n=188) of ~0.3g and 0.5 cm thick were collected at 5 cm intervals starting at a base depth of 1103 cm (Appendix X). Samples were packed into clean glass vials, stored at −20°C, dried, and ground using mortar and pestle (clean technique). Total Hg content was analyzed at the Stanford Carnegie Institute Department of Global Ecology by thermal decomposition followed by preconcentration of Hg on a gold trap and cold vapor atomic absorption spectrophotometry using a DMA-80 direct Hg analyzer (Milestone, CT, USA). Approximately 50 mg of dried and homogenized sediment was processed per run with a Method Detection Limit of 2 ng/g. Samples of certified reference material (TIL-3 and BCR-482) were analyzed every 10 samples and were within acceptable recovery limits. Blanks were run every 10 samples as well as before and after reference material to limit possible contamination and carryover effect. QA/QC protocol was in accordance with US EPA Method 7473 (U.S.EPA 1998). See Redondo (2022) and Redondo et al (in prep) for Hg measurements and for further details.

Appendix 13. Analysis of pollen, spores, and non-pollen palynomorphs

Inaperturate grains with papilla were referable to *Sequoia sempervirens*, but others without the papilla were grouped as TCT (Taxodiaceae- Cupressaceae-Taxaceae; Adam, 1967); *Pinus* were all diploxylon, most probably *P. radiata*); *Olea* was not differentiated from *Ligustrum*; the Asteraceae group was differentiated into bursage type (*Ambrosia*); dandelion-type (Lactuceae); sagebrush (*Artemisia*); and thistle-type (*Cirsium*); Poaceae was differentiated into the general Poaceae and Cerealia, which was subdivided into *Secale*-type and *Zea*-type. Fern spores were divided on morphological differences. For algae, all *Pediastrum* is *P. simplex*, but was differentiated into four morphotypes.

Pollen, spores and NPPs were grouped into general function groups, based upon several references on the vegetation of JRBP (Common Plants, 1995; JRBP Plant List, 2016). Groups included total trees; shrubs; herbs; introduced species; common oak woodland species; common chaparral species; common grassland species; rooted aquatic species; pelagic and floating aquatic species; coprophilous fungi; and total NPPs.

Pollen, spore, and NPP counts are reported in Anderson et al. (in prep).

Appendix 14. Sedimentation rates.

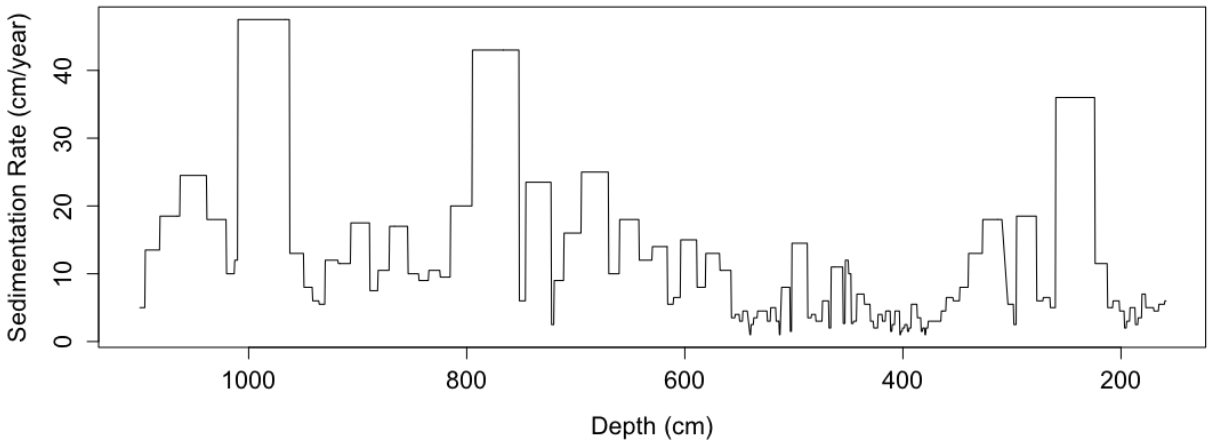

Figure S14.1 Sedimentation rates for Searsville core JRBP2018-VC01B.

Appendix 15. Radiocarbon Analysis

Table S15.1. Radiocarbon and calibrated radiocarbon dates for Searsville core JRBP2018-VC01B.

Upper Depth	ETH ID	^{14}C Age	1 σ	$F^{14}C$ (^{4}C)	1 σ ($F^{14}C$)	d13C	1 σ ($d^{13}C$)	calibrated 2.5%	calibrated 50%	calibrated 97.5%
158.5-160	116208	8459	26	0.349	0.0011	-25.8	1	9438	9489	9528
201-202	116209	3412	22	0.654	0.0018	-27.6	1	3580	3655	3806
275-276	116210	11883	31	0.228	$9.00x10^{-4}$	-25.2	1	13612	13719.5	13803.025
337-338	116211	3362	22	0.658	0.0018	-28.5	1	3499	3600	3682
357-358	116212	3638	22	0.636	0.0018	-26	1	3879	3947	4068
377-378	116213	12154	43	0.22	0.0012	-25.5	1	13870	14057	14170
397-398	116214	14860	39	0.157	$8.00x10^{-4}$	-23.8	1	18080	18204	18256
407-408	116215	7709	26	0.383	0.0012	-25.3	1	8422	8485	8570
417-418	116216	16463	62	0.129	0.001	-25.1	1	19614	19866	20083
427-428	116217	10725	30	0.263	0.001	-24	1	12692	12724	12744
437-438	116218	4041	23	0.605	0.0017	-27.6	1	4428	4483	4589
447-448	116219	13638	50	0.183	0.0011	-25	1	16310	16473	16664
452-453	116220	5533	24	0.502	0.0015	-27.3	1	6291	6332	6390
467-468	116221	7185	25	0.409	0.0013	-24.3	1	7947	7991	8024
477-478	116222	13013	34	0.198	$8.00x10^{-4}$	-23.7	1	15393	15589	15727.025
487-488	116223	16202	42	0.133	$7.00x10^{-4}$	-23.6	1	19455	19544	19760
497-498	116224	3883	22	0.617	0.0017	-27.7	1	4200.975	4328	4405
507-508	116225	6571	24	0.441	0.0013	-26.8	1	7430	7468	7556
517-518	116226	5981	24	0.475	0.0014	-26.4	1	6744	6818	6889

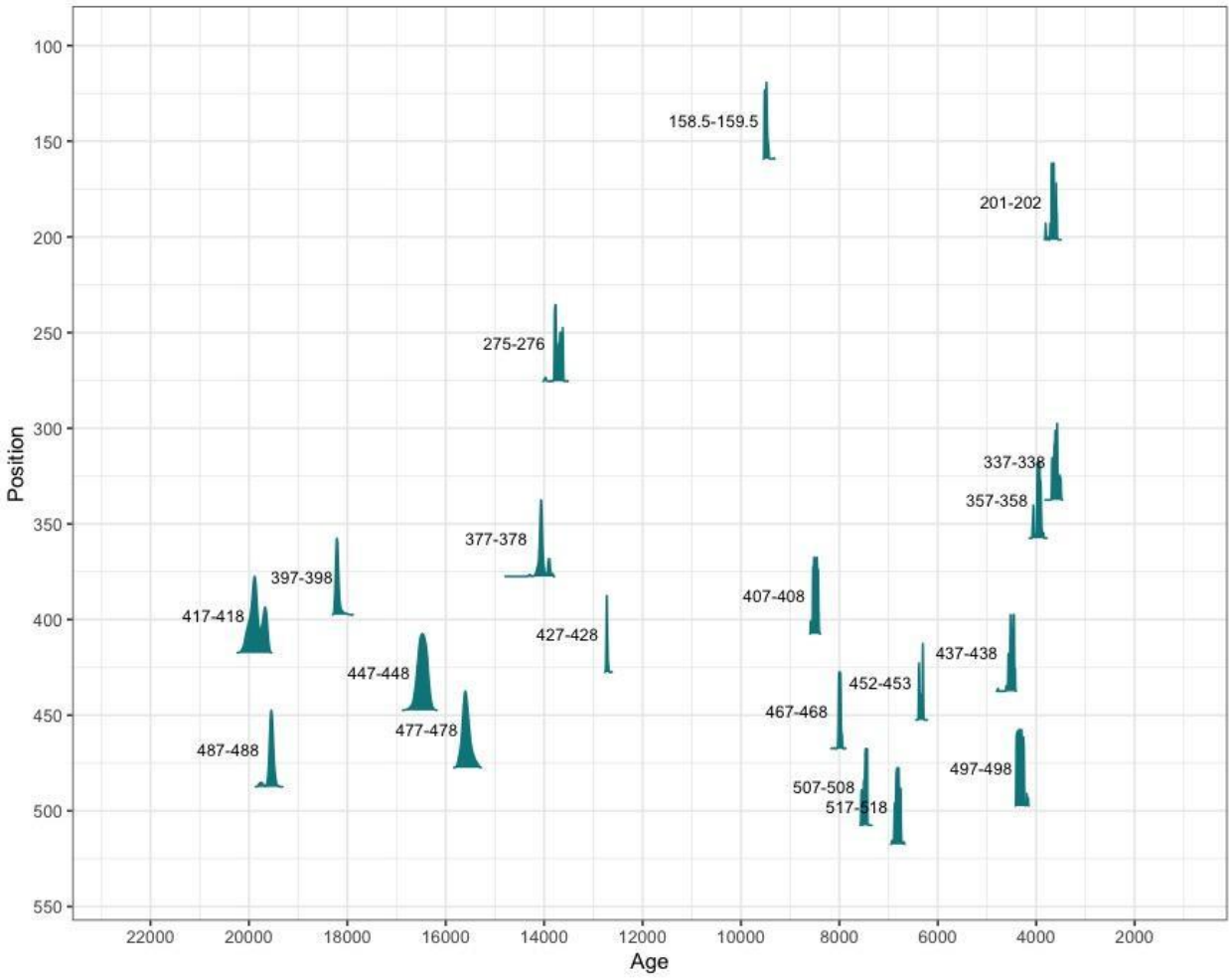

Figure S15.1 Calibrated radiocarbon dates for Searsville core JRBP2018-VC01B. Turquoise distributions are the radiocarbon probability density curves.